Metadolerites as quantitative P-T markers for Sveconorwegian metamorphism, SW Sweden

Birgit Fredrich

Dissertations in Geology at Lund University,
Master's thesis, no 415
(45 hp/ECTS credits)

Department of Geology
Lund University
2014

Metadolerites as quantitative P-T markers for Sveconorwegian metamorphism, SW Sweden

Master's thesis

Birgit Fredrich

Department of Geology
Lund University
2014

Contents

Cover Picture: View on charnockitic rocks at Apelviken (Varberg). Picture is taken from sampling site AV1. (Photo: Birgit Fredrich)

P-T estimates on metadolerites, SW Sweden

Birgit Fredrich

Fredrich, B., 2014: Metadolerites as quantitative P-T markers for Sveconorwegian metamorphism, SW Sweden. *Dissertations in Geology at Lund University*, No. 415, 62 pp. 45 hp (45 ECTS credits) .

Abstract: : Structurally late and roughly N-S trending high-grade metamorphic dolerites occur in the Eastern Segment along the coast from Varberg to Kullaberg and inland (eastwards) to the Sveconorwegain Front. Locally these mafic dykes cross-cut the gneissic foliations of the host gneisses. Metadolerites have a high-pressure granulite facies metamorphic mineral assemblage and some of them have well-preserved primary magmatic structures such as layering and "cross-bedding". These dykes are younger than the Hallandian metamorphism and thus provide a means to determine indisputable quantitative P-T markers for the Sveconorwegian metamorphism. The estimated temperatures and pressures range between 770-850 °C and 8-10 kbar. These high-grade metamorphic conditions represent the transition between upper amphibolite and granulite facies at medium to high pressure and refine the previously published P-T estimates (680-800 °C and 8-12 kbar) for the southern part of the Eastern Segment. Geochemical data indicate a within-plate and volcanic arc setting. It also suggests that the intrusion is related to late-orogenic extension and exhumation of the Sveconorwegian orogen. A Nb-anomaly for all samples indicates a source affected by subduction. High LIL elements (mafic layers at Gåsanabbe and Söndrum dykes) indicate metamsomatic processes, which is supported by the presence of scapolite and epidote veins.

Keywords: Getterön, Träslövsläge, Apelviken, Söndrum, Stensjöstrand, Gåsanabbe, Kullaberg, metadolerite, granulite, Sveconorwegian, P-T estimate, subduction, late-orogenic extension, Nb-anomaly, Blekinge-Dalarna dykes

Supervisor: Charlotte Möller

Birgit Fredrich, Department of Geology, Lund University, Sölvegatan 12, SE-223 62 Lund, Sweden.

Tryck-temperatur-bestämning i metadiabaser, sydvästra Sverige

Birgit Fredrich

Fredrich, B., 2014: Metadolerites as quantitative P-T markers for Sveconorwegian metamorphism, SW Sweden. *Dissertations in Geology at Lund University*, No. 415, 62 pp. 45 hp (45 ECTS credits) .

Abstract: Strukturellt unga och N-S-ligt strykande högmetamorfa metadiabaser förekommer i Östra segmentet längs västkusten från Varberg till Kullaberg, och i inlandet mot öster till den Svekonorvegiska fronten. Dessa basiska gångar skär ställvis gnejsiga strukturer i värdbergarterna. Några har välbevarade primärmagmatiska strukturer som exempelvis lagring och “cross-bedding”. Metadiabaserna består av högtrycksgranulit-facies mineral. Eftersom gångarna är yngre än den Hallandiska metamorfosen i sydvästra Sverige erbjuder de möjlighet att beräkna tryck och temperatur som otvetydigt gäller Svekonorvegisk metamorfos. Värden för metadiabaser längs kusten har beräknats med geotermobarometri (TWEEQE, Thermocalc) och faller i intervallet 770-850 °C och 8-10 kbar. Detta representerar övergången från övre amfibolitfacies till granulitfacies vid medelhöga till höga tryck. Bulk-geokemisk sammansättning är tholeiitisk och dataplotter indikerar ”within-plate” och ”volcanic arc”; Nb-anomalier för samtliga prov indikerar magmabildning i en subduktionspåverkad kemisk miljö. Gångarna intruderade vid sen-orogen extension under den senare delen av den Svekonorvegiska bergskedjebildningen. Höga halter av LIL-element i vissa prov är kopplade till förekomst av skapolit (basiska veckade lager, Gåsanabbe) respektive epidot i närheten av sena sprickor (metadiabaser i Söndrum), och indikerar metamsomatiska processer.

Nyckelord: Getterön, Träslövsläge, Apelviken, Söndrum, Stensjöstrand, Gåsanabbe, Kullaberg, metadiabas, granulit, Sveconorvegisk, tryck-temperatur-bestämning, subduktion, sen-orogen extension, Nb-anomali, Blekinge-Dalarna diabas

Supervisor: Charlotte Möller

Subject: Bedrock Geolog

Birgit Fredrich, Department of Geology, Lund University, Sölvegatan 12, SE-223 62 Lund, Sweden.

1 Introduction

The Eastern Segment of the Sveconorwegian Orogen underwent two metamorphic cycles: the 1.47-1.38 Ga Hallandian and the 0.99 – 0.90 Ga Sveconorwegian metamorphism, which led to a polymetamorphic nature of the high-grade metamorphic gneisses and metabasic rocks. Sveconorwegian metamorphism reached high-pressure granulite and upper amphibolite facies in the southern part of the Eastern Segment at 680-750 °C and 8-10 kbar (Johansson et al 1991, Wang & Lindh 1996, Möller 1998). Partly exposed relics of late Sveconorwegian (990-980 Ma) retrogressed eclogite indicate however pressures in excess of 15 kbar for parts of the Eastern Segment (Möller 1998; 1999, Johansson et al. 2001, Hegardt, 2010, Möller et al. 2013).Hallandian metamorphism at c. 1.43 Ga involved regional-scale migmatization (Söderlund et al. 2002, Möller et al. 2007); local charnockitization took place at 1.40 Ga, in association with emplacement of high-temperature intrusions in the coastal area south of Varberg (Harlov 2006, Rimša 2007) The pervasive character of the Sveconorwegian overprint however impedes determination of the extent and the character of the Hallandian event in detail and has led to different interpretations regarding the orogenies. Quantitative P-T estimates of the Hallandian event reached 750 °C and 4-5 kbar for the region around Romeleåsen (Ulmius et al. 2013)

Structurally late and roughly N-S trending high-grade metamorphic dolerites occur along the coast from Varberg in the north to Kullaberg. These mafic dykes cross-cut the gneissic foliations of the host gneisses in some cases. They have a high-pressure granulite metamorphic mineral assemblage and some of them have well-preserved primary magmatic structures such as layering and “cross-bedding”. At two localities (Träslövsläge and Kullaberg) a Sveconorwegian intrusion age is indicated (Johansson & Kullerud 1993; Söderlund et al. 2008). These dykes are younger than the Hallandian metamorphism and thus provide a means to determine indisputable quantitative P-T markers for the Sveconorwegian metamorphism.

2 Geological Background

2.1 Regional Geology

The Sveconorwegian Province is a tectonic counterpart to the Grenville Province in the Canadian Shield. It forms a circa 500 km wide orogenic belt in the (present-day) south-west Baltic Shield and is delimited by the Sveconorwegian Front in the east. The province is divided into five principal lithotectonic segments, separated by roughly N-S trending crustal scale deformation zones of Sveconorwegian age (Fig. 1, Bingen et al. 2005, 2008). The lithotectonic segments are, from east to west; the Eastern Segment, the Idefjorden Terrane, the Bamble Terrane, the Kongsberg Terrane and the Telemarkia Terrane, which differ from one another in their crustal evolution of Pre- and Sveconorwegian time, regarding timing and character of crustal growth, deformation and metamorphism. The segments west of the Eastern Segment (Fig. 1A) are regarded as Sveconorwegian allochthons and are separated from the parautochthonous Eastern Segment by a shear belt of ductile deformation, the Mylonite Zone (Park et al. 1991; Andersson et al. 2002). The Eastern Segment is mainly composed of reworked equivalents to igneous rocks of the Transscandinavian igneous belt, 1.70-1.65 Ga orthogneisses (e.g. Persson et al. 1995; Connelly et al. 1996; Söderlund et al. 1999; Åhäll & Larson 2000; Söderlund et al. 2008).

Records of Sveconorwegian metamorphic and intrusive age are present west of the Caledonian front. However the reworking of these rocks during the Caledonian orogeny makes it difficult to relate the tectonic characteristics to the Sveconorwegian orogen southeast of the Caledonian Front (Bingen et al. 2008, Roffeis et al. 2012). Bingen et al. suggested a four-phase history for the Sveconorwegian metamorphic evolution (Bingen et al. 2008). The early Arendal phase at 1.14-1.08 Ga took place at high-temperature and low to moderate pressures, reaching metamorphic conditions of the granulite facies. The mid-Sveconorwegian phase at 1.05-1.03 Ga was characterized by metamorphism in the greenschist-, to upper amphibolite facies, with a few local occurrences of high pressure granulite (Bingen et al. 2008, Söderlund et al. 2004).

At 990-980 Ma, the late Sveconorwegian phase (Falkenberg phase) reached regionally high-pressure metamorphism, in the Eastern Segment (Johansson et al. 2001; Bingen et al. 2008, Möller et al. submitted). Retrograde eclogites occur in one tectonic unit (Möller 1998, 1999; Möller et al. 2013). This high-pressure metamorphism was followed by regional-scale partial melting at 0.98-0.96 Ga (Andersson et al. 1999; Söderlund et al. 2002; Möller et al. 2007, submitted) and mafic dyke intrusions at 0.97-0.94 Ga (Söderlund et al. 2005, 2008). In the foreland region, these mafic dykes occur as an extensive orogen parallel dyke swarm, the Blekinge Dalarna Dolerites. The youngest phase of Sveconorwegian metamorphism, the Dalane phase at about 930-920 Ma was a thermomagmatic event with voluminous anorthosite-mangarite-charnockite intrusions, in Rogaland, southwestern Norway, and associated low-pressure and high- to ultra-high temperature metamorphism (Bingen et al. 2008).

The Eastern Segment has been divided into three different levels – the upper, middle and lower - which differ in their metamorphic grade from one another. Semi-penetrative Sveconorwegian ductile deformation and metamorphic conditions of amphibolite to greenschist facies characterize the upper level. The middle level is dominated by

penetrative ductile Sveconorwegian deformation at amphibolite facies conditions (Wahlgren et al., 1994; Möller et al. 2007).

The studied area is situated within the lower level. This level contains 1.73-1.66 Ga high-grade migmatitic orthogneisses of granite-quartzmonzonite to quartz-monzodiorite composition and minor 1.41-1.18 Ga syenitoid intrusions. The gneisses host metamorphosed mafic rocks like migmatitic garnet amphibolite and high-pressure granulite (Möller et al. 2007). Partly exposed relics of late Sveconorwegian (990-980 Ma) retrogressed eclogite indicate pressures of over 15 kbar in a recumbent fold nappe (Möller 1998, 1999; Johansson et al. 2001; Möller et al. 2013, submitted).

Regional geological mapping supported by high-resolution airborne magnetic anomaly maps reveal folding of the high-grade gneissic foliation. Roughly E-W to WNW-ESE trending folds with gently plunging fold axes are reoriented by large scale regional open folding along N-S trending axes (Möller et al. 2007, submitted). The metamorphic conditions within the lower level reached high-pressure granulite and upper amphibolite facies. Geothermobarometry of mafic rocks estimate a temperature of 680-850 °C and corresponding pressures of 8-12 kbar during metamorphism (Johansson et al.,1991; Wang & Lindh, 1996; Möller, 1998, 1999, Hansen et al. submitted). The Eastern Segment records also a pre-Sveconorwegian high-grade metamorphic event between 1.46-1.42 Ga, however the pre-Sveconorwegian minerals have recrystallized and/or re-equilibrated during the Sveconorwegian high-grade overprint (Christoffel et al., 1999; Söderlund et al., 2002, Möller et al. 2007). This Hallandian orogeny is preserved as regional scale migmatization and at least locally a gneissic layering, which have been dated at 1.46-1.42 Ga (Hubbard, 1975; Christoffel et al., 1999; Söderlund et al., 2002; Möller 2007). Additionally the U-Pb mineral isotope system of zircons show recrystallization, new growth of zircons and overgrowth of igneous zircon (Söderlund et al. 2002; Möller et al. 2007). This metamorphic event is partly coeval with widespread 1.47-1.44 mafic intrusions (diabase sills and dykes) and felsic plutonism of anorogenic origin in SW Fennoscandia (Brander & Söderlund 2009, Ulmius et al. submitted). This was followed by 1.40-1.38 Ga intrusions of charnockitic granite and syenitoid rocks and a charnockitization of gneisses around felsic dyke intrusions at the same time (Bogdanova 2001). Orogenic activity in this time range has also been termed Danapolonian (Bogdanova 2001). Pervasive Sveconorwegian overprint impede however the record of the extent and the character of the Hallandian event in detail.

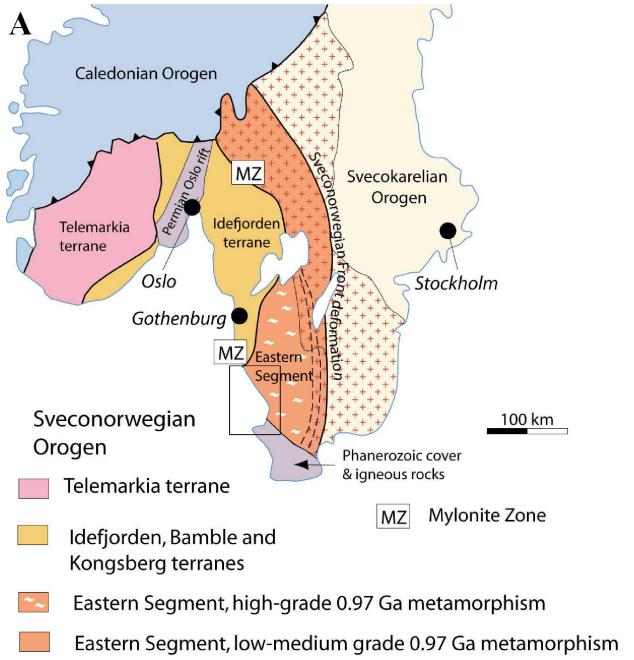

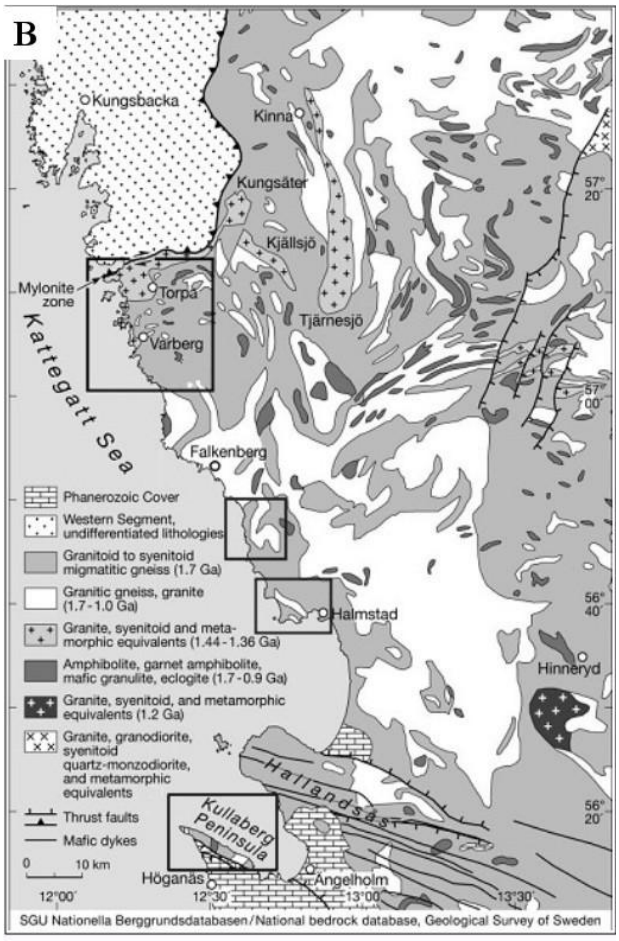

Fig. 1. A: Sketch map of southern Sweden and Norway showing the Eastern Segment (modified after Möller et al 2007). Box marks the study area. B. Simplified geological map of the southwestern Eastern Segment (modified after the National bedrock database of the Geological Survey of Sweden compiled at scale 1:1 Million) showing the studied localities.

3 Methods

3.1 Fieldwork

Field work was carried out during eight days in August and September 2013, using as map data the airborne magnetic anomaly map (SGU), Bedrock Map 5B Varberg NO (SGU) and a lithological map of the Stensjö association (Hansen et al. submitted). Eleven localities have been mineralogically and structurally investigated. Coordinates refer to the SweRef 99TM coordinate system.

3.2 Petrography, Scanning Electron Microscope—Energy Dispersion Spectroscopy (EDS)

Thirty thin sections were investigated using polarizing microscope (Nicon, eclipse E400 Pol) and seven of them additionally with a scanning electron microscope (SEM; Hitachi S3400N) coupled with an EDX analyser (Link INCA) at the Department of Geology, Lund University. All samples were polished and carbon coated. An acceleration voltage of 15-25 kV was used. The SEM-analysis data of all samples and minerals can be seen in appendix A. Amphibole endmembers were classified by the method of Leake et al. (Leake et al. 1997). Pyroxene endmembers were classified after Morimoto (Morimoto, 1988). A Wo-En-Fs plot of all pyroxenes can be seen in appendix B.

3.3 Geochemical Analysis

Major and trace elements including Fe^{2+} - contents were determined of 15 samples (Table). The geochemical analysis were done by Acme Analytical Laboratories (Vancouver) Ltd. The Mg# was calculated via Mg/(Mg+Fe) = Mg# . Diagrams were created using the program GCDkit Win 3.0 (Janousek et al 2006). Normative mineral assemblages of all the samples were calculated by the calculation-spreadsheet by Kurt Hollocher following the CIPW norm (Appendix E).

3.4 P-T estimates

Equilibrium P-T estimates were done by using the WinTWQ (Thermobarometry with estimation of equilibration state) program with two different databases; TWQ v. 1 (Berman 1988,1990) and TWQ v. 2.32 (Berman & Aranovich, 1996).Reactions containing pargasite or enstatite were calculated with version 1, all other minerals with version 2 .

Average P-T estimations were calculated by using the software Thermocalc (Powell & Holland 1988).

4 Field Relationships

Structurally young meta-mafic dykes are exposed along the Kattegatt coast from Varberg and southwards to the Kullaberg peninsula. They locally cross-cut the gneissic fabric of the country rock and record metamorphic conditions at high-pressure granulite facies, which sets a minimum age for the igneous emplacement at circa 0.95 Ga (Möller et al. 2007). It is indicated by Söderlund et al. (2005; 2008) that these dykes are likely equivalent to the 975-940 Ma orogen-parallel Blenkinge-Dalarna Dolerite dyke swarm in the adjacent foreland region and possibly formed in response to an orogenic collapse (Johansson & Kullerud 1993; Wang et al. 1998; Möller et al. 2007; Söderlund et al. 2008). The youngest rocks in the lower level are late-tectonic pegmatitic and granitic dykes 0.96-0.94 Ga old which cut the country rock discordantly (Möller & Söderlund 1997; Andersson et al. 1999; Möller et al. 2007).

4.1 Localities

The studied area is situated in the southern part of the Eastern Segment along the Kattegatt coast (Fig.1). The chosen localities are from north to south, Getterön

Locality	Coordinates	Sample-ID	Sample-type	Figures
Getterön	N6334005 E0330010	GT1	metadolerite	2,3,12
Träslövsläge	N6327477, E0334758	TL1	metadolerite	2,4,13
Apelviken	N6330104, E0333328	AV1	metadolerite	2,4,11
Stensjö harbour	N6297034, E0354076	StSD	metadolerite	5,6,14
Gåsanabbe	N6297542, E0353692	Gas3A	metadolerite	5,6,15
	N6297542, E0353692	Gas3B	metadolerite	5,6,15
	N6297550, E0353700	StHD1	metadolerite	5,6
	N6297550, E0353699	StHD2	metadolerite	5,6
	N6297564, E0353709	StML1	mafic layer	5,6,16
	N6297560 E353710	StML2	mafic layer	5,6,16
	N6297560, E353710	StML3	mafic layer	5,6,16
Söndrum harbour	N6279827, E0363564)	SöHf1	metadolerite	7,8,17
Söndrum	N6280273, E0362838	SöM1	metadolerite	7,8,17
	N6280252, E0362843	SöPD1	Plagioclase-rich lens in sample SöM1	7,8,18
	N6280228, E0362857	SöKG	contact gneiss-dolerite	7,8,18
Kullaberg	N6242741, E0342236	KB2	metadolerite	9,10,19

Table 1; Overview of studied localities and samples. Coordinates refer to the SweRef 99TM coordinate system.

(Varberg), Apelviken (Varberg), Träslövsläge (Varberg), Stensjöstrand, Söndrum and Kullaberg (Table1).

4.1.1 Varberg

In Varberg (Fig. 2) is the only occurrence of intrusive charnockite in southern Sweden. It is a part of a plutonic suite called the Varberg-Granite-Charnockite association (Hubbard 1975) and consists of granite (Torpa granite) and several textural different varieties of charnockites. The crystallization of the magmatic mineral assemblage was dated at 1399 ± 6Ma by Christoffel et al. (1999). Åhäll et al. (1997) dated a charnockite portion in the Torpa granite at 1380 +/- 6 Ma. A moderate foliation which cuts the magmatic structures in the charnockite indicates a high-grade Sveconorwegian metamorphic event (Johansson & Kullerud 1993). P-T estimates have recorded temperatures of 750-850°C and pressures of 8.0-8.5 kbar (Harlov et al. 2013).

At **Getterön**, a peninsula in the north-western part of Varberg, the coarse grained charnockite

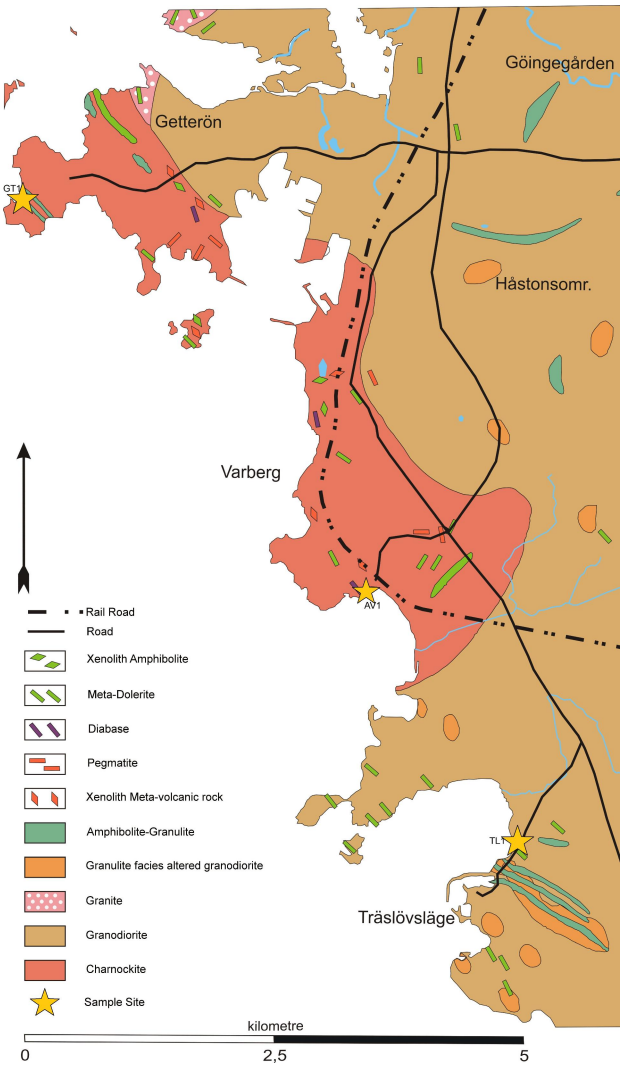

Fig. 2. Geological map of Varberg (SGU basemap, modified after Lundqvist 2008).

contains orthoclase megacrysts and shows minor deformation only. Within the charnockite occurs a mafic dyke with well preserved magmatic structures. This metagabbroic dyke is concordant to the foliation of the charnockite and trends NW-SE. At the contacts, the charnockite and the mafic dyke have stronger gneissic foliation and the charnockite has lost its orthoclase megacrysts (Fig. 3C). The metadolerite is fine-grained and blacker at the contacts, indicating hydration and formation to hornblende in the marginal zone. Magmatic structures such as primary igneous layering, "slumping" and "cross-bedding" are well preserved (Fig. 3A). The layers alternate between light plagioclase-rich layers and darker layers richer in pyroxenes and hornblende. The scale of the magmatic layering varies between a cm up to a metre. There is also a < 10 cm thick garnet-band which follows the igneous layering (Fig. 3B). A weak foliation indicates a deformation event. A close look shows locally elongated black aggregates made of clinopyroxene, orthopyroxene and hornblende. This elongation trends roughly NW-SE and is subparallel to the magmatic layering and the contacts of the dyke.

A garnet-free fine-grained mafic dyke is preserved in front of the local surfing school at a beach of **Apelviken**, south of Varberg (Fig.4A). The thickness of the dyke is circa 1m. The dyke trends NW -SE and has a weak folitation parallel to the contacts. The southern contact has a brittle overprint.

There are several elongated mafic dykes within a granulite facies felsic gneisses, at the beach, ca. 7 km south of Varberg near the harbour of **Träslövsläge** (locality studied by Johansson & Kullerud 1993). The dykes trend WNW-ESE and is slightly discordant to the NW-SE trending foliation of the surrounding gneiss. Like the metagabbro dyke in Getterön, the intrusions show well preserved primary igneous layering of alternating light plagioclase-rich and darker layers richer in pyroxenes and hornblende (Fig. 4B). The layers trend NW-SE and their thickness vary between ca. 1 cm and 90 cm. There is a subhorizonatal E-W lineation. Together with the preservation of the igneous layering, it indicates that the dyke was undeformed and unmetamorphosed before its high-grade metamorphic overprint.

4.1.2 Stensjöstrand

The Stensjö association consists of sillimanite-bearing and sillimanite-free felsic migmatitic gneiss interbanded with mafic layers. They crop out along along the Kattegatt coast in Halland within the Naturreservat Stensjöstrand northwest of the village Steninge (Fig.5). The association underwent upper amphibolite to lower granulite metamorphic conditions. P-T estimates on the mafic metatexites suggest a pressure of 0.9-1.03 GPa and a temperature of c. 850 °C (Hansen et al. submitted). The Stensjö association is structurally complex. A predominant N-S to NE-SW trending gneissic foliation (S1) with

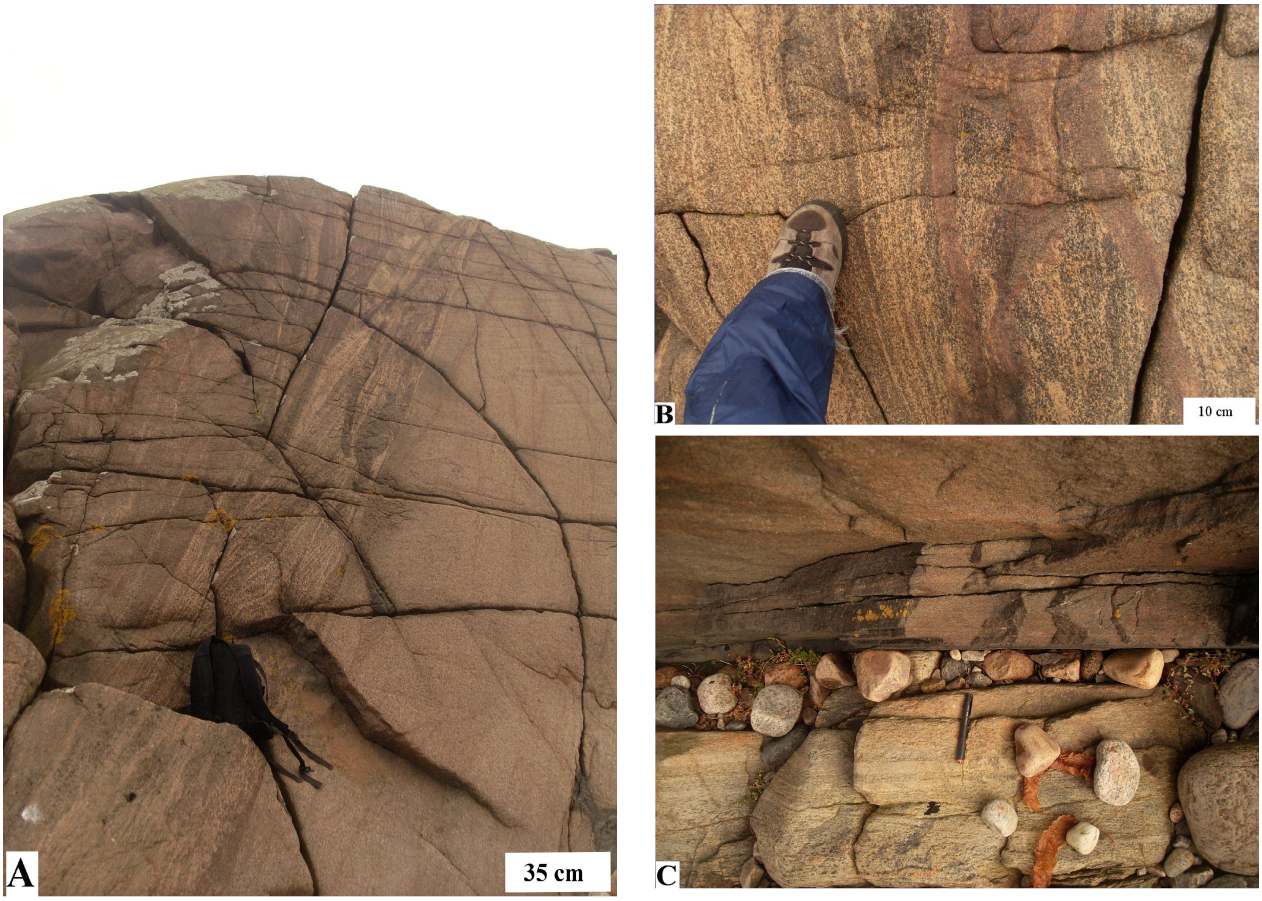

Fig.3; A:Magmatic layering and „slumping“ structures of metadolerite. B: Garnet-band within the magmatic layering of the dyke. C: Local deformation at the contact to the charnockite. Hatched lines indicate the foliation.

Fig. 4; A: Metadolerite dyke in Apelviken. The dyke has a thickness of 1m. B: Magmatic layering in metadolerite at Träslövsläge. The orientation of the layering is indicated by the hatched lines.

preserved intrafolial folds (F1) and a ESE-plunging lineation (L1) defined by polymineralic aggregates were followed by metric to km-scale asymmetric F2 folding. The F2 folds have one subhorizontal and one steep limb, angular hinges and N-S to E-W trending axes (Pinan-Llamas et al. 2013). All these structures are affected by cm to km-scale concentric, roughly SE verging F3 folds with subhorizontal to steeply E to NE or SW plunging axes. The interpretation of these D1-D3 ductile structures is a mainly WNW-ESE transport which was followed by E-W shortening of the Eastern Segment during the Sveconorwegian orogeny (Pinan-Llamas et al. 2013). Geochronological analysis by zircons from all rock types show a Hallandian metamorphic and igneous activity at c. 1400 Ma and subsequent migmatization (coeval with F1-F3 folding) during the late Sveconorwegian orogeny at c. 970 Ma. (Pinan-Llamas et al. 2013).

There are several metadolerite dykes at Stensjöstrand. One at the harbour; this small dyke has a thickness of 1,5 - 2 m and trends roughly N-S. It cuts the E-W trending foliation of the surrounding quartzo-felddspathic gneiss (Fig. 6A). Compared to the other dykes it is more fine-grained. There are no deformation structures or textures visible with the naked eye.

A second dyke is located within a small bay (Fig. 6B). It crops out over c. 35m along the coast and it concordant to the surrounding gneiss. The gneiss shows small, tight and angular F2 folds with roughly E -W trending axes. These smaller folds are enclosed within an open-gentle upright F3 antiform, with NE plunging axes. It is not clear if the dyke is discordant to the F2 folds but it is clearly enclosed in the F3 antiform.The dyke trends roughly NE. Its foliation dips 45° SE at the southeastern contact, is horizontal in the middle and dips 40° at the northwestern contact. A 3 cm thick plagioclase- and quartz-rich vein within the metadolerite also shows a gentle bending. With the exception of these structures the dyke is homogenous. There are no magmatic structures. This dyke has not been sampled.

Some smaller roughly NE trending garnet-poor dykes with a thickness of around 15 cm are located close to the locality Gåsanabbe. They are discordant to the surrounding sillimanite-bearing gneiss and dip 40° W (Fig. 6C). These dykes have not been sampled.

Another garnet-rich mafic dyke is located at **Gåsanabbe** (Fig. 6D). This dyke consists of three roundish sheets of mafic composition with a thickness of circa 70 cm and traceable for circa 20 m in northeastern direction. They are discordant to the isoclinal F1 folds in the host gneiss (Fig. 6E). The gneiss between those sheets is totally recrystallized. The sheets are boudinaged and folded by F3 upright folds. The mineral aggregate foliation of the dolerite sheets trend E-W. Some c. 4 mm long black minerals are oriented NW-SE. Partly there are some elongated greyish plagioclase grains (c.1 cm long) which have a red garnet-rich rim. The dyke forms also apophysises.

A ca. 2,5m high wall some metres east of the dykes has fine-grained mafic layers within migmatitic gneiss. The mafic layers are pinch and swell-shaped, strongly elongated and form rootless folds (Fig. 6F). These mafic layers (Fig. 6G) have been sampled (STML1-3).

4.1.3 Söndrum

Söndrum near Halmstad (Fig. 7) is a key-locality for Hallandian zonal charnockitization due to solid-state dehydration along pegmatoid dykes (Harlov et al. 2006). This charnockitization and coeval formation of clinopyroxene megacrysts formed due to CO2-rich fluids and has been dated at 1397 ± 4Ma (Rimša et al. 2007). The charnockite and the clinopyroxene-bearing rocks show subvertical stretching and recrystallization,

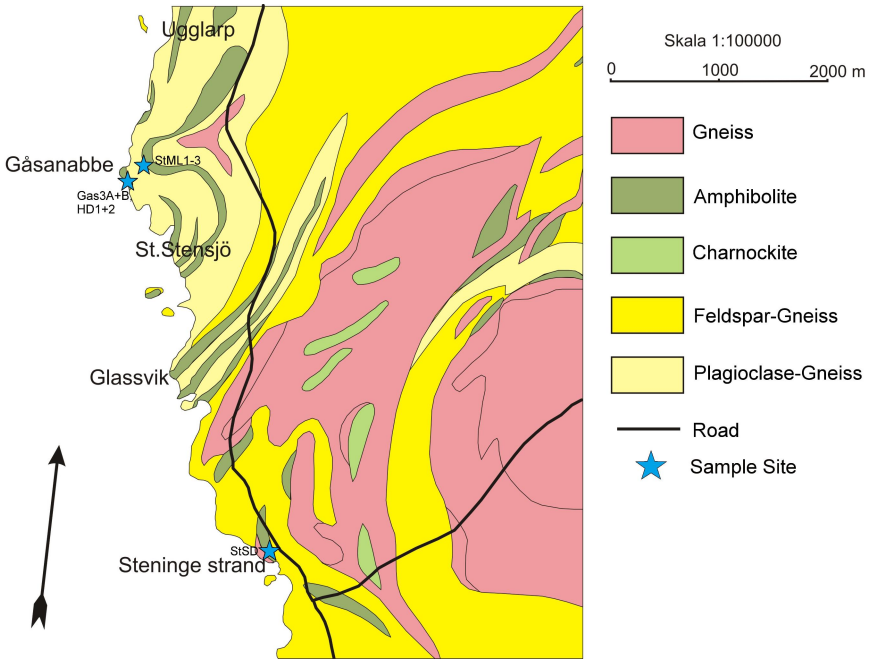

Fig. 5. Geological map of Stensjöstrand, showing the sample sites (SGU basemap, modified after Larsson 1966).

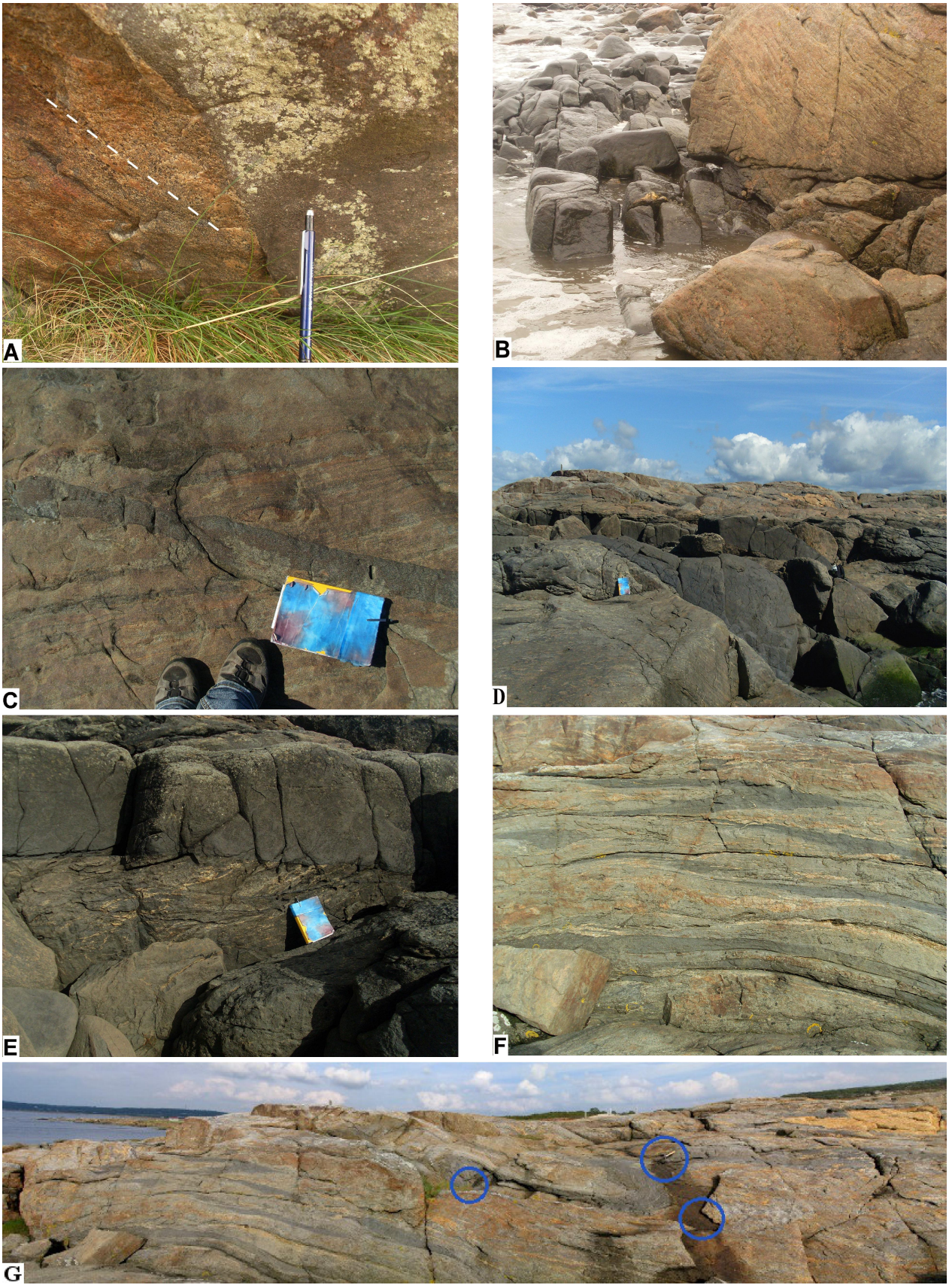

Fig. 6. A: Discordant contact of metadolerite and the surrounding gneiss in Stensjö harbour. B: Contact of metadolerite and the surrounding gneiss. Gneiss and dyke are both deformed by F3 folding. C: Thin discordant dykes. D: Folded and boudinaged dykes at Gåsanabbe. E: Gåsanabbe dykes cutting tight F1 folds. F: Mafic, pinch– and swell-shaped layers forming rootless fold-hinges(isoclinal F1). Samples StML1-3 were collected from mafic layers of this outcrop. G: Sampling sites of StML1-3 (Photo: Leif Johansson). Right circle = StML1, left circle = StML2 and top circle = StML3.

which is most likely of Sveconorwegian age.

Three mafic dykes occur in this area and cut the gneissosity at a high angle. Two are in a quarry at the harbour and one is located south of the key-locality of the zonal charnockitization at the coast.

The metadolerite dyke south of the charnockitization locailty crops out for circa 60 m along the coast, is NNW-SSE trending, and cuts the gneissic foliation of the host gneiss. Both contacts to the gneiss are exposed over a length of 2-5 m The contact is clearly sharp and discordant to the NE-SW trending foliation of the gneiss (Fig. 8A). The gneiss has locally a strong reddish colour.
A magmatic layering trending on average N-S can be seen in central parts of the dyke (Fig. 8C). Other primary igneous features are “crossbedding” and irregular-shaped inclusions of plagioclase-rich composition (Fig. 8B). A steep E-W lineation defined by strechted light and dark mineral aggregates is present in both the metadolerite and the host gneiss. The igneous and ductile metamorphic structures within the dyke are cut by green net-like epidote veins. They vary in thickness of some mm to 3 cm (Fig. 8D). A faulted plagioclase-rich patch demonstrates that the epidote filled late brittle structures were associated with sinistral/dextral strike-slip movement (Fig. 8E).

Two other metadolerite dykes are located at the quarry near the harbour.They trend roughly N-S, are 1,5 m wide and cross-cut the foliation of the host gneiss. There are gneiss fragments within one of the metadolerites (Fig. 8F). Central parts of the meta-dolerite are homogenous with a foliation which trends NE-SW.

4.1.4 Kullaberg

Kullaberg in NW Skåne is located between Skälderviken bay in the northeast and the Helsingborg lowland area in the south. It is the northwesternmost exposure of one of the major horsts in the Sorgenfrei-Tornquist zone. The horsts consist of Precambrian crystalline rocks, mainly gneiss and amphibolite, locally overlain by Palaeozoic sedimentary rocks. Younger sedimentary rocks are preserved within the grabens. The crystalline basement of the Kullaberg peninsula is part of the Eastern Segment and experienced Sveconorwegian high-pressure granulite facies metamorphism (Wang 1996). The regional gneissic foliation in the biotite- and hornblende-gneiss at the tip of Kullaberg dips shallowly to the west, but steepens towards the east (Forsell 1962, Söderlund et al. 2008).

The studied area is located at Paradishamn, where a ca 50 m wide metadolerite sheet is exposed, dipping shallowly WSW (Fig. 9). It has a strongly migmatized contact to the overlying biotite-gneiss (Fig. 10A). The metadolerite loses its garnet content in direction to the contact, whereas the sugary leucosomes are rich in garnet and of a granitic composition. The locally stromatic and partly net-like leucosomes are parallel to the contact of the metadolerite dyke, the biotite-gneiss and the foliation of the biotite-gneiss (Söderlund et al. 2008). This migmatized contact has locally a sharp and locally a gradual transition into the unmigmatized metadolerite dyke (Fig. 10B). The amount of leucosomes increases away from the metadolerite. Near the biotite-gneiss,

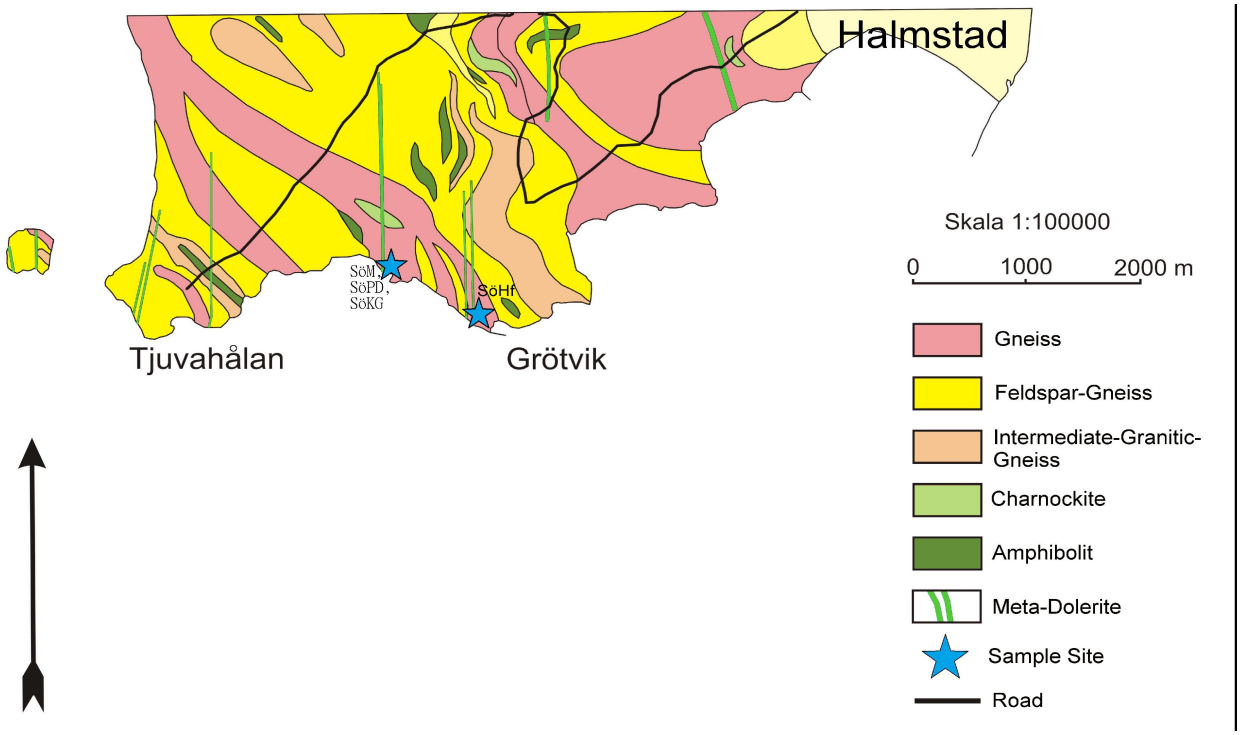

Fig. 7. Geological map of Söndrum showing the sample sites (SGU basemap, modified after Larsson 1968). Note that the dykes are highly exaggerated in length.

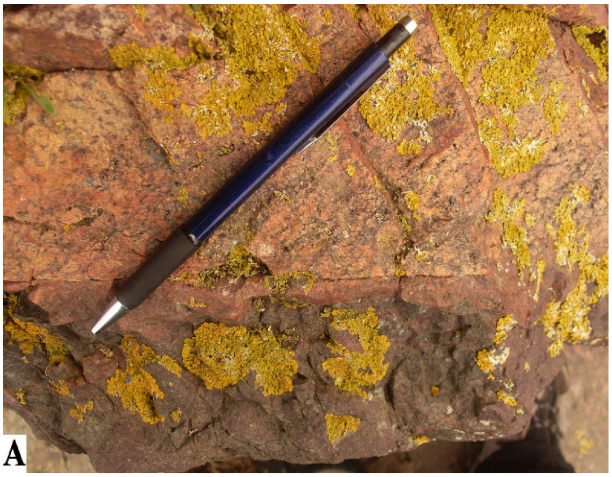

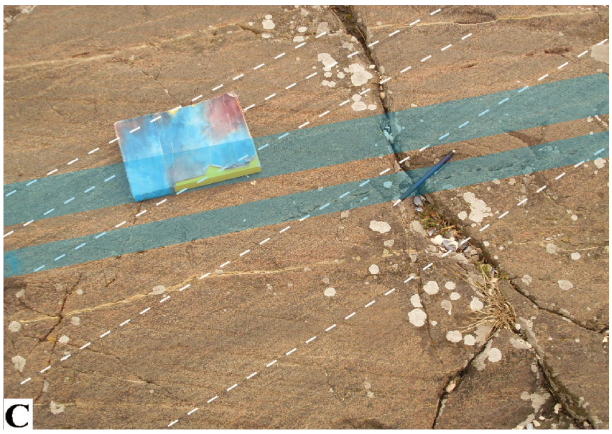

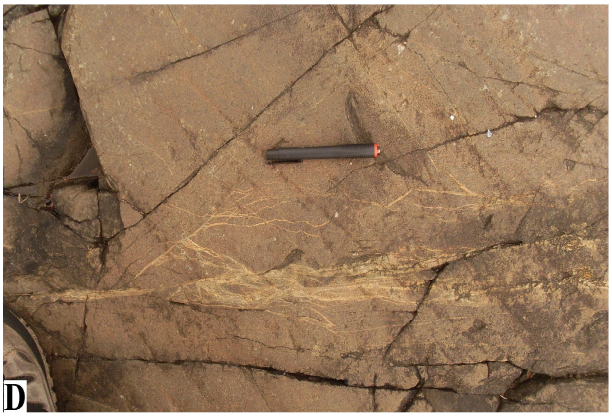

Fig. 8. A: Metadolerite cutting the gneissic foliation (foliation-orientation indicated by pencil). B: Irregular plagioclase-rich inclusions in metadolerite. C: Foliation oblique to magmatic layering (blue = magmatic layering, hatched line = foliation). D: Green net-like epidote veins of varying size. E: faulted plagioclase-rich lens shows that late brittle deformation were associated with shear movements (eastern block up—western block down). F: Gneissic fragments within metadolerite dyke.

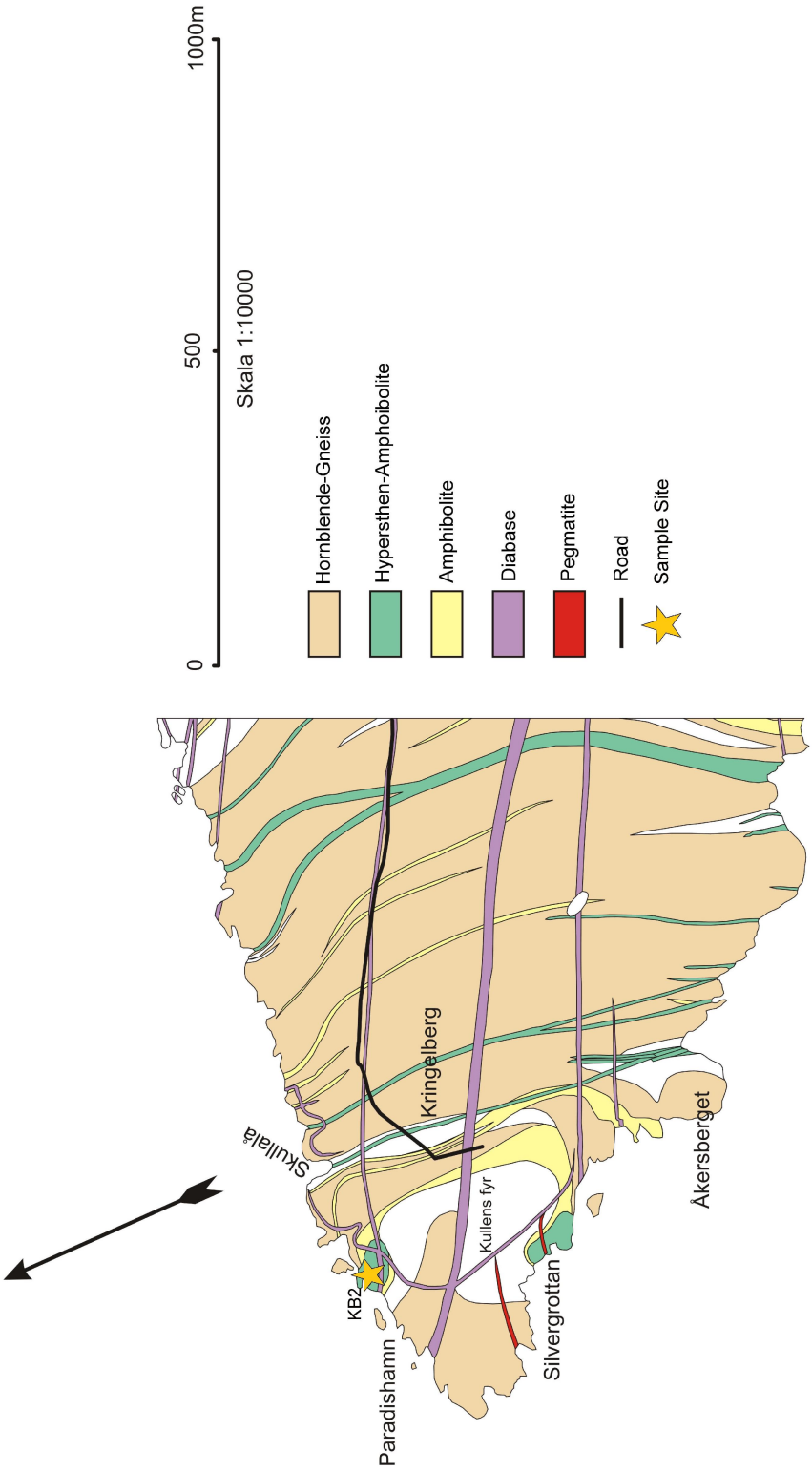

Fig. 9. Geological map of Kullaberg (SGU basemap, modified after Forsell 1962).

disrupted mafic lenses (Fig. 10C) can be found within the gneiss indicating mingling and possibly mixing during the intrusion (Söderlund et al. 2008). U-Pb dating of zircon in the granitic mobilisate has given an age of 961+/- 6 Ma which was interpreted as the age of the dolerite intrusion (Söderlund et al. 2008). The eastern contact between the dyke and the hornblende-gneiss is sharp with the metadolerite cross-cutting the gneissic foliation in the gneiss. The hornblende-gneiss is grey in colour, but gets reddish close to the dyke contact. Central parts of meta-dolerite are homogenous and shows neither primary magmatic structures nor migmatization, but an E-W trending (Sveconorwegian) foliation.

Two younger ca 1m wide subhorizontal umetamorphosed diabase dykes cut the metadolerite dyke in E-W and NE-SW directions. These dykes are parallel to the fractures created by the horst-graben system and have been dated at ca. 280 Ma (Klingspor 1976).´

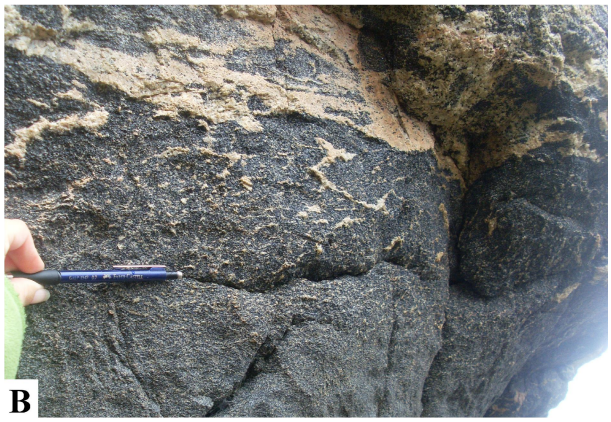

Fig. 10. A: Strongly migmatized metadolerite at the contact to overlying biotite-gneiss.. B: Migmatitic metadolerite with a gradual transition into unmigmatized metadolerite. C: Roundish mafic lenses within the gneiss.

5 Petrography and mineral chemistry

5.1 Varberg

5.1.1 AV1 - Apelviken (N6330104, E0333328)

The Apelviken metadolerite is fine-grained, black and homogenous. The thin-section shows a granoblastic texture (Fig.11). It is dominated by hornblende, plagioclase, clinopyroxene, biotite, cummingtonite (?) and scapolite. Primary clinopyroxene is larger in size and show abundant exsolution of orthopyroxene. Brownish Ti-rich hornblende is locally twinned and slightly oriented. Plagioclase shows twinning, undulatory extinction and is locally seritized. Colourless scapolite with low relief and spotted pinkish-orange interference colours of the 2nd order is found close to hornblende. A pale green – colourless pleochroistic mineral, which shows the same lath-like growth as hornblende and some intergrowth with it has blue to green interference colours of the 2nd order and is interpreted as – cummingtonite. Brown altered clots are interpreted as altered biotite due to local lath-like shapes.This sample has no garnet. No quantitative EDX analysis has been done on this sample.

5.1.2 GT1 – Getterön (N6334005, E0330010)

The metadolerite Getterön is fine-grained with a medium-coarse grained domainal texture in the form of lens-shaped, greenish mineral aggregates in a whitish matrix. The sample is dominated by clinopyroxene, plagioclase, hornblende, garnet, opaques, orthopyroxene, biotite, quartz and zircon. White domains are rich in plagioclase and dark domains are rich in clinopyroxene. One of the plagioclase-rich domains shows a typical plagioclase lath shape with a length of 1,8 (Fig.12A). Undulatory, partly seritized plagioclase and garnet compose this domain. The plagioclase also shows compositional zoning. Garnet grains appear locally corona-like as pearls on a string at the border to the clinopyroxene-rich domains; they host plagioclase inclusions. The average composition is $Grs_{19}Prp_{16}Alm_{62}Sps_{3}$. Grossular and almandine increase to the rim, whereas pyrope and spessartine decrease (Fig. 12B). Most plagioclase inclusions are seritized. Plagioclase inbetween the garnet-chain and the clinopyroxene-rich domains is twinned, antiperthitic and extincts undulatory. The composition of plagioclase is $Alb_{60}An_{38}Or_{2}$ with Alb_4Or_{96} K-Feldspar exsolution blebs. The An-content of plagioclase varies from An_{33} to An_{38} (Fig. 12E) Clinopyroxene-rich domains are made up of 2 x 3mm large mostly twinned diopside with inclusions of quartz, ilmenite and hematite (Fig. 12C). They also show exsolution lamellae of orthopyroxene (En_{47}) and replacement textures to ferro-pargasitic hornblende. These igneous pyroxene relics are diopside with average Fe/Fe+Mg = 0.36. The diopside grains are also surrounded by smaller orthopyroxene grains (En_{50}), opaques and small polygonal clinopyroxene neoblast aggregates with a composition of Fe/ Fe+Mg=0.37 (Fig. 12D). Orthopyroxene grains have a distinct pleochroism from green to light red, and show partial replacement to ferro-pargasitic hornblende and biotite (Ann_{51}) along the fractures. Ilmenite and hematite are often associated and partly rimmed by orthopyroxene.

5.1.3 TL1 – Träslövsläge (N6327477, E0334758)

The Träslövsläge metadolertite is fine-grained with a medium-coarse grained domainal texture in the form of lens-shaped, greenish mineral aggregates distributed in a whitish matrix. The thin section shows a fine-grained texture, dominated by clinopyroxene, plagioclase, hornblende, garnet, opaques, orthopyroxene, biotite, quartz, rutile and pyrite. White domains are rich in plagioclase and dark domains are

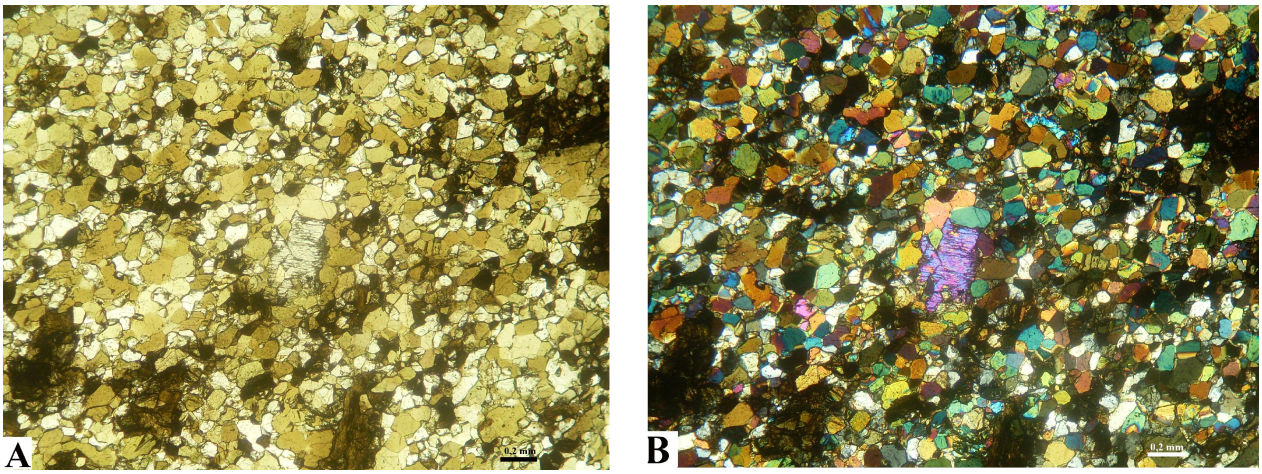

Fig. 11. A: Photomicrograph (PPL), fine-grained granoblastic texture. Large relict igneous have exsolution textures. *B:* Photomicrograph (XPL), of Fig. 11A.

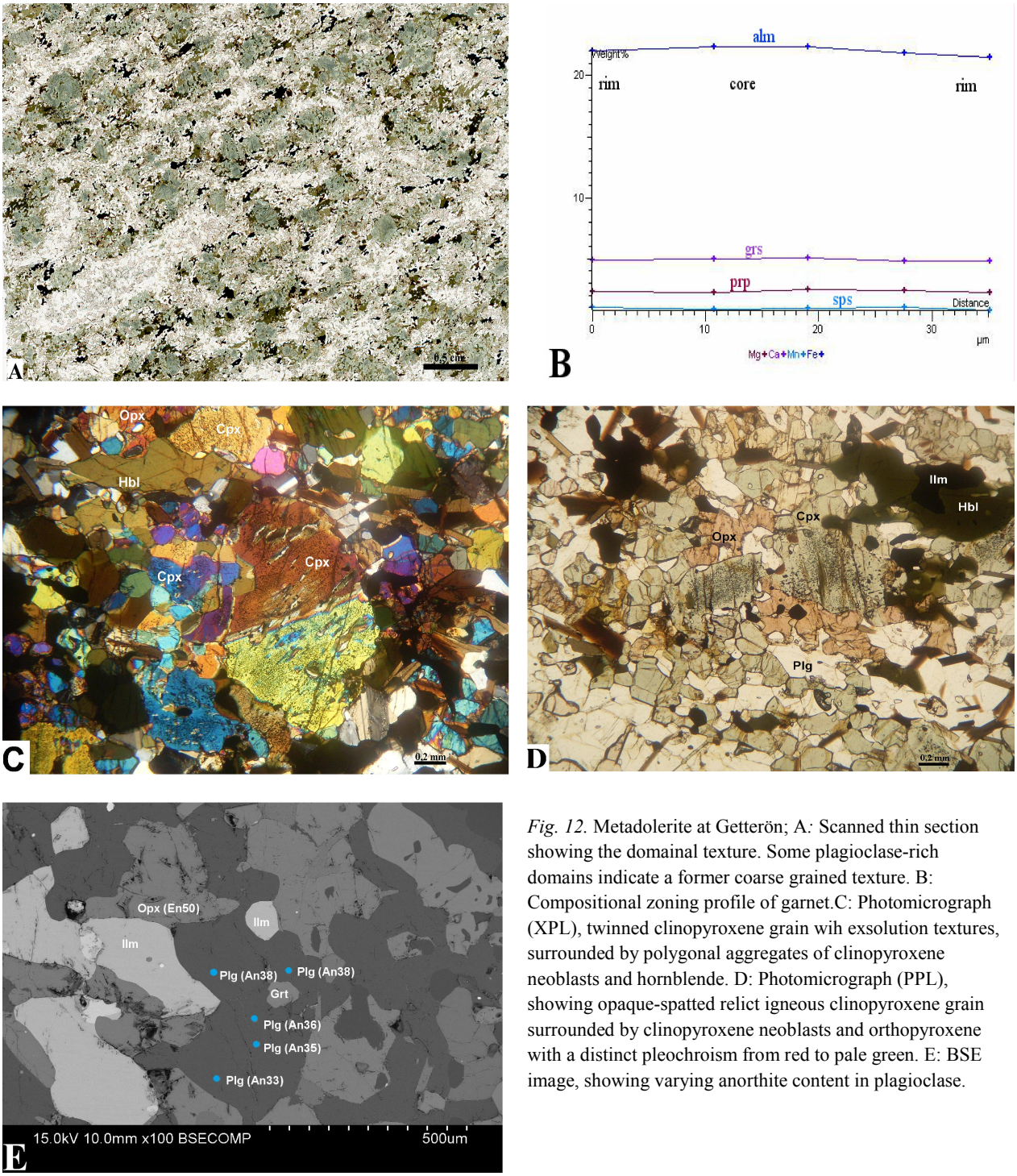

Fig. 12. Metadolerite at Getterön; A*:* Scanned thin section showing the domainal texture. Some plagioclase-rich domains indicate a former coarse grained texture. B: Compositional zoning profile of garnet.C: Photomicrograph (XPL), twinned clinopyroxene grain wih exsolution textures, surrounded by polygonal aggregates of clinopyroxene neoblasts and hornblende. D: Photomicrograph (PPL), showing opaque-spatted relict igneous clinopyroxene grain surrounded by clinopyroxene neoblasts and orthopyroxene with a distinct pleochroism from red to pale green. E: BSE image, showing varying anorthite content in plagioclase.

rich in clinopyroxene. The plagioclase-rich domain is composed of antiperthitic plagioclase, garnet and small clinopyroxene grains. Plagioclase extincts undulatory and has tapering twins. Garnet grains are mainly at the border of the plagioclase-rich to the clinopyroxene-rich domain (Fig. 13). They have inclusions of plagioclase and rutile.

The clinopyroxene-rich domains are made up of large twinned primary clinopyroxene grains rimmed by orthopyroxene (and locally together with garnet) and surrounded by opaques and polygonal clinopyroxene neoblasts. Relict igneous clinopyroxene shows a pronounced exsolution texture with lamellae in different orientations. Some of these textures are related to hornblende replacement and some are exsolved orthopyroxene. Typical is also small opaque inclusions. These clinopyroxene crystals are often surrounded by smaller orthopyroxene grains with biotite replacements. The pleochroism of orthopyroxene is generally strong from greenish to reddish. Opaque phases are often found close to orthopyroxenes. Biotite and hornblende form within the fractures of the orthopyroxene. No quantitative EDX analysis has been done on this sample.

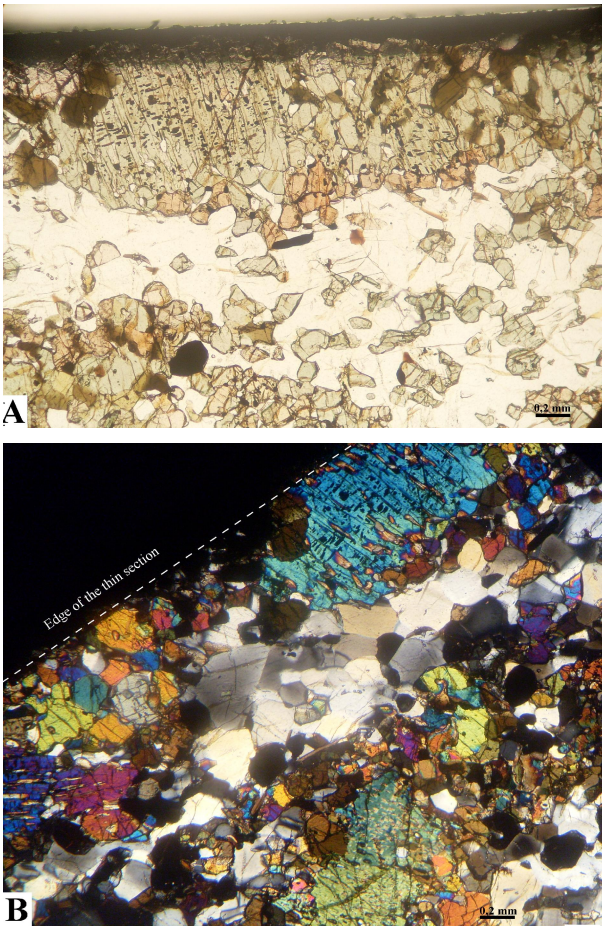

Fig. 13. Metadolerite Träslövsläge; A: Photomicrograph (PPL), showing twinned, exsolved clinopyroxene surrounded by clinopyroxene neoblasts and orthopyroxene. There are domains rich in polygonal plagioclase aggregates. B: Photomicrograph (XPL), of the same area like A.

5.2 Stensjöstrand

5.2.1 StSD – Stensjö Harbour (N6297034, E0354076)

The metadolerite at Steninge harbour is fine-grained and blackish. The thin section shows a granoblastic texture dominated by clinopyroxene, garnet, plagioclase, biotite, ilmenite, hematite, scapolite, hornblende, orthopyroxene, quartz and pyrite (Fig. 14 A,B). There are also accessory zircons. Large diopside grains have inclusions of hematite, V-bearing ilmenite, plagioclase ($Ab_{56}An_{42}Or_2$) and quartz, and show rare exsolution of orthopyroxene (Fig. 14C). Some diopside grains (Fe/Fe+Mg =0.28) show sector zoning outlined by opaque inclusions in form of an hour-glass. Biotite (Phl_{64}) is mainly anhedral and occurs inbetween clinopyroxene and/or orthopyroxene grains. Plagioclase shows undulatory extinction, is antiperthitic and forms polygonal aggregates. It has an average composition of An_{46}. Garnet has quartz and plagioclase ($Ab_{57}An_{43}$) inclusions and is on average $Grs_{19}Prp_{22}Alm_{54}Sps_5$ in the core. Grossular and pyrope decrease slightly and almandine increase towards the rim (Fig. 14E). Orthopyroxene is Mg-rich (En_{60}) and are often associated with ilmenite and hematite. Some opaque phases have a blue reflectance colour (Fig. 14D). They are interpreted as CuS.

5.2.2 Gas3A – Gåsanabbe (N6297542, E0353692)

The metadolerite at Gåsanabbe is fine-grained and granoblastic. It is dominated by hornblende, plagioclase, clinopyroxene, ilmenite biotite, orthopyroxene, hematite, garnet quartz and apatite. The rock doesn't show an obvious domainal, but there are small areas rich in plagioclase and areas rich in clinopyroxenes, hornblende and opaques. Plagioclase is twinned, occurs in polygonal aggregates and is locally antiperthitic. It has undulatory extinction. Sometimes there are very fine bent fractures.

Large clinopyroxene crystals show opaque inclusions of ilmenite and hematite. They also have exsolution lamellae of orthopyroxene and replacement to mainly pargasitic hornblende. If the blast is not surrounded by hornblende it often has Mg-rich orthopyroxene (En_{58}) and clinopyroxene neoblasts next to it. Those neoblasts have different compositions. Neoblasts with inclusions of ilmenite have a composition of Fe/Fe+Mg=0.27 and neoblasts without inclusions and less Ca have a composition of Fe/Fe+Mg=0.34. At one spot the interfence colours of relict igneous diopside shows sector zoning in the form of an hour-glass (Fig. 14F). The location of opaque inclusions outlines this texture as well. From 0.38 in the core to 0.28 at the rim. The opaque inclusion are Cr-bearing ilmenite. Garnet has an average composition of $Grs_{19}Prp_{21}Alm_{55}Sps_5$ in the core with decreasing grossular and increasing almandine towards the rim ($Grs_{18}Prp_{21}Alm_{57}Sps_5$). They also have inclusions of quartz and plagioclase.

Fe-sulphide locally show a net-like texture enclosing orthopyroxene and/or plagioclase (Fig. 14G). They can also have rim-like textures made of quartz and orthopyroxenes. Biotite ($Phl_{57}Ann_{43}$) can be often found along the cleavage of. Garnet grains in this microdomain are poorer in Mg and richer in Fe ($Grs_{18}Prp_{17}Alm_{60}Sps_5$).

5.2.3 Gas3B – Gåsanabbe (N6297542, E0353692)

The metadolerite Gåsanabbe is a fine-grained, granoblastic and dominated by clinopyroxene, plagioclase, hornblende, orthopyroxene, garnet, ilmenite, biotite, quartz, apatite and pyrite. There is a faint domainal texture with domains rich in plagioclase and others rich in pyroxenes, hornblende and ilmenite. The pyroxene-rich domain is made up of large relict igneous diopside grains (Fe/Fe+Mg=0.30) with opaque inclusions, exsolution lamellae of orthopyroxene and replacement textures to pargasitic hornblende. Locally, the diopside lacks Na. The diopside grains are

surrounded by orthopyroxene (En_{59}) and clinopyroxene neoblasts with the same composition as diopside. Apatite can be found close to the large diopside grains.

Garnet has an average composition of $Alm_{54}Prp_{22}Grs_{20}Sp_4$ within the core. Almandine increases towards the rim whereas pyrope and grossular decrease (changes < 0,3wt%) . Ilmenite can show a net-like texture enclosing orthopyroxene and/ or plagioclase. Plagioclase is antiperthitic and commonly with undulatory extinction. The average composition is $Alb_{62}An_{35}Or_3$ in the core and $Ab_{58}An_{40}Or_2$ at the rim. Plagioclase without antiperthite textures have an average composition of $Ab_{63}An_{37}$. It is locally Ba-bearing. Sometimes plagioclase grains have very fine bent fractures. Biotite is rich in Mg (Phl_{56}, which changes to an average of Phl_{58} for biotites in contact with garnet).

5.2.4 StHD1 – Gåsanabbe (N6297550, E0353700)

The metadolerite is fine-grained and shows no oritental fabric. It is dominated by greenish hornblende, biotite, garnet, opaques, clinopyroxene and scapolite. Hornblende has abundant inclusions of plagioclase, biotite and opaques. Garnet and clinopyroxene have plagioclase inclusions; plagioclase shows antiperthite texture, twinning and has quartz inclusions. Opaque phases often form a net-like textures enclosing plagioclase and hornblende (Fig. 15A). No quantitative EDX analysis has been done on this sample.

5.2.5 Sample StHD2 – Gåsanabbe (N6297550, E0353699)

The metadolerite is fine-grained and shows no orientated fabric (Fig. 15B). It is dominated by greenish hornblende, biotite, garnet, opaques and scapolite. It is very similar to StHD1, but it has more and smaller sized opaque grains randomly distributed. Plagioclase has more quartz inclusions. No clinopyroxene was found in this sample, however the amount of scapolite is higher. No quantitative EDX analysis has been done on this sample.

5.2.6 StML1 – Gåsanabbe (N6297564, E0353709)

The mafic layer is fine-grained and foliated. Leucosomes have a sugary texture. The sample is dominated by pargasitic hornblende, clinopyroxene, scapolite, garnet, hematite, ilmenite, plagioclase, quartz, pyrite and monazite. The foliation defined by light plagioclase-rich aggregates in a matrix of clinopyroxene, scapolite, plagioclase and hornblende. Lens-shaped scapolite aggregates are oriented parallel to the foliation (Fig. 16A, B). Scapolite is of Mei_{75} and have inclusions of quartz and hematite. Garnet has an average composition of $Grs_{23}Prp_{17}Alm_{52}Sps_8$. Hematite and ilmentite show exsolution textures. Plagioclase has a composition of $Ab_{59}An_{29}Or_2$ within cores and $Ab_{58}An_{35}Or_2$ at the rim.

5.2.7 StML2 – Gåsanabbe (N6297560 E353710)

The mafic layer is coarser grained, richer in felsic minerals than StML1 and resembles an intermediate part of the layered sequence. It has an isotropic fabric, dominated by plagioclase, greenish hornblende, biotite, garnet, opaques, K-feldspar, quartz, titanite and chlorite. There are plagioclase- and quartz-rich domains. Plagioclase shows antiperthite textures, tapering twins and undulous extinction (Fig. 16C). Sometimes the antiperthite textures show bending (Fig. 16D). Antiperthite textures and tapering twins are often found randomly oriented within the same grain. Plagioclase is locally seritized. Yellowish polygonal quartz can be found within some plagioclase grains.

Biotite is often affected by chloritization. Garnet grains are small and poikilitic. They have inclusions of plagioclase, biotite and quartz. No quantitative EDX analysis has been done on this sample.

5.2.8 StML3 – Gåsanabbe (N6297560, E353710)

This sample is the most mafic type of the mafic-intermediate layers in the folded sequence. It is coarser -grained than StML1 and shows a weak foliation defined by hornblende. The thin section is dominated by greenish hornblende, plagioclase, biotite, garnet, opaques, K-feldspar, quartz, titanite, rutile and chlorite. There are domains rich in plagioclase and quartz and domains rich in hornblende. Plagioclase extincts undulatory, shows tapering twins and has sometimes slightly bent fractures. Plagioclase is locally seritized. Quartz appears as polygonal within the plagioclase-rich domains (Fig. 16E). Garnets are small and have inclusions of plagioclase and rutile. No quantitative EDX analysis has been done on this sample.

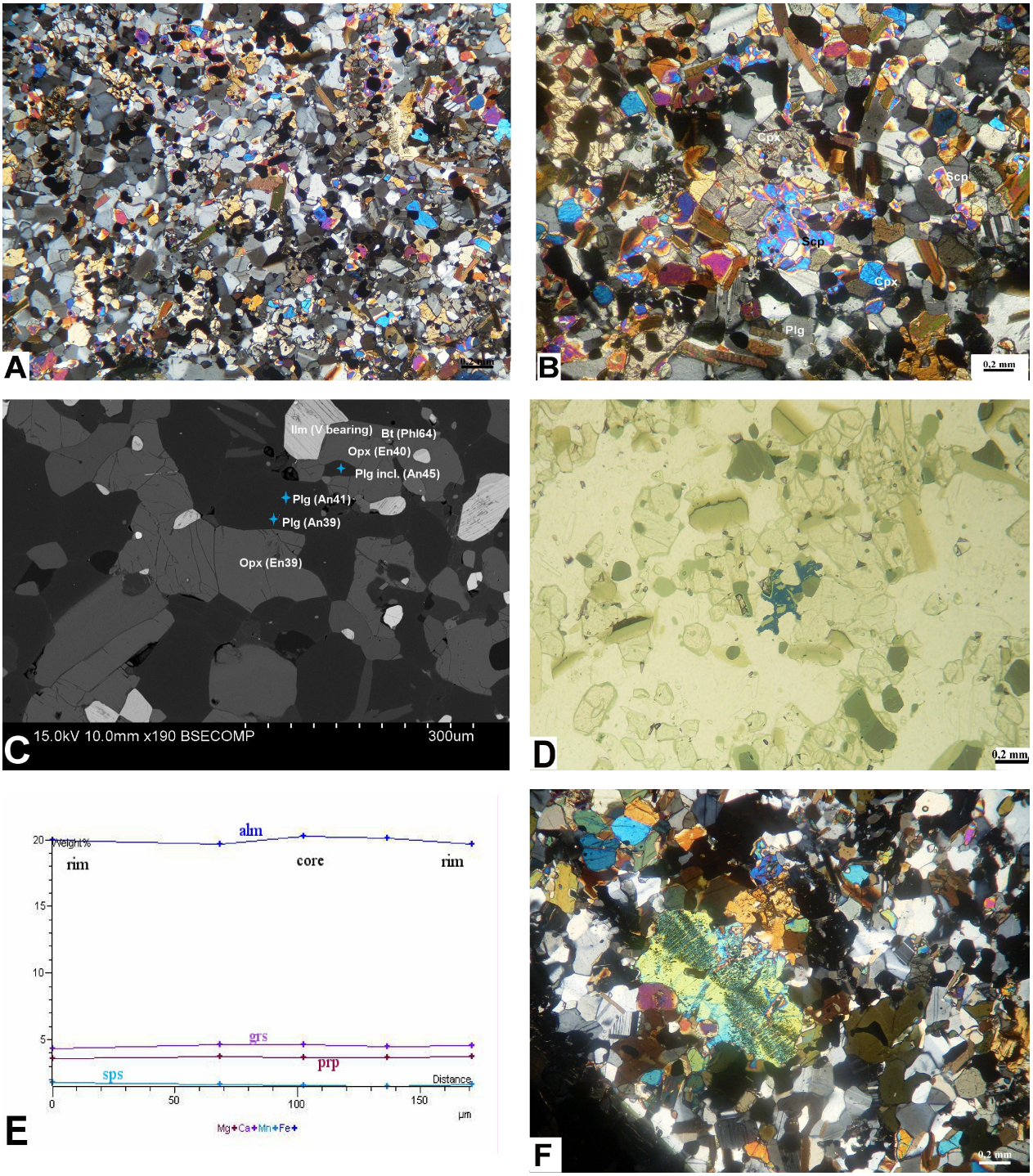

Fig. 14. Metadolerite at Stensjöstrand; A: Photomicrograph (XPL), showing granoblastic texture of metadolerite at Stensjö harbour. B: Photomicrograph (XPL), illustrating relict igneous clinopyroxene surrounded by scapolite. C: BSE image, shwoing varying anorthite content. Opaque phases are exsolved hematite-ilmenite, partly V-bearing. D: Photomicrograph (reflected light), shwoing that some opaque phases have a blue reflectance colour. They are interpreted as CuS. E: Compositional zoning profile of garnet. F: Photomicrograph (XPL) of metadolerite at Gåsanabbe (Gås3A), showing sector zoned relict igneous clinopyroxene. G: BSE-image, illustrating hematite-ilmenite and Fe-sulphides enclosing plagioclase.

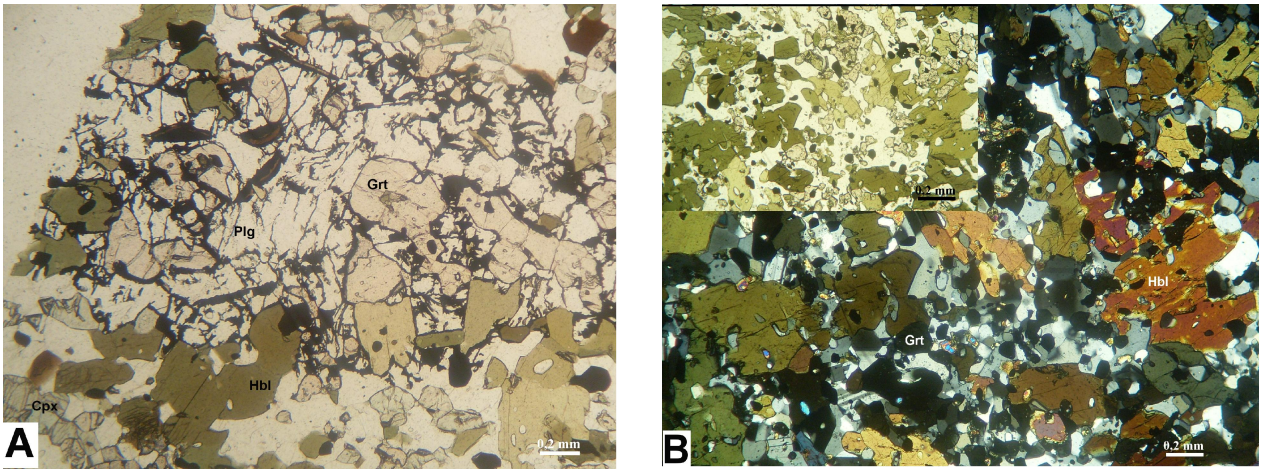

Fig. 15. Metadolerite at Gåsanabbe; A: Photomicrograph (PPL), showing opaque phases forming net-like textures, enclosing plagioclase and hornblende (and locally orthopyroxene). B: Photomicrograph (XPL), illustrating hornblende dominated texture with small opaque grains. Hornblende has plagioclase and quartz inclusions. Plagioclase shows strong undulatory extinction.

5.3 Söndrum

5.3.1 SöM1 (N6280273, E0362838)

The metadolerite at Söndrum is black in colour and has slighly coaser black minerals within a dark matrix. The thin section shows a fine-grained granoblastic texture, dominated by clinopyroxene, garnet, plagioclase, hornblende, biotite, orthopyroxene, ilmenite, hematite, quartz, K-feldspar, pyrite, rutile and chalcopyrite. There is a domainal texture with domains rich in plagioclase and others rich in pyroxenes and opaque phases. Twinned primary diopside grains (Fe/Fe+Mg = 0,31) within the clinopyroxene-rich domain have exsolution lamellae of orthopyroxene (En_{56}) and Fe-oxides (Fig. 17A, B, C, E). There are also inclusions of quartz and rutile. Diopside grains are surrounded by Ti-bearing pargasitic hornblende and smaller clinopyroxene neoblasts, arranged in polygonal aggregates. The clinopyroxene neoblasts are slightly poorer in Fe (Fe/Fe+Mg = 0,35) and Ca than the primary clinopyroxenes and lack a Na-component. Garnet grains are often poikilitic, with inclusions of quartz, plagioclase and sometimes rutile. Garnet has an average composition of $Alm_{58}Prp_{21}Grs_{18}Sps_{2.}$ Pyrope and spessartine decrease to the rim, whereas almandine and grossular increase, but the changes minimal (< 0,2 wt. %). Ilmenite and Fe-oxides, locally associated with chalcopyrite, are often surrounded by orthopyroxene (En_{56}). Orthopyroxene shows replacement to pargasitic hornblende and Ti-rich biotite (Phl_{56}) along rims and cleavage planes (Fig. 17D). Plagioclase is antiperthitic and has an average composition of $An_{37.}$ Plagioclase close to garnet and orthopyroxene have a composition of An_{42} in the core (Fig. 17F). Plagioclase-rich domains are strongly seritized.

5.3.2 SöPD1 (N6280252, E0362843)

The sample of the lens-shaped inclusion shows a irregular layer-like texture, with black and white layers. The thin-section shows fine-grained clinopyroxene, garnet, opaque phases, plagioclase, hornblende and quartz. There is a strong elongation of plagioclase-rich and dark domains consisting of opaque phases, garnet and clinopyroxene. Garnets and opaque phases form lens-shaped aggregates (Fig. 18A). Clinopyroxenes is locally made up of polygonal aggregates (Fig. 18B). Plagioclase grains show a strong seritization. No quantitative EDX analysis has been done on this sample.

5.3.3 SöKG (N6280228, E0362857)

This sample is from a boulder which shows the contact of the metadolerite to the surrounding gneiss. The gneiss is reddish and oxidized. Quartz ribbons and domains rich in opaque phases, clinopyroxene, hornblende and rutile define the foliation (Fig. 18C). There are also domains rich in chlorite. The contact to the metadolerite is defined by a greenish fracture which is mainly filled with epidote (Fig. 18D). The metadolerite is dominated by hornblende, epidote, chlorite, plagioclase, quartz and K-feldspar. There is a orientation of hornblende, which is parallel to the gneissic foliation. Another 8mm thick fracture within the metadolerite part shows roundish and angular fragments of the gneiss and metadolerite in a very fine -grained dark matrix (Fig. 18E). Abundant fine green epidote veins cross the metadolerite randomly. No quantitative EDX analysis has been done on this sample.

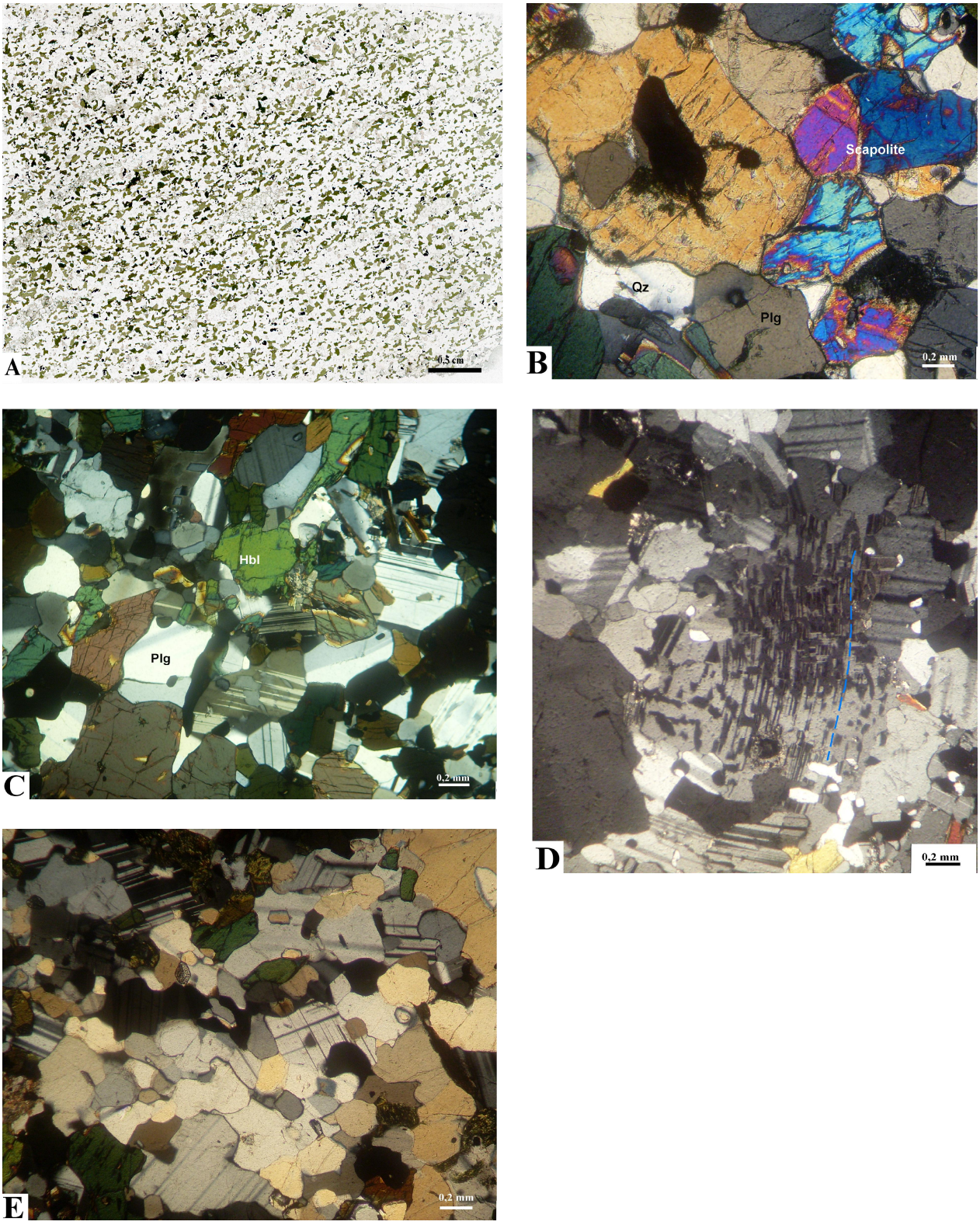

Fig. 16. Mafic layers at Gåsanabbe; A: Scanned thin section demonstrating colourless lens-shaped scapolite agregates within a foliated rock dominated by hornblende. B: Photomicrograph (XPL), showing scapolite of the lens-shaped aggregates from Fig. 16A. C: Photomicrograph (XPL), showing tapering plagioclase twins together with antiperthite textures within the same grain. D: Photomicrograph (XPL), illustrating plagioclase with antiperthite textures in different shapes and orientation.The lamellae are slightly bent, indicated by the blue hatched line. E: Photomicrograph (XPL) of polygonal quartz within plagioclase. Some grains have a dihedral angle of 120°.

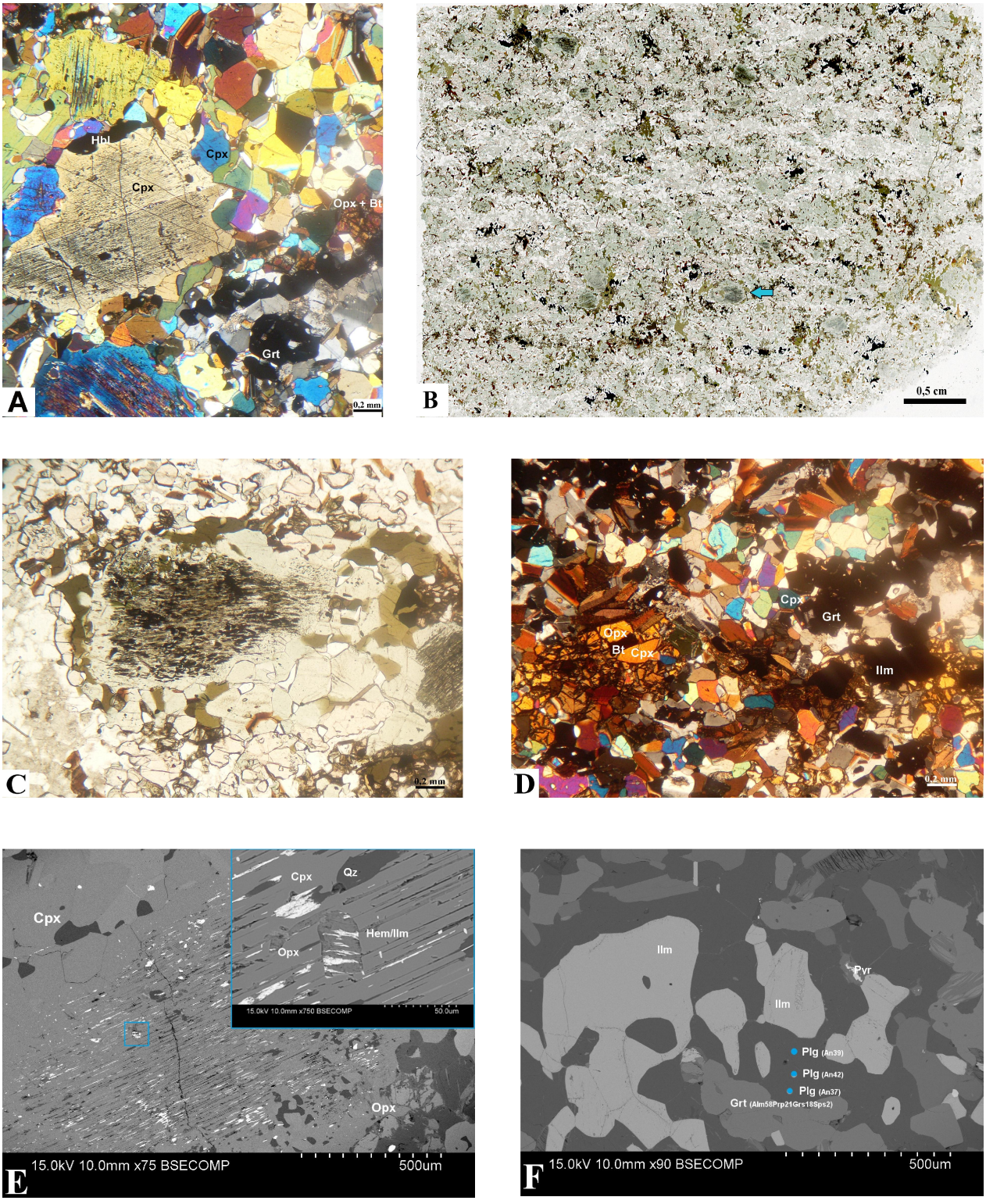

Fig. 17. Metadolerite at Söndrum; A: Photomicrograph (XPL), twinned relict igneous diopside grain with orthopyroxene exsolution lamellae and surrounded by clinopyroxene neoblasts and hornblende. B: Scanned thin section showing the domainal texture with plagioclase-rich domains and domains rich in pyroxenes, hornblende and opaque phases. Large primary slinopyroxene grains can be seen in the lower half of the picture (arrow), recognizable at its pale green colour and the exsolution texture together with many opaque inclusions. C: Photomicrograph (PPL), diopside with exsolution texture, opaque inclusions and replacement textures to hornblende. D: Photomicrograph (XPL), orthopyroxene replaced by biotite and hornblende along the fractures. Ilmenite grains are often surrounded by orthopyroxene. E: BSE-image, exsolution texture of relict igneous clinopyroxene with quartz and hematite-ilmenite exsolved inclusions. F: BSE-image, varying an-content between ilmenite and garnet.

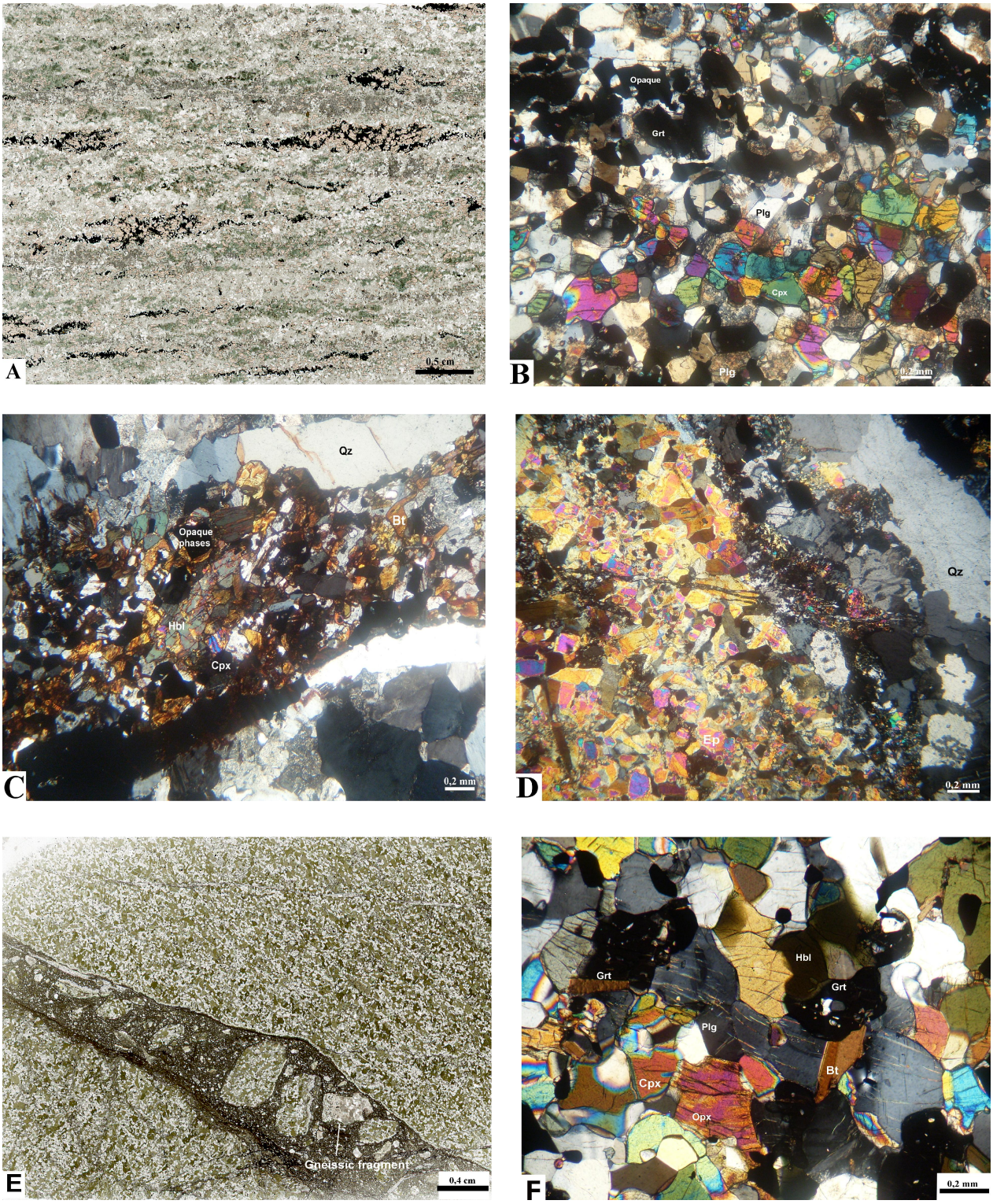

Fig. 18. Plagioclase-rich lens at Söndrum; A: Scanned thin section, showing pronounced deformation fabric with elongated aggregates of clinopyroxene, garnet, plagioclase and opaques. B: Photomicrograph (XPL), polygonal clinopyroxene aggregates within plagioclase-rich domain. C: Photomicrograph (XPL), gneissic part of the rock showing elongated aggregates of opaque phases, hornblende, biotite and clinopyroxene. D: Contact between gneiss and metadolerite at Söndrum; photomicrograph (XPL), fracture between gneiss and metadolerite, filled with epidote. E: Scanned thin-section, roundish and angular fragments of the gneiss and metadolerite in a very fine-grained dark matrix. F: Metadolerite at Söndrum harbour; photomicrograph (XPL), slightly bent fractures in plagioclase.

5.3.4 SöHf1 – Söndrum Harbour (N6279827, E0363564)

The metadolerite at Söndrum harbour is coarser grained than the sample SöM1. It has slightly coarser black minerals within a dark matrix. The thin section shows a granoblastic texture, dominated by hornblende, clinopyroxene, garnet, plagioclase, quartz, orthopyroxene, opaques, biotite and rutile. There is a domainal texture with domains rich in hornblende and others rich in garnets, clinopyroxene and plagioclase. Large clinopyroxene grains show exsolution of orthopyroxene and have inclusions of opaque phases. Orthopyroxene shows replacement to hornblende along fractures. Garnet is poikilitic, with inclusions of plagioclase, quartz, pyroxenes, biotite and rutile. antiperthitic, has tapering twins and is often affected by seritization. All minerals show slightly bent fractures, but most often plagioclase (Fig. 18F). No quantitative EDX analysis has been done on this sample.

5.4 Kullaberg

5.4.1 KB2 – Kullaberg (N6242741, E0342236)

The metadolerite at Kullaberg is fine-grained and and has slightly coarser black minerals evenly spread in a whitish matrix. The thin section shows a texture dominated by clinopyroxene, garnet, plagioclase, pargasitic hornblende, ilmenite, orthopyroxene, quartz, pyrite and rutile. There is a domainal texture with domains rich in plagioclase and others rich in pyroxenes, hornblende and ilmenite (Fig. 19A). Large primary, greenish diopside grains ($Jd_3Di_{88}En_9$) within the pyroxene-rich domain have inclusions of ilmenite, quartz, plagioclase, Fe-sulfides, and exsolution lamellae of orthopyroxene (En_{58}). Clinopyroxene shows a partial replacement to pargasitic hornblende along the rim of the grain, as well as within exsolution lamellae. Polygonal aggregates of clinopyroxene neoblasts around the large diopside have the same

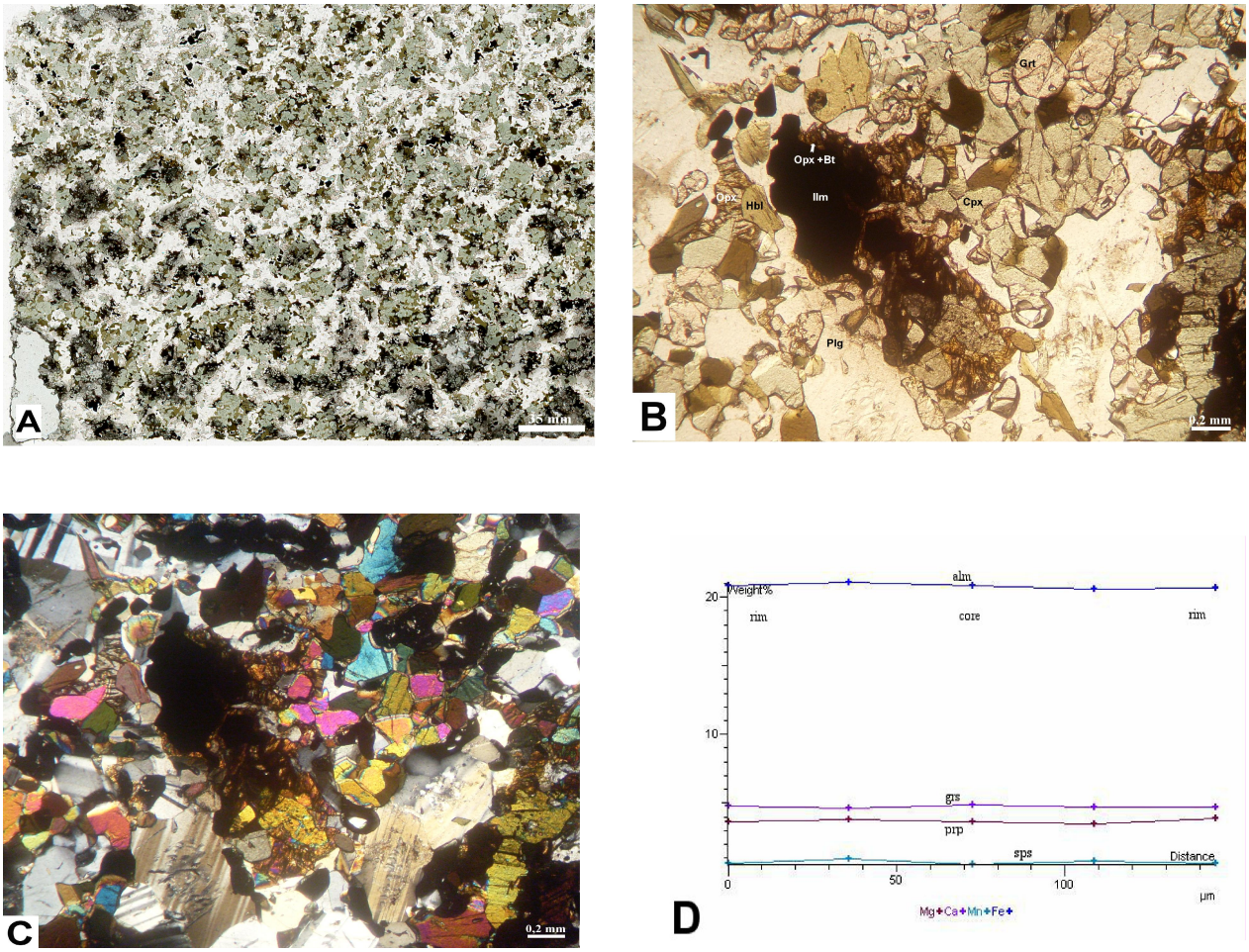

Fig. 19. Metadolerite at Kullaberg; A:Scanned thin section showing the domainal texture of plagioclase-rich domains and domains rich in pyroxene, hornblende and ilmenite. The sample is unfoliated. B: Photomicrograph (PPL), ilmenite surrounded by orthopyroxene. Orthopyroxene is partly replaced by biotite. C: Photomicrograph (XPL), same view as B, plagioclase on the right side shows undulatory extinction and seritization. Plagioclase on the left side shows tapering twins and antiperthitic textures. D: Zonation profile of garnet.

average composition as the diopside. The grains lack exsolution textures and inclusions.

Ilmenite grains are often surrounded by orthopyroxene (Fig. 19B, C). Those orthopyroxenes are Mg-richer (En_{71}) than the ones not in contact with ilmenite (En_{58}). They show partial replacement by pargasitic hornblende and Mg-rich biotite (Phl_{54}) along fractures and cleavage planes.

Garnet has an average composition of $Alm_{57}Prp_{22}Grs_{18}Sp_3$. Grossular and spessartine decrease slightly towards the rim whereas pyrope increases (Fig. 19D).

Plagioclase shows antiperthite textures, tapering twins and compositional zoning. The average composition at the rim is $An_{39;}$ within the core An_{44}. Plagioclase inclusions within diopside have a higher anorthite content and an orthoclase component is present. The average composition is $Ab_{51}An_{47}Or_2$.

6 Geochemical Data

Two groups are identified: the metadolerites (group 1) and the mafic layers at Stensjö (group 2).

6.1 Group 1 (samples: GT1, TL1, AV1, Gas3A, Gas3B, StSD, SöM, SöHf, KB2)

All metadolerites have silica contents characteristic for basic rocks (Table 2), between 47 % (TL1) and 48 % (AV1). In general the FeO-content varies in these samples between 14 % (SöHf1, 13% in GT1) and 7 % (AV1). Sample SöHf1 has the highest TiO_2 content (3 %) and sample AV1 the lowest (1 %). Sample GT1 has also a high TiO_2 content (3 %) compared to the other samples, which fall between 1-2 %. The sample SöHf has the lowest MgO content (5 %) and AV1 the highest (12 %). All other samples vary between 6-7 %. Sample AV1 also has a very high Cr_2O_3 (2150 ppm) and Ni (147 ppm) content compared to the others with 70-340 ppm Cr_2O_3 and 21-94 ppm Ni. Sample SöHf1 (51 ppm), SöM (39 ppm) and GT1 (32 ppm) are rich in Rb compared to the others which range between 12-16 ppm. All samples from Stensjö have more Sr (530-580 ppm) compared to the others with 168-219 ppm. Sample KB2 is with 94 ppm very poor in Ba. The Stensjö samples are rich in Ba and range between 663 and 713 ppm with a maximum of 818 ppm in sample StSD1. All others range between 161 and 279 ppm.

There is also a minor variation of Mg#. The lowest Mg# (0.34) is formed in sample SöPD and SöHf wih 0.37. The highest Mg# has AV1 with 0.74.

6.1 Group 2 (samples: StML 1-3)

The mafic layers from Stensjö are richer in SiO_2 (51 % and 55 %) than in the mafic dykes. StML3 has the highest FeO content with 7 % and StML1 the lowest with 5 %. The TiO_2 content is homogenous and varies between 1-1,1 %. StML3 has also the highest MgO content with 6 % and StML1 the lowest with 3 %. StML2 is with 1,5 % slightly richer in K_2O compared to the others which range between 0,9 and 1 %. StML3 is richer in Cr_2O_3 (´140 ppm) and Ni (42 ppm) compared to the others, which have 20 ppm Cr_2O_3 and <20 ppm Ni. StML2 is richer in Rb (60 ppm) compared to the other samples with 14 and 15 ppm. The Ba content varies a lot among the three samples. The sample ML3 has the highest Mg# number with 0.61. The other samples have 0.52 and 0.49.

6.3 Group 1+2

In the TAS diagram (Cox et al. 1979) (Fig. 20), the samples fall within the gabbro field and on the tholeitic side, except for sample SöPD1, which is on the alkaline side. All dyke-samples are within the basic field. Sample StML2 is on the line between basic and intermediate and sample StML1 is within the intermediate field. In the R_1-R_2 diagram by DeLaRoche (1980) all samples fall into the gabbro field except StML1-3 and SöHf1 which are in gabbro-diorite field, SöPD in the monzo-gabbro field and KB2 which lies on the line between gabbro and gabbro-norite (Fig. 20).

The AFM diagram (Irvine & Baragar, 1971) show that the samples from Stensjö as well as the sample GT1 have a tendence to be more calc-alkaline and the rest of tholeiitic(Fig. 20). In the SiO_2-FeO[tot]/MgO diagram of Miyashiro (1974, not shown) only StML1, STML3 and GT1 plot in the calc-alkaline field. The SiO_2-K_2O diagram of Peccerillo and Taylor (Peccerillo and Taylor, 1976, not shown) puts all the samples within the calc-alkaline field, except SöM which plots in the high-K calc-alkaline field. In a Na_2O-K_2O-Al_2O_3 discrimination diagram, all the samples fall into the metaluminous field (Fig. 20).

All samples from Stensjö (dyke samples and mafic layer samples) show a positive Ba-anomaly in the spider plot normalized to the primordial mantle (Fig. 21, Wood et al. 1979). The samples KB2 and SöHf have a small negative Ba-anomaly. All samples except for SöHf show a positive K-anomaly. All samples have negative Ta and Nb-anomalies but the sample AV1 the strongest concerning the Ta-anomaly. All dyke-samples except for the samples from Stensjö show negative Sr-anomalies. All three mafic layer samples from Stensjö show positive Sr-anomalies. Sample KB2, TL1 and GT1 show also weak P-anomalies. All samples show negative Hf and Ti anomalies. An enrichment in LIL elements and no depletion of HFS elements can be seen. Sample SöPD has the highest enrichment in LIL elements.

The chondrite-normalized spider plot (Boynton, 1984) shows subparallel curves, except for sample StML2, which cut the other samples with a steeper curve (Fig. 21). In general the slopes for LREEs vary between 1,8-2,4 and between 3-6 for HREEs. Sample StML2 has with 3,6 a slightly higher ratio in $(La/Sm)_N$

In wt %	STSD1	STHD1	STHD2	GAS3B	GAS3	KB2	AV1	TL1	GT1	SöHf1	SöM1	SöPD1	STML1	STML2	STML3
SiO_2	47,48	47,12	47,46	46,95	47,34	48,47	48,12	46,56	47,41	47,63	48,45	49,35	54,61	52,12	51,30
TiO_2	2,24	2,22	2,18	2,30	2,39	1,77	0,96	1,89	2,88	3,17	1,83	2,17	0,96	1,08	1,06
Al_2O_3	14,63	14,94	14,87	14,80	14,54	14,43	12,11	15,97	12,22	12,49	14,37	18,93	17,39	18,45	15,39
$[Fe2O3]_{tot}$	14,73	14,47	14,51	14,69	15,00	12,82	10,40	14,74	17,13	18,94	14,10	12,23	9,15	10,98	11,59
Fe_2O_3	6,36	5,21	5,37	5,22	5,58	3,41	3,12	4,88	4,09	4,74	3,64	3,33	4,24	4,61	4,49
FeO	8,37	9,26	9,14	9,47	9,42	9,41	7,28	9,86	13,04	14,20	10,46	8,90	4,91	6,37	7,10
MgO	6,52	6,54	6,80	6,72	6,18	7,10	11,57	7,18	6,84	4,63	6,80	2,63	2,97	3,48	6,23
CaO	9,45	9,71	9,40	9,56	9,51	11,11	10,39	9,44	9,42	8,70	9,79	7,68	8,94	7,64	8,91
Na_2O	2,49	2,51	2,32	2,78	2,66	2,33	2,85	2,59	2,19	2,32	2,32	3,53	3,02	3,06	2,81
K_2O	1,05	0,94	0,93	0,95	1,02	0,48	0,65	0,76	1,00	1,28	1,00	2,27	0,92	1,46	1,02
P_2O_5	0,40	0,39	0,38	0,37	0,40	0,17	0,11	0,23	0,36	0,38	0,21	0,29	0,46	0,49	0,36
MnO	0,23	0,23	0,24	0,23	0,23	0,19	0,15	0,20	0,24	0,25	0,21	0,15	0,16	0,19	0,22
Cr2O3 [ppm]	90,00	100,00	90,00	80,00	70,00	340,00	2150,00	190,00	280,00	30,00	190,00	20,00	20,00	20,00	140,00
Totals	99,66	99,67	99,66	99,67	99,65	99,79	99,84	99,78	99,75	99,72	99,75	99,7	99,36	99,61	99,59
LOI	0,40	0,60	0,60	0,30	0,40	0,90	2,30	0,20	0,00	-0,10	0,60	0,5	0,80	0,70	0,70
Mg#	0,58	0,56	0,57	0,56	0,54	0,57	0,74	0,56	0,48	0,37	0,54	0,34	0,52	0,49	0,61
In ppm															
Ba	818,00	681,00	663,00	697,00	713,00	94,00	177,00	161,00	247,00	279,00	261,00	683,00	1179,00	717,00	187,00
Be	1,00	1,00	1,00	1,00	1,00	2,00	2,00	1,00	1,00	2,00	1,00	1,00	1,00	1,00	1,00
Co	61,40	69,00	69,40	65,40	75,30	72,30	69,80	72,40	67,60	78,10	86,00	57,70	88,20	45,10	55,90
Cs	0,10	0,20	0,10	0,20	0,20	0,20	0,30	0,30	0,80	2,30	0,80	0,70	0,70	0,90	0,10
Ga	18,80	18,90	19,20	21,10	18,90	16,20	11,70	17,50	18,40	20,10	16,70	20,60	19,40	18,80	16,00
Hf	3,30	3,80	3,90	3,80	4,30	3,10	2,10	3,30	3,90	5,20	3,20	3,80	1,80	2,80	2,70
Nb	9,00	8,90	8,30	9,20	9,60	7,60	4,30	10,00	12,70	13,50	8,50	11,00	4,10	5,30	3,90
Rb	15,60	13,90	12,10	13,50	13,80	14,90	15,80	22,20	31,50	51,30	39,00	100,30	13,60	60,30	14,80
Sn	1,00	1,00	2,00	1,00	1,00	1,00	1,00	1,00	1,00	1,00	1,00	1,00	1,00	2,00	1,00
Sr	529,60	528,80	526,90	579,80	529,80	167,90	198,40	219,10	173,70	193,80	198,50	375,20	2781,20	1326,50	1628,80
Ta	0,60	0,50	0,60	0,60	0,60	0,40	0,20	0,80	0,80	0,90	0,70	0,80	0,30	0,30	0,30
Th	0,70	0,70	0,70	0,90	0,70	1,60	1,30	2,40	2,70	5,00	3,20	4,00	2,90	2,60	1,30
U	0,20	0,20	0,10	0,20	0,20	0,40	0,30	0,70	0,90	1,40	0,90	1,10	1,50	0,80	0,60
V	386,00	381,00	371,00	386,00	399,00	352,00	241,00	296,00	374,00	476,00	331,00	249,00	238,00	272,00	273,00
Zr	144,40	143,30	142,70	155,40	144,10	116,70	68,50	144,50	180,40	180,30	125,00	154,10	99,90	108,60	101,00
Mo	0,30	0,20	0,20	0,10	0,20	0,40	0,20	0,40	0,30	0,50	0,30	0,50	0,10	0,10	0,20
Cu	25,80	80,60	192,60	57,40	125,40	110,00	44,80	74,10	116,70	123,90	123,60	139,20	31,20	23,80	334,10
Pb	1,00	0,70	0,80	0,30	0,40	0,50	0,70	0,70	1,00	1,00	1,30	2,40	9,50	0,80	5,10
Zn	41,00	38,00	21,00	36,00	49,00	34,00	34,00	30,00	41,00	39,00	48,00	36,00	26,00	62,00	26,00
Ni	23,70	28,20	21,10	30,70	27,00	45,30	146,60	94,00	59,70	22,50	67,90	24,30	5,90	8,70	19,30
As	0,60	0,50	0,50	0,50	0,50	0,50	0,50	0,50	0,50	0,50	0,50	0,50	1,00	0,50	0,80
Cd	0,10	0,10	0,10	0,10	0,10	0,10	0,10	0,10	0,10	0,10	0,10	0,10	0,10	0,10	0,10
Sb	0,10	0,10	0,10	0,10	0,10	0,10	0,10	0,10	0,10	0,10	0,10	0,10	0,10	0,10	0,10
Bi	0,10	0,10	0,10	0,10	0,10	0,10	0,10	0,10	0,10	0,10	0,10	0,10	0,10	0,10	0,10
Ag	0,10	0,10	0,10	0,10	0,10	0,10	0,10	0,10	0,10	0,10	0,10	0,10	0,10	0,10	0,10
Au	0,60	0,50	0,50	0,50	0,50	0,50	2,60	0,80	0,50	0,50	2,70	1,30	0,50	1,40	1,00
Hg	0,01	0,01	0,01	0,01	0,01	0,01	0,01	0,01	0,01	0,01	0,01	0,01	0,01	0,01	0,01
Sc	38,00	38,00	38,00	38,00	38,00	43,00	34,00	30,00	42,00	39,00	39,00	20,00	22,00	25,00	35,00
Y	29,70	29,90	29,10	32,00	30,30	29,10	17,20	29,50	38,50	41,20	29,40	31,60	19,70	23,40	24,10
La	23,10	22,60	23,40	23,80	22,50	11,70	10,90	18,40	22,00	27,50	15,50	20,30	23,60	40,40	19,50
Ce	52,20	49,20	52,40	52,70	51,50	27,60	21,60	40,10	48,90	59,50	37,80	45,50	60,60	73,50	44,40
Pr	6,92	6,81	6,79	7,09	6,95	3,69	2,97	5,26	6,54	7,67	4,76	6,20	7,60	10,35	6,00
Nd	28,30	30,50	28,20	29,10	28,90	16,80	12,60	23,80	29,30	32,30	21,30	25,90	31,30	38,60	25,70
Sm	6,35	6,24	6,41	7,02	6,62	4,10	3,02	5,63	7,04	7,41	5,07	6,37	6,10	7,06	5,40
Eu	2,03	1,96	2,08	2,27	2,30	1,33	0,92	1,58	2,10	2,03	1,60	1,87	1,93	1,85	1,48
Gd	6,47	6,59	6,80	6,90	7,09	5,34	3,12	6,28	7,76	8,79	5,84	6,74	5,37	5,73	5,04
Tb	0,98	0,98	1,01	1,04	1,05	0,84	0,49	0,92	1,23	1,31	0,85	0,98	0,67	0,74	0,68
Dy	6,19	5,81	5,85	6,30	6,15	5,41	3,15	5,57	7,20	7,92	5,38	6,06	3,42	4,35	4,20
Ho	1,24	1,20	1,16	1,23	1,12	1,09	0,58	1,18	1,43	1,53	1,11	1,11	0,66	0,71	0,89
Er	3,09	3,28	3,46	3,42	3,15	2,88	1,74	3,46	4,28	4,55	3,32	3,00	1,75	2,22	2,54
Tm	0,45	0,46	0,46	0,47	0,50	0,47	0,24	0,48	0,57	0,62	0,45	0,51	0,28	0,33	0,40
Yb	2,83	2,99	2,95	2,99	3,13	2,97	1,67	3,11	3,83	4,34	2,99	3,05	1,60	2,21	2,42
Lu	0,41	0,42	0,40	0,44	0,44	0,45	0,22	0,48	0,55	0,60	0,41	0,45	0,25	0,32	0,38
$(La/Yb)_N$	5,56	5,14	5,40	5,42	4,89	2,68	4,44	4,03	3,91	4,31	3,53	4,49	10,04	12,44	5,48
$(La/Sm)_N$	2,28	2,27	2,29	2,12	2,13	1,79	2,26	2,05	1,96	2,33	1,92	2,00	2,42	3,59	2,26

Table 2. Major, trace and REE element concentrations for 11 dyke and 3 mafic layer samples. Major element concentrations are given in wt%, trace element and REE concentrations in ppm. The ratios of $(La/Nb)_N$ and $(La/Sm)_N$ were calculated by the normalization of McDonough and Sun (1995).

and also the $(La/Yb)_N$ ratio with 12 is an exception. Although sample STML1 fits into the general slope trend for LREEs, it has also an exceptionally high $(La/Yb)_N$ ratio of 10. The sample AV1 has the lowest content in LREE as well as HREE. The STML2 sample has the highest content in LREE and sample SöHf has the highest content in HREE. It also shows the strongest negative Eu-anomaly. KB2, SöM1, StML3, TL1 and GT1 show a smaller negative Eu-anomaly. All the other samples show no Eu-anomalies.

The NMORB-normalized plot (Sun & McDonough, 1989) and the one for primitive mantle (Sun & McDonough, 1989) confirm the trends seen in the plot by Wood et al. and especially the positive Ba-anomaly of the Stensjö samples, the negative Nb-anomaly for all the samples and the positive Sr-anomaly for the mafic layer samples are even clearer (Fig. 22). This plot also shows a negative Pb-anomaly for all the samples except for SöM and SöPD. Sample StML1 and StML3 even have a positive Pb-anomaly. In this plot the enrichment of LIL elements/LREE and a rather shallow to flat line of HFS elements/HREE is more pronounced than in the plot by Wood et al.

In the geotectonic discrimination diagram by Pearce & Cann (1973) all the samples fall into the field of the within-plate basalts, with the exception of the mafic layers of Stensjö, GT1 and KB2, which fall into the overlapping field of MORB/CAB/IAT. StML1 and StML2 are within the calc-alkaline basalts field. A similar trend is seen within the Zr-Ti discrimination diagram (Fig. 23) by Pearce (1982). Most samples are within the overlapping MORB field on the within-plate basalts field. The Söndrum samples and TL1 are within in the within-plate basalts field. Sample AV1 is within the overlapping MORB field on the island arc basalts field. All three Stensjö mafic layer samples are within the island arc basalt field.

In the Zr-Nb-Y discrimination diagram by Meschede (1986) are all samples within the within-plate tholeiites and volcanic arc basalts (Fig. 23). All samples are within the continental flood basalts field in the V-Ti discrimination diagram (Fig. 23) by Shervais (1982). In the MnO-TiO2-P2O5 discrimination diagram by Mullen (1983, not shown) are STML2 and StML3 within the calc-alkaline, AV1 in the island arc tholeiitic, SöHf and TL1 in the ocean island tholeiitic and KB2, GT1 and SöM within the MORB field. All other samples are on the line between the OIT, OIA, MORB and IAT field.

Normative mineral assemblages of all the samples were calculated by the calculation-spreadsheet by Kurt Hollocher following the CIPW norm (Appendix E). The program includes trace elements like Sr, Ba, Ni, Cr and Zr as well.Pyroxenes are classified as diopside, hypersthen and wollastonite. The used iron-oxidation ratio is based on the chemical analysis. Except for the mafic layers from Stensjö, SöHf, STSD1 and StHD2 there is a normative olivine content.

7 P-T Estimates

7.1 Geothermobarometry—WinTWQ

Microprobe analyses of six samples were performed in order to determine the P-T conditions of the Sveconorwegian granulite facies metamorphism. Disequilibrium textures like garnet-zonations were avoided, and only microdomains with minerals in equilibrium were used. Phase equilibria was calculated by the program TWQ using classical geothermobarometry calibrations. T-dependant ion-exchange reactions (e.g. exchange of Fe and Mg) were used as geothermometers. P-dependent net transfer reactions (e.g. GAES-GAFS) with a large ΔV were used as geobarometers.

7.1.1 The garnet-biotite exchange geothermometer

The Mg-Fe exchange of the garnet-biotite thermometer is based on experiments by Ferry and Spear (1978) and described by the reaction:

$Fe_3Al_2Si_3O_{12} + KMg_3Si_3AlO_{10}(OH)_2 = Mg_3Al_2Si_3O_{12} + KFe_3Si_3AlO_{10}(OH)$
almandine + phlogopite = pyrope + annite (1)

Garnet prefers to incorporate Fe, whereas at higher temperatures the minerals get less selective due to the greater thermal vibration in the mineral lattice. The ion distribution will thus be more evenly at higher temperatures. This temperature-dependent reaction has a small ΔV and has a steep isopleth-slope in a P-T diagram. Additionally considered geothermometers are the garnet-hornblende (Graham & Powell 1984) and the garnet-clinopyroxene (Råheim & Green 1974) thermometer, which are also both based on a Fe-Mg exchange reaction. The reactions are:

$3\ NaCa_2(Mg_4Al)(Si_6Al_2)O_{22}(OH)_2 + 4Fe_3Al_2Si_3O_{12} = 4\ Mg_3Al_2Si_3O_{12} + 3NaCa_2(Fe_4Al)(Si_6Al_2)O_{22}(OH)_2$
pargasite + almandine = pyrope + Fe-pargasite (2)

$2Mg_3Al_2Si_3O_{12} + CaFeSi_2O_6 = Fe_3Al_2Si_3O_{12} + CaMgSi_2O_6$
pyrope + hedenbergite = almandine + diopside (3)

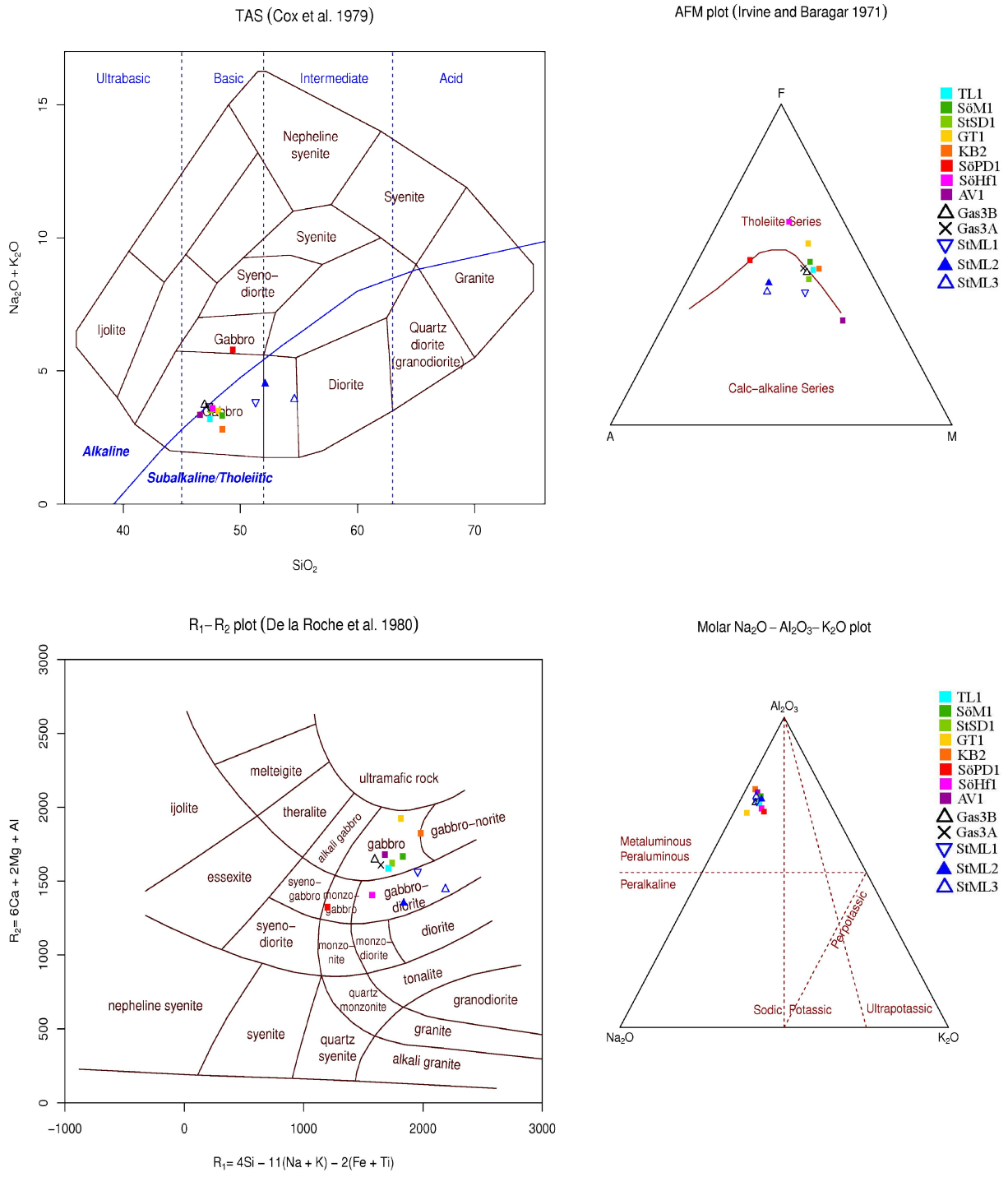

Fig. 20. Upper, left: TAS diagram for plutonic rocks by Cox et al. (1979). Upper, right: AFM diagram; the line distinguishs between calc-alkaline and tholeiitic (Irvine & Baragar, 1971). Lower, left: R_1-R_2 diagram by DeLaRoche (1980) with R_1=4Si-11 (Na+K)-2(Fe+Ti) and R_2=6Ca+2Mg+Al. Lower, right: molar Na_2O-Al_2O_3-K_2O plot showing a metaluminous composition of the samples.

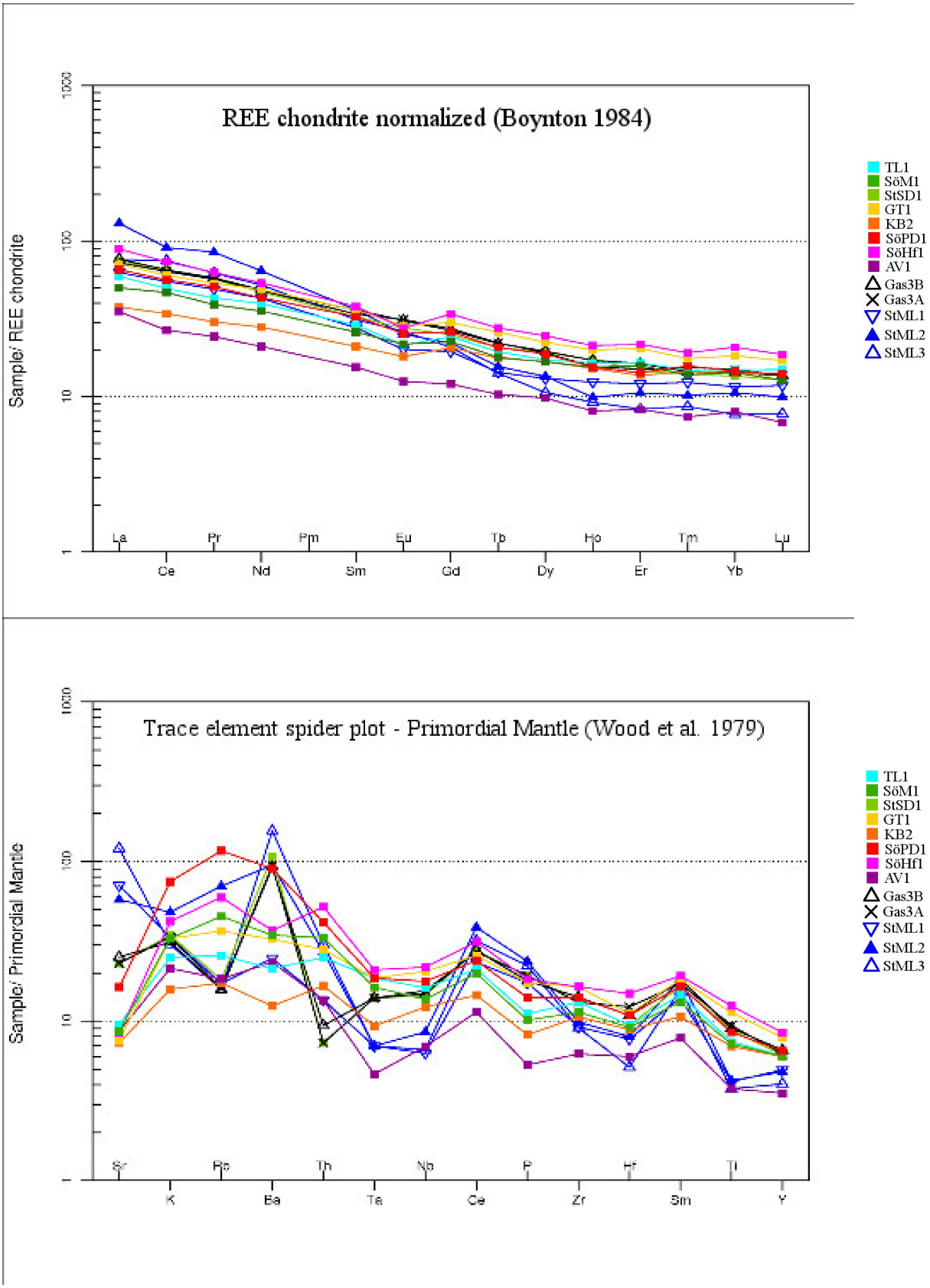

Fig. 21. Upper: chondrite-normalized spider diagram by Boynton (1984). Lower: trace elements normalized with the primordial mantle (Wood et al. 1979).

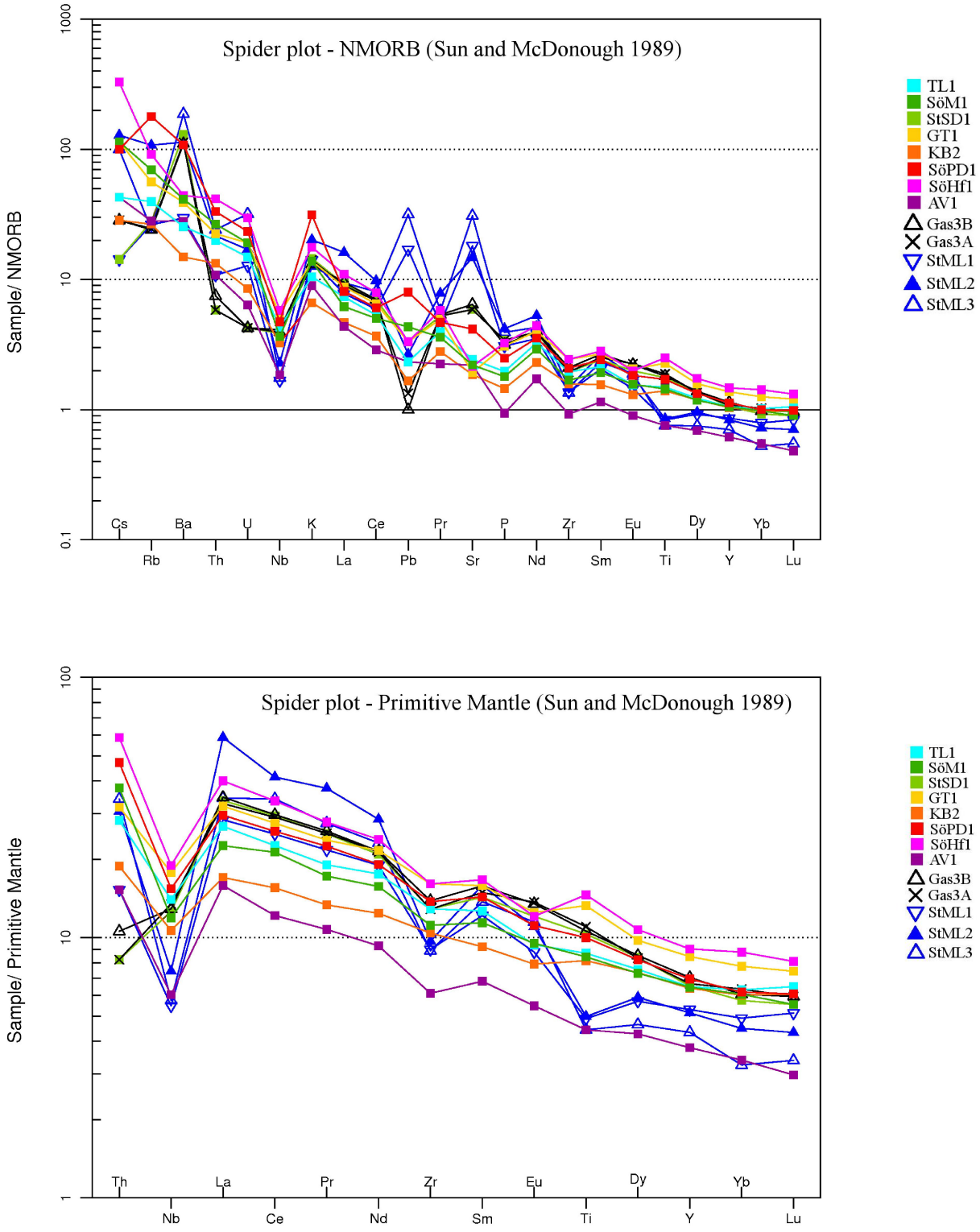

Fig. 22. Upper: NMORB-normalized spider diagram by Sun & McDonough (1989). Lower: spider diagram primitive-mantle-normalized by Sun & McDonough (1989).

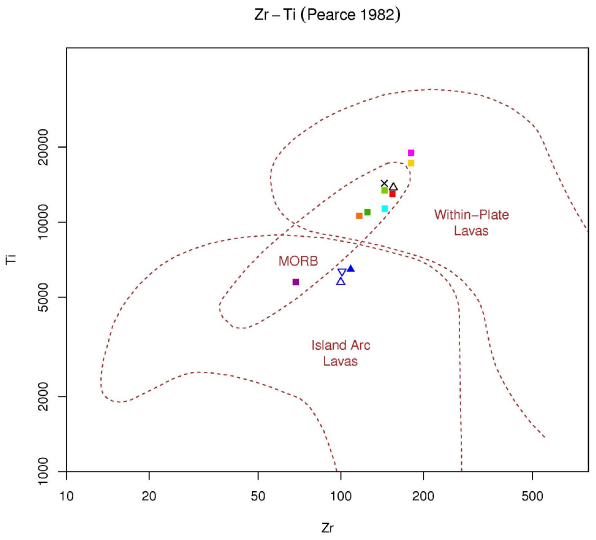

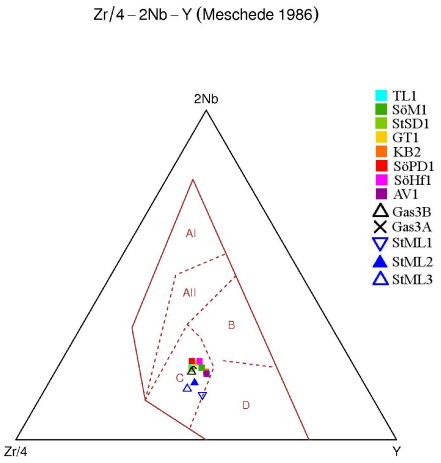

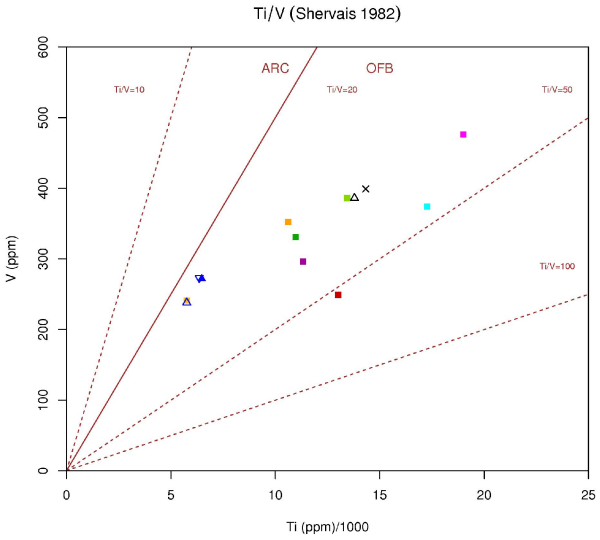

Fig. 24. Upper, left: the Zr-Ti discrimination diagram by Pearce (1982) plots most of the samples within the overlapping MORB field on the within-plate lavas side. Upper, right: In the Zr-Nb-Y discrimination diagram by Meschede (1986) all samples are within the within-plate tholeiites and basalts of volcanic arcs. AI=within-plate alkali-basalts, AII=within-plate alkali basalts and tholeiites, B=EMORB (midocean-ridge basalts), C=within-plate tholeiites and volcanic arc basalts, D=NMORB and island arc basalts. Middle, left: all samples are within the continental flood basalt field in the V-Ti discrimination diagram by Shervais (1982). Ti/V=50—Ti/V=100: ocean island and alkali basalts, Ti/V=20—Ti/V=50: OFB (ocean floor basalts, MORB and back-arc basin basalts), <Ti/V=20: ARC (arc tholeiitic). Legend (Fig. 23).

7.1.2 Theory of Grt-opx-pl-qtz (GAES-GAFS)

The GAES-GAFS geobarometer (Wood 1975) is based on two net transfer reactions, depending on the different end-members of orthopyroxene. The large ΔV of these reactions creates a shallow isopleth-slope in a P-T diagram. They are called the Fe- and the Mg-reaction.

$Ca_3Al_2Si_3O_{12} + 2Mg_3Al_2Si_3O1_2 + 3SiO_2 = 3Mg_2Si_2O_6 + 3CaAl_2Si_2O_8$
grossular + pyrope + quartz = enstatite + anorthite (4)

$Ca_3Al_2Si_3O_{12} + 2Fe_3Al_2Si_3O1_2 + 3SiO_2 = 3Fe_2Si_2O_6 + 3CaAl_2Si_2O_8$
grossular + almandine + quartz = ferrosillite+anorthite (5)

Additionally considered geobarometers are the grt-cpx-pl-qz (GADS-GAHS, Newton & Perkins 1982) and the grt-cpx-opx-pl-qz barometer (Paria et al. 1988). The associated reactions are:

$Ca_3Al_2Si_3O_{12} + Mg_3Al_2Si_3O_{12} + 3\ SiO_2 = 3\ CaAl_2Si_2O_8 + 3CaMgSi_2O_6$ (GADS-GAHS)
grossular + pyrope + quartz = anorthite + diopside (6)

$Fe_3Al_2Si_3O1_2 + CaFeSi_2O_6 + SiO_2 = 2\ Fe_2Si_2O_6 + CaAl_2Si_2O_8$ (7)
almandine + hedenbergite + quartz = ferrosillite + anorthite

7.1.3 Results WinTWQ

The results of the P-T estimates are summarized in Table 3. The chosen mineral assemblage in the microdomains for winTWQ is; garnet, plagioclase, orthopyroxene, clinopyroxene, biotite and quartz.

All geothermobarometer reactions plot similarily within each microdomain of each sample. In all samples, the Mg-reaction of the GAES-GAFS barometer tends to yield lower pressures than the Fe-reaction and the garnet-clinopyroxene and garnet-hornblende thermometer give lower temperatures as garnet-biotite (Appendix D).

The exchange equilibria of the Fe-reaction of the GAES-GAFS barometer and the garnet-biotite thermometer are plotted within a P-T diagram (Fig. 24). No biotite was analysed in sample StML1. Therefore, no biotite-garnet thermometer could be applied for this sample. The temperature in the P-T diagram for this sample is based on the garnet-hornblende thermometer. Sample KB2 has the highest temperature and pressure (926 °C, 12,3kbar). All other samples are within a range of 788-830 °C and 8,9 – 10,5 kbar. Sample StML1 plots at 744°C and 8,7 kbar.

	Temperature (grt-bt)	Pressure (grt-opx-pl-qtz): Fe
KB2	914 – 938 °C	11,6 – 13,0 kbar
SöM	798 – 804 °C	10,1 – 11,0 kbar
StSD	795 – 801 °C	7,9 – 9,9 kbar
Gas	779 – 796 °C	9,5 – 11,1 kbar
Gas3B	827 – 832 °C	8,9 – 10,7 kbar
StML1	–	–
GT1	788 – 812 °C	9,1 – 10,1 kbar

	Temperature (grt-bt)	Pressure (grt-opx-pl-qtz): Mg
KB2	905 – 925 °C	9,9 – 10,2 kbar
SöM	791 – 793 °C	7,9 – 8,1 kbar
StSD	798 – 800 °C	8,3 – 9,4 kbar
Gas	773 – 788 °C	7,8 – 8,5 kbar
Gas3B	821 – 823 °C	7,6 – 8,0 kbar
StML1	–	–
GT1	786 – 806 °C	7,7 – 8,6 kbar

	Temperature (grt-amph)	Pressure (grt-opx-pl-qtz)
KB2	779 – 790 °C	8,4 – 10,0 kbar
SöM	691 – 703 °C	7,3 – 9,5 kbar
StSD	762 – 766 °C	8,1 – 9,2 kbar
Gas	695 – 707 °C	7,4 – 9,8 kbar
Gas3B	724 – 727 °C	8,4 – 9,0 kbar
StML1	744,12 °C	8,7 kbar
GT1	723 – 732 °C	7,7 – 9,1 kbar

	Temperature (grt-cpx)	Pressure (grt-opx-pl-qtz)
KB2	-	-
SöM	741 – 749 °C	7,8 – 9,9 kbar
StSD	697 – 703 °C	7,3 – 9,2 kbar
Gas	668 – 675 °C	7,2 – 9,6 kbar
Gas3B	747 – 750 °C	8,7 – 9,2 kbar
StML1	744,12 °C	8,7 kbar
GT1	684 – 687 °C	7,4 – 8,8 kbar

Table 3. Results of the PT-estimation for different geothermobarometer calculated by WinTWQ.

7.2 AvePT—Thermocalc

Average P-T estimations were done by using the AvePT module of the program Thermocalc, which uses an internally-consistent thermodynamic dataset to calculate phase diagrams for metamorphic rocks (Powell & Holland 1988). Like WinTWQ, Thermocalc searches for reactions involving a stable mineral assemblage. Thermocalc uses however the activity of an end-member as a variable within the uncertainty of the activity model. It then calculates the P-T point via least square and estimates the overall activity model uncertainty (Powell & Holland 1988).

Several microdomains with the same or similar mineral assemblage were used to calculate the pressure and the temperature of a sample. The average of those results (Table 4) is shown in Fig. 24. The full analysis can be seen in appendix C. The chosen mineral assemblage in the microdomain is; garnet, plagioclase, orthopyroxene, clinopyroxene, biotite and quartz. Hornblende and ilmenite/hematite as well as end-members with e* > 2,5 were excluded because the estimated temperatures were unrealistically high.

All samples plot within a similar P-T range of 767-853 °C and 9,1-10,2 kbar. Sample Gas3B plots within the kyanite field and yield the lowest temperatures. Sample Gas yields the highest temperature and pressure. It plots with the other samples in the sillimanite field. Sample GT1 has the lowest pressure.

Sample	avT	sd(T)	avP	sd(P)	corr
KB	813	96	9,6	1,2	0,639
Gas3B	770	92	9,9	1,2	0,702
StSD	806	92	9,7	1,2	0,622
SöM	802	94	10,1	1,3	0,704
Gas	853	94	10,3	1,2	0,645
GT	767	81	9,1	1,2	0,732

Table 4. Results of the PT-estimation by AvePT (Thermocalc). avT = average temperature, sd(T) = standard deviation for temperature, avP = average pressure, sd(P) = standard deviation for pressure, corr = correlated ellipse

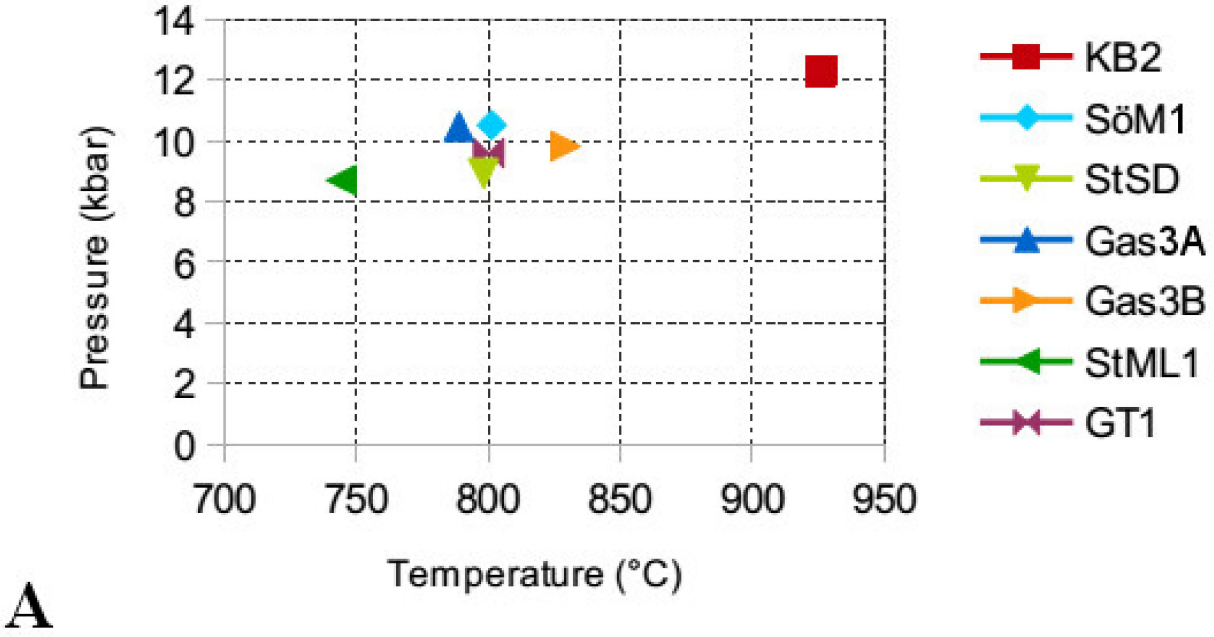

A

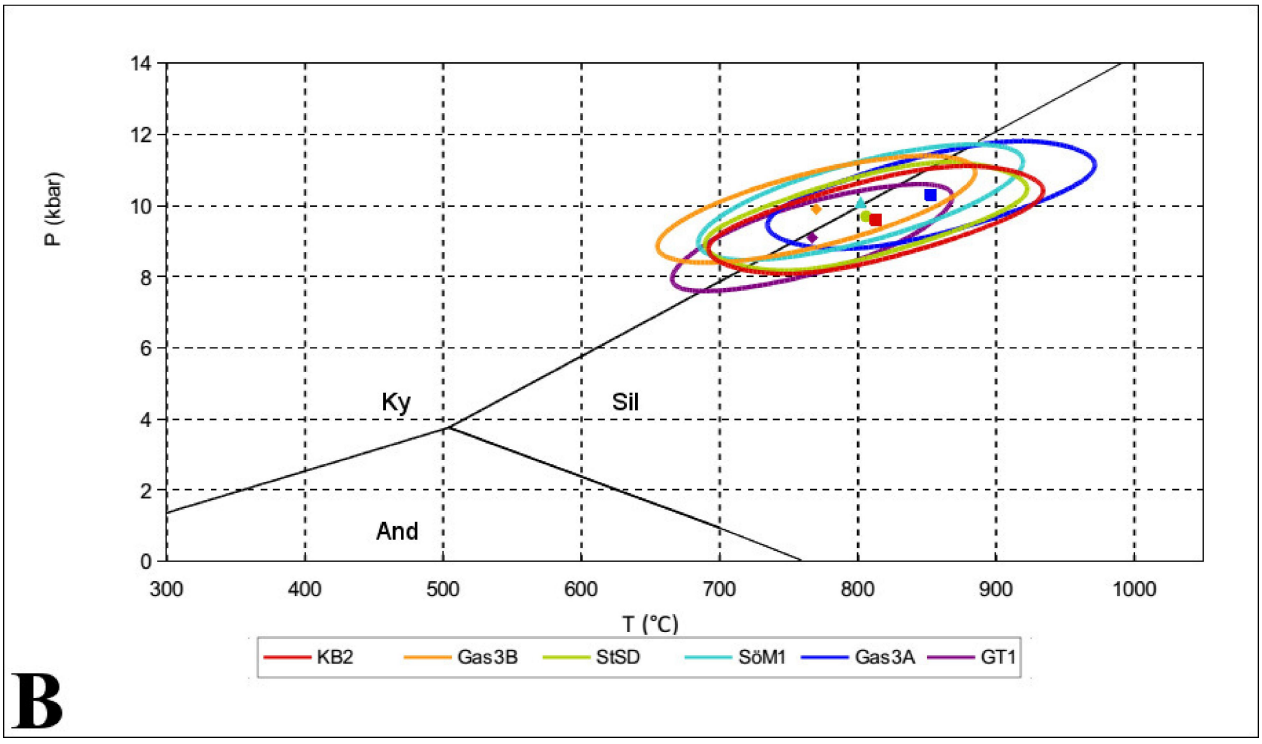

B

Fig. 24. A: Results of PT-estimates by WinTWQ based on average analysis. Sample StML1 was calculated with a different thermometer. The used assemblage is; clinopyroxene, orthopyroxene, garnet, biotite and plagioclase. B: Results of PT-estimates by AvePT (Thermocalc) with error ellipses representing the standard deviation.

8 Discussion

8.1 Metamorphism

8.1.1 Field-relationship

All dykes are roughly N-S to NE-SW trending and show an E-W trending Sveconorwegian foliation or lineation. There are three clearly distinguishable groups of rocks if compared in terms of deformation and composition: the dykes at Getterön, Träslövsläge and Söndrum (1a), the dykes at Stensjö harbour, Söndrum harbour and Kullaberg (1b), the dykes at Gåsanabbe (1c), the mafic layers at Gåsanabbe (2) and the dyke at Apelviken (3). Group 1a-c differ in grade of deformation and field appearance. Group 2 and 3 are different in composition. Group 2 occurs as folded layers.

8.1.1.1 Group 1a

All dykes at Getterön, Träslövsläge and Söndrum are only locally deformed at the contacts. They have a preserved non-graded, rhythmic magmatic layering. Accumulations of single minerals within the layers indicate cumulate textures. Slumping and "cross-bedding" textures wihtin the layering suggest an activity within the magma chamber during the intrusion and crystallization. The presence of this magmatic layering indicates that there was neither a deformation nor a metamorphic event during the intrusion and crystallization or before the granulite metamorphic overprint.

The hornblende-rich marginal part in Getterön indicates hydration probably during retrogression. Clinopyroxene and orthopyroxene break down to hornblende via hydration reactions.

At Söndrum the dyke shows additionally a foliation/lineation which is at an angle to the compositional rhythmic layering. Both, the layering and the foliation are cut sharply by plagioclase-rich lenses. Due to the composition of these lenses, which characterizes the lenses as a primary igneous feature of the dyke, the foliation must have formed earlier than the lenses, but later than the layering. They are therefore also interpretated as an igneous texture. This foliation could have formed due to imbrication or laminar flow within the magma chamber. It is suggested that the direction of this imbrication can determine the sense of magmatic flow (McBirney 1996, Winter 2010). In this case the direction is NNE-SSW. The plagioclase-rich lenses are probably formed by the same process than the plagioclase-rich lenses in the layered gabbro in Lower Zone of the Skaergaard intrusion, Greenland (McBirney 1996). McBirney suggests that those lenses formed by deformation, which led to a segregation of liquids into zones of minimum stress.

At Söndrum the contact to the country rock is discordant to the foliation within the host gneiss and underwent minor deformation. This shows that the intrusion of the dyke is younger than the metamorphic event which caused the coarse gneissic layering in the gneiss (Hallandian event). The marginal portion of the dyke was affected by later brittle deformation together with metasomatic processes, which affected also interior parts of the dyke, seen at the small epidote-filled veins.

8.1.1.2 Group 1b

The dykes in this group are discordant to the foliation of their host gneisses and are therefore younger than the metamorphic event which caused the coarse gneissic foliation within the host gneiss. They show no magmatic layering.

At Kullaberg the intrusion let to a melting of the granitic host rock along the eastern contact zone. This felsic magma mingled with the intruded mafic magma and underwent shearing along a soft contact zone (Söderlund et al. 2008). Crystallization was followed by a granulite metamorphic overprint. The presence of anhydrous minerals such as garnet in the stromatic leucosomes indicate water-undersaturated melting like the breakdown-reaction of biotite.

The dykes at Stensjö harbour and Söndrum harbour indicate that the grain size can be correlated with the original dyke thickness. Both dykes are smaller than all others and have a smaller grain size. Smaller bodies lose their heat quicker than larger bodies. The time to develop a coarse-grained texture was therefore not given.

8.1.1.3 Group 1c

At Stensjö, the less ductile dykes separated into boudins during a stretching event. They are clearly deformed by ductile deformation and subsequent folding which affected the whole Stensjö sequence. The less ductile dykes separated into boundins, while the surrounding rocks underwent deformation by ductile flow. The dykes cut locally the foliation of the host gneiss and locally some small, tight and angular folds. This would indicate that the intrusion and crystallization was post-tectonic to the first isoclinal folding but pre-tectonic to the late folding.

8.1.2 Petrography

8.1.2.1 Groups 1a-c

All samples of groups 1a-c have a domainal texture with domains rich in plagioclase and others rich in pyroxenes, hornblende and opaque phases. This suggests a protolith precursor with a medium- to coarse-grained texture, typical of a dolerite. Primary magmatic clinopyroxene grains and the biotite-lath shape of the plagioclase-rich domains suggests a primary ophitic texture.The large grain size indicates a slow cooling-rate after intruding the country rock. Sample Gas3A, StSD and StHf have only minor

domainal textures. The size of the dyke and the marginal location of sample Gas3A suggests rapid cooling and crystallization.

Disequilibrium growth is indicated by a sector-zoned primary clinopyroxene. This is due to rapid growth or slow growth combined with a low diffusion rate, which prevent the crystal from equilibrating with the liquid. Since the protolith was coarse-grained, a low-diffusion rate during crystallization is suggested to be more likely.

All samples in this group were affected by a pervasive re-equilibration under upper amphibolite to high-pressure granulite facies metamorphic conditions. The key assemblage is orthopyroxene, clinopyroxene, plagioclase, quartz and garnet with variable amounts of hornblende and biotite. Some dykes have scapolite, which forms during medium to high temperatures and indicates a presence of (S– and) CO_2 –rich fluids.

Except for the large primary clinopyroxene grains and the domainal texture, there are no signs of relict igneous textures. All samples have a granoblastic texture which formed by recrystallization after deformation at high temperatures. With this process the grain boundaries are reduced to minimize the surface area and the result is an equilibrium texture in which grains meet along straight boundaries, ideally in triple junctions as it is often the case with plagioclase and clinopyroxene together with hornblende. These polygonal aggregates of clinopyroxene and hornblende indicate equilibrium and simultaneous growth at some point. Hornblende was therefore stable during high pressure and temperature metamorphism. Replacement textures of primary clinopyroxene to hornblende along the rims and within exsolved lamellae indicate that more hornblende formed during retrogression, as a result of hydration reactions and the break-down of primary clinopyroxene grains to amphibole and metamorphic clinopyroxene under lower temperature conditions. This would indicate a clockwise PT path.

Large primary clinopyroxene grains show exsolution, which is also a retrograde texture formed by an intragranular solid-state processes. During decreasing temperature or decompression the homogenous solid solution of clinopyroxene gets unstable and breaks down. The result is the development of lamellae of low Ca-orthopyroxene within the exsolving host. The sample from Kullaberg has no exsolved pyroxene grains, which indicates a rapid uplift and the preservation of the solid solution. However the primary pyroxene grains in all dykes have many inclusions of ilmenite-hematite. They probably formed due to an exsolution of a Ti-Fe-rich phase (Griffin & Raheim 1973).

Plagioclase inclusions (An46) in primary clinopyroxene grains may represent high temperature (igneous) plagioclase which gets unstable at lower temperatures. Within clinopyroxene this process releases Ca and Al which produced hornblende. General igneous plagioclase breakdown in the matrix produces albite or oligoclase which would explain compositionally zones plagioclase and recrystallized plagioclase in polygonal assemblages with a lower an-content, but a low orthoclase-component.

The locally tapering twins of those metamorphic plagioclase grains form due to zoned crystals but could also indicate rapid growth during deformation. They have also antiperthitic textures, which are typical of high metamorphic temperatures. Plagioclase exsolves K-feldspar in spot-like textures at lower temperatures. Garnet grains show only little zonation and are small. This indicates that those grains did not underwent a change in chemical composition due to P-T changes and represent therefeore a single metamorphic event. It assumes a rapid uplift.

The presence of Fe-pargasite and the composition of relict igneous clinopyroxene indicates that the dyke in Getterön is richer in Fe compared to the others. No difference can be seen between sample Gas3A from the centre of the dyke and the marginal sample Gas3B.

8.1.2.2 Group 2

The mafic layers form long lens-shaped bodies isoclinally folded within the quartzo-feldspathic-gneiss. The layers differ in composition and deformation from the metadolerites. There is a foliation defined by light plagioclase-rich aggregates in a matrix of clinopyroxene, scapolite, plagioclase and hornblende. Lense-shaped scapolite assemblages are oriented within the foliation. The mineral assemblage is not the typical granulite facies assemblage but rather amphibolite facies with the key assemblage; pargasitic hornblende, clinopyroxene, plagioclase, garnet, scapolite (hematite, ilmenite, quartz, pyrite and monazite). Microprobe analysis revealed Ba-bearing plagioclase, which indicates an enrichment of LIL elements through metasomatism or crustal contamination. Which is supported by the presence of scapolite. There are no small scale deformation textures except for very fine bent fractures in plagioclase.

8.1.2.3 Group 3

The dyke at Apelviken has a slightly different composition than the other dykes. The high Mg# and high contents of Ni and Cr characterize this rock as ultramafic. However the mineral assemblage is like group 1 granoblastic and has the same metamorphic mineral assemblage, with the same key minerals plus cummingtonite. The only difference is, that this dyke is garnet-free.The presence of scapolite indicate the presence of CO_2-rich fluids.

8.2 P-T estimates

The estimated temperatures and pressures range between 770 and 850 °C and 8 to 10 kbar. These conditions represent the transition between upper amphibolite and high-pressure granulite facies at medium to high pressure and fit with the previously

published P-T estimates for the southern part of the Eastern Segment of 680-800 °C and 8-12 kbar (e.g. Johanson et al., 1991, Wang & Lindh, 1996, Möller, 1998).

The large error ellipses in winTWQ might be a result of disequilibrium, errors in the activity-model or disturbences in the Fe/Mg ratio. Perkins & Chapera (1985) mention that the activity of enstatite might be underestimated or the pyrope activity overestimated in Fe-rich rocks, leading to different pressure and temperature estimates in using the garnet-orthopyroxene-plagioclase-quartz barometer. Therefore, the Fe-endmember reactions are more reliable. Retrograde textures such as exsolution lamellae and replacements were avoided, because retrograde effects might have upset the system. However the mineral assemblage might not represent the metamorphic peak temperature because Fe-Mg equilibria can reset during cooling.

Another source of error might be the use of garnet-core compositions. Although the garnets were little zoned and rather small, it might have been more precise to use the garnet composition of the rim, because the rims are more likely in equilibrium with the matrix.

To use the garnet-biotite thermometer on Ca-bearing garnets could have caused another error, because Ca in garnet has a non-ideal effect on the Fe/Mg ratio. Therefiore, the garnet-biotite thermometer has to be applied carefully. A correction of the activity -composition might decrease the error.

Also, the ratio of Fe2+/Fe3+ is calculated on the basis of charge balance and not an actual measured ratio. For complex minerals the charge-balance-calculation can be a source of error because several valences for ions have to be considered as well as factors like the varying H_2O content and cation site vacancies. A miscalculated ratio of the Fe oxidation state influences significantlly the ratio of Fe/Mg and with that the temperature estimate.

8.3 Geochemistry

There are three distinguishable groups; the dykes at Gåsanabbe (1), all other dykes (2) and the mafic layers at Gåsanabbe (3). Note that sample GT1 annd TL1 represents only the very mafic part of the metadolerite and does not represent the average whole rock geochemistry.

8.3.1 REE chondrite-normalized

All groups have similar negative slopes with little LREE enrichment which is accomplished by low degrees of partial melting of primitive mantle or a heterogeneous mixture of depleted MORB an enriched OIB types. There is no depletion in HREE. The lines are almost flat. It suggests that garnet was not in quilibrium with the melt in time of segregation. This indicates that there was no garnet in the source and the origin of the melt was in the upper mantle.

Sample StML2 shows a steeper slope, which indicates a higher degree of fractionation. The small negative Eu-anomaly in sample SöHf reflects the substitution of Eu^{2+} for Ca^{2+} in plagioclase and indicates that the sample was in equilibrium at some point with (now absent) igneous plagioclase.

8.3.2 MORB– and primitive-mantle-normalized

Group 1 has positive Rb- and Ba-anomalies. These LIL elements are mobile, easily extracted from the mantle and concentratied in the crust. The anomalies suggest either metasomatism or the contamination by a crustal component. They only show a little negative Nb-anomaly, but a strong negative Pb-anomaly.

Group 2 has a strong negative Nb-anomaly and indicates the presence of a residual Nb-Ta bearing mineral. The HFS elements are controlled by the source region and fractionation during magma evolution. Nb is found in Ti-rich phases such as ilmenite and hornblende, which hold the element in the source. It is characteristic for subduction-related melts and indicates crustal involvement in the magma process. A negative P-anomaly suggest an equilibrium at some point with (now absent) apatite.

All groups have no Y- or Yb-anomaly. This suggests that the magma source was not garnet bearing. It could indicate a shallow slab dip and a lesser depth of the magma genesis.

Group 3 shows the same positive Rb- and Ba anomalies as group 1 and has the same negative Nb-anomaly as group 2. It is also enriched in mobile Pb, except for StML2. A positive Sr-anomaly indicates the presence of plagioclase. A negative Zr-anomaly assumes equilibrium at some point with now absent zircon.

8.3.3 CIPW-norm calculations

Most of the samples have normative olivine and hypersthene and are therefore classified as Si-saturated basalts (olivine-tholeiites) according to the classification of Yoder and Tilley (1962). Clearly different are the mafic layers from Gåsanabbe which are Si-oversaturated (quartz-tholeiites) with normative quartz and hypersthene and the dyke at Apelviken which is Si-undersaturated (alkali basalt) and has normative olivine and nepheline.

The norm calculation is sensitive to any changes in the iron oxidation state. Since the samples are metamorphic, it is very unlikely that the present iron ratio will reflect the iron ratio of the protolith.

8.3.4 Geotectonical discrimination

Geotectonic discrimination diagrams indicate a within-plate and volcanic arc setting and also the Nb-anomaly for all samples indicate subduction-related magma generation. It also shows that the mafic layers and

dykes have a similar history. It might be possible that the tholeiitic dykes are related to an extension event after subduction, where magma reaches the surface through normal faults, without experiencing fractionation or contamination by the crust. This fits with the extensional movements along crustal-scale shear zones during the latest phase of Sveconorwegian metamorphism It suggest that the intrusion is related to the late-orogenic extension and exhumation of the Sveconorwegian orogen.

The high LIL elements in case of the Gåsanabbe dykes, SöPD,SöHF and SöM are probably due to metasomatic processes, which is supported by the presence of scapolite and epidote veins, however a crustal contamination may not be excluded.

Dykes like KB2 and AV1 are only slightly enriched in LIL elements. The reason could be the metamorphic overprint. Granulites tend to be not enriched in LIL elements. However it is still unknown if this is caused by depletion by fluids, melts or compositional differences (Sørensen & Winter 1989). The dyke at Apelviken is more mafic compared to the other dykes and has a different average bulk rock composition.

9 Conclusions

- N-S trending high-grade metamorphic dolerite dykes occur along the coast from Varberg to Kullaberg. The discordance to the gneissic foliation of the country rock indicates that the dykes are of late Sveconorwegian age. U-Pb dating of zircon at Kullaberg gave an age of 961+/- 6 Ma which was interpreted as the age of the dolerite intrusion (Söderlund et al. 2008).
- Geochemical and petrographical data distinguishes 3 groups: young tholeiitc dolerites, a more mafic and tholeiitc dyke at apelviken and older calc-alkaline mafic layers. The metadolerites have a domainal texture with domains rich in plagioclase and others rich in pyroxenes, hornblende and opaque phases, suggesting a protolith precursor with a coarse-grained texture, typical of a dolerite. Primary magmatic clinopyroxene grains and the biotite-lath shape of the plagioclase-rich domains suggests a primary ophitic texture. The large grain size indicates a slow cooling-rate after intrusion. All samples are affected by a pervasive re-equilibration under upper amphibolite to high-pressure granulite facies metamorphic conditions. The key assemblage is orthopyroxene, clinopyroxene, hornblende, biotite, plagioclase, quartz, apatite and garnet. Some dykes have scapolite, which indicates the presence of (S– and) CO_2-rich fluids. The texture is generally granoblastic, with relicts of large primary clinopyroxene. Equilibrium textures of metamorphic clinopyroxene and hornblende indicate amphibolite facies metamorphic conditions for the formation of pargasitic hornblende. This suggests a clockwise P-T-path. The dyke from Apelviken is garnet-free.
- The estimated temperatures and pressures are 770-850 °C and 8-10 kbar. These conditions represent the transition between upper amphibolite and granulite facies at medium to high pressure and fit with the previously published P-T estimates for the southern part of the Eastern Segment of 680-800 °C and 8-12 kbar (e.g. Johanson et al., 1992, Möller, 1998).
- Geotectonic discrimination diagrams indicate a within-plate and volcanic arc setting. The Nb-anomaly for all samples indicate subduction-related magma generation. It also shows that the mafic layers and dykes have a similar history. The tholeiitic dykes are related to an extension event after subduction, where magma reaches the surface through normal faults, without experiencing fractionation or contamination by the crust. This fits with the extensional movements along crustal-scale shear zones during the latest phase of Sveconorwegian metamorphism. It suggests that the intrusion is related to the late-orogenic extension of the Sveconorwegian orogen. High LIL elements (Gåsanabbe and Söndrum dykes) indicate metasomatic processes, which is supported by the presence of late epidote veins (and scapolite)and late (cretaceous) hematite-alteration at Stensjö. However a crustal contamination may not be excluded. The correspondance to the Blekinge-Dalarna dykes is therefore possible. A similar conclusion, based on Nd-isotopes, was made by Johansson & Kullerud (1993). Dykes like KB2 and AV1 are only slightly enriched in LIL elements. However it is still unknown if this is caused by depletion by fluids, melts or compositional differences (Sørensen & Winter 1989).

10 Suggestions for future studies

- Since in Getterön only the most mafic layer was sampled and investigated, it would be interesting to investigate the intermediate and the plagioclase-rich layer as well, in order to get a picture of the whole rock chemistry and perhaps an idea of the mechanism of fractionation.
- In order to get a better insight into the PT estimates and the associated metamorphic reactions, it would be useful to create pseudosections (e.g. with Thermocalc, Theriak Domino etc.)

- To date the intrusion and metamorphic peak. Some additional isotopic data could also give a better insight in the geotectonic nature of the rocks.

11 Acknowledgements

I would like to thank my supervisor Charlotte Möller for her immense support and for introducing me into a beautiful field area. Thanks to Lorraine Tual and Victoria Beckman for helping me with Thermocalc and the possibility to come by at any time for some discussions. Thanks to Leif Johansson for sampling the mafic layers at Gasanabbe and to review parts of this thesis. Thanks to Anders Scherstén for comments and tips. Finally, to my friends and parents; thank you for all the support!

12 References

Åhäll, K.-I., Gower, C.F., 1997: The Gothian and Labradorian orogens: variations in accretionary tectonism along a late Paleoproterozoic Laurentia–Baltica margin. *GFF* 119, 181–191.

Åhäll, K.-I., Samuelsson L., Persson P., 1997: Geochronology and structural setting of the 1.38 Ga Torpa granite; implications for charnockite formation in SW Sweden, *GFF* 119, 1, 37-43.

Åhäll, K.-I., Cornell, D.H., Armstrong, R., 1998: Ion probe zircon dating of three metasedimentary units bordering the Oslo Rift; new constraints for early Mesoproterozoic growth of the Baltic Shield. *Precambrian Research* 87,117–134.

Åhäll, K.-I. & Larson, S.-Å., 2000: Growth-related 1.86–1.55 Ga magmatism in the Baltic Shield; a review addressing the tectonic characteristics of Svecofennian, TIB 1-related, and Gothian events. *GFF* 122, 193–206.

Åhäll, K.-I., Connelly, J.N., 2008: Long-term convergence along SW Fennoscandia: 330 m.y. of Proterozoic crustal growth. *Precambrian Research* 163, 402–421.

Andersson, J., Söderlund, U., Cornell, D., Johansson, L. & Möller, C., 1999: Sveconorwegian (-Grenvillian) deformation, metamorphism and leucosome formation in SW Sweden, SW Baltic Shield: constraints from a Mesoproterozoic granite intrusion. *Precambrian Research* 98, 151–171.

Andersson, J., Möller, C. & Johansson, L., 2002: Zircon geochronology of migmatite gneisses along the Mylonite Zone (S Sweden): a major Sveconorwegian terrane boundary in the Baltic shield. *Precambrian Research* 114,121–147.

Andersson, J. et al., 2014/2015: unpublished manuscript, Geological Survey, Sweden.

Austin Hegardt E., 2010: Pressure, temperature and time constraints on tectonic models for southwestern Sweden. Earth Science Centre Doctoral Thesis A134. Department of Earth Sciences, University of Gothenburg. 26pp. ISBN 978-91-628-8211-2.

Berman, R. G., 1988: Internally-consistent thermodynamic data for minerals in the system Na2O-K2O-CaO-MgO-FeOFe2O3-Al2O3-SiO2-TiO2-H2O-CO2, *Journal of Petrology* 29, 2, 445 – 522.

Berman, R. G., 1990: Mixing properties of Ca−Mg−Fe−Mn garnets. *Am Mineral* 75, 328–344 .

Berman, R. G. & Aranovich, L. Y., 1996: Optimized standard state and solution properties of minerals, *Contributions to Mineralogy and Petrology 126, 1, 1-24.*

Bingen, B., Skår, Ø., Marker, M.et al., 2005: Timing of continental building in the Sveconorwegian orogen, SW Scandinavia. *Norwegian Journal of Geology* 85,87–116.

Bingen, B., Nordgulen, Ø., Viola, G., 2008: A four-phase model for the Sveconorwegian orogeny, SW Scandinavia. *Norwegian Journal of Geology* 88, 43–72.

Bogdanova, S.V., Page, L.M., Skridlaite, G. & Taran, L.N., 2001: Proterozoic tectonothermal history in the western part of the East Europen Craton: 40Ar/39Ar geochronological constraints. *Tectonophysics* 339, 39–66.

Boynton, W. V., 1984: Cosmochemistry of the rare earth elements: meteorite studies, *Developments in geochemistry*, 2, 63-114.

Brander, L. & Söderlund, U., 2009: Mesoproterozoic (1.47-1.44 Ga) orogenic magmatism in Fennoscandia; Baddeleyite U-Pb dating of a suite of massiftype anorthosite in S Sweden. *International Journal of Earth Sciences* 98, 499-516.

Christoffel, C.A., Connelly, J.N., Åhäll, K.-I., 1999: Timing and characterization of recurrent pre-Sveconorwegian metamorphism and deformation in the VarbergHalmstad region of

SW Sweden. *Precambrian Research* 98, 173–195.

Connelly, J. N., Berglund, J. & Larson, S. Å., 1996: Thermotectonic evolution of the Eastern Segment of SW Sweden; tectonic constraints f rom U–Pb geochronology. In: Precambrian Crustal Evolution in the North Atlantic Region (ed. Brewer, T.S.),*Geological Society Special Publication* 112, 297–313.

Cox K. G, Bell, J. D., Pankhurst, R. J., 1979: The Interpretation of Igneous Rocks, Allen and Unwin, London.

De La Roche, H., Leterrier, P., Grandclaude, P. & Marchal, M., 1980: A classification of volcanic and plutonic rocks using the R1-R2 diagram and major element analyses - It's relationship with current nomenclature, *Chemical Geology* 29, 183-210.

Ferry, J.M. & Spear, F.S., 1978: Experimental calibration of the partitioning of Fe and Mg between biotite and garnet, *Contributions to Mineralogy and Petrology* 66, 2, 113-117.

Forsell, P., 1962: Kullabergs berggrund . *Kullabergs natur* 7, 45.

Graham, C.M. & Powell,R., 1984: A garnet–hornblende geothermometer: calibration, testing, and application to the Pelona Schist, Southern California, *Journal of Metamorphic Geology* 2, 1, 13–31.

Griffin, W. L. & Raheim, A. , 1973: Convergent metamorphism of eclogites and dolerites, Kristiansund area, Norway, *Lithos* 6, 1, 21-40.

Hansen, E., Johansson, L, Andersson, J., LaBarge, L, Harlov, D., Möller, C., submitted. Partial melting in amphibolites in the parautochtonous basement of the Sveconorwegian orogen, SW Sweden. Submitted to Lithos April, 2014.

Harlov, D. E., Johansson, L., Van den Kerkhof, A. & Förster, H.-J., 2006: The role of advective fluid flow and diffusion during localized, solid-state dehydration: Söndrum Stenhuggeriet, Halmstad, SW Sweden, *Journal of Petrology* 47, 3-33.

Harlov, D.E., Van Den Kerkhof, A., Johansson, L., 2013. The Varberg–Torpa charnockite–granite association, SW Sweden: mineralogy, petrology, and fluid inclusion chemistry. *Journal of Petrology* 54, 3-40.

Hollocher, K.: CIPW-norm calculation spreadsheet, http://www.neiu.edu/~kbartels/norm3.xls.

Hubbard, F.H., 1975: The Precambrian crystalline basement of southwestern Sweden. The geology and petrogenitic development of the Varberg region. *GFF* 97, 223–236.

Irvine, T. N. & Baragar, W.R.A.,1971: A guide to the chemical classification of the common volcanic rocks, *Canadian Journal of Earth Sciences* 8, 523-48

Janousek V., Farrow C.M. & Erban V., 2006: Interpretation of whole-rock geochemical data in igneous geochemistry: introducing Geochemical Data Toolkit (GCDkit). *Journal of Petrology* 47, 6, 1255-1259.

Johansson, Å. , 2009: Baltica, Amazonia and the SAMBA connection – 1000 million years of neighbourhood during the Proterozoic? *Precambrian Research* 175, 221-234.

Johansson, L., Lindh, A. & Möller, C., 1991: Late Sveconorwegian (Grenville) high-pressure granulite facies metamorphism in southwest Sweden. *Journal of Metamorphic Geology* 9, 283–292.

Johansson, L. & Kullerud, L., 1993: Late Sveconorwegian metamorphism and deformation in southwestern Sweden. *Precambrian Research* 64, 350–353.

Johansson, L., Möller, C. & Söderlund, U. 2001: Geochronology of eclogite facies metamorphism in the Sveconorwegian Province of SW Sweden. *Precambrian Research* 106, 261-275.

Klingspor, I., 1976: Radiometric age-determinations of basalts, dolerites and related syenite in Skåne, southern Sweden. *GFF* 98, 195–216.

Larsson, W., 1966: Berggrundskarta till bladet Halmstad (SGU aA 198), SGU biblioteket.

Larsson, W., 1968: Berggrundskarta till bladet Laholm (SGU aA 197), SGU biblioteket.

Leake, B. E., Woolley, A. R., Arps, C. E. S., Birch, W. D., Gilbert, M. C., Grice, J. D., Hawthorn, F.C., Kato, A., Kisch, H.J., Krivovichev, V. G., Linthout, K., Laird, J., Mandarino, J. A., Maresch, W. V., Nickel, E. H., Rock, N. M. S., Schumacher, J. C., Smith, D. C., Stephenson,

N. C. N., Ungaretti, L., Whittaker, E. J. W. & Youzhi, G., 1997: Nomenclature of amphiboles: Report of the subcommittee on amphiboles of the international Mineralogical Association, commission on new minerals and mineral names, *Can Mineral* 35, pp. 219 – 246.

Li, Z.X., Bogdanova, S.V., Collins, A.S., Davidson, A., De Waele, B., Ernst, R.E., Fitzsimons, I.C.W., Fuck, R.A., Gladkochub, D.P., Jacobs, J., Karlstrom, K.E., Lu, S., Natapov, L.M., Pease, V., Pisarevsky, S.A., Thrane, K., & Vernikovsky, V., 2008: Assembly, configuration, and break-up history of Rodinia: a synthesis. *Precambrian Research* 160, 179–210.

Lundqvist, I., 2008: Berggrunskartan 5B Varberg NO, SGU biblioteket.

McBirney, A., R. & Nicolas, A. 1996: The Skaergaard Layered Series. Part II. Magmatic flow and Dynamic Layering, *Journal of Petrology 38, 5, 569-580.*

McDonough, W. F. & Sun, S.-s., 1995: The composition of the Earth. *Journal of Chemical Geology* 120, 223-253.

Meschede, M., 1986: A method of discriminating between different types of mid-ocean ridge basalts and continental tholeiites with the Nb-Zr-Y diagram, *Chemical Geology*, 56, 3- 4, 207-218.

Miyashiro, A., 1974: Volcanic rock series in island arcs and active continental margins, *American Journal of Science* 274, 321-355.

Möller, C., 1998: Decompressed eclogites in the Sveconorwegian (-Grenvillian) orogen of SW Sweden: petrology and tectonic implications. *Journal of Metamorphic Geology* 16, 641–656.

Möller, C., 1999: Sapphirine in SW Sweden: a record of Sveconorwegian (Grenvillian) late-orogenic tectonic exhumation. *Journal of Metamorphic Geology* 17,127–141.

Möller, C. & Söderlund, U., 1997: Age constraints on the regional deformation within the Eastern Segment, S. Sweden: Late Sveconorwegian granite dyke intrusion and metamorphic-deformational relations. *GFF* 119, 1–12.

Möller, C., Andersson, J., Lundqvist, I. & Hellström, F., 2007: Linking deformation, migmatite formation and zircon U-Pb geochronology in polymetamorphic orthogneisses, Sveconorwegian Province, Sweden. *Journal of Metamorphic Geology* 25, 727–750.

Möller, C., Andersson, J., Dyck, B. & Antal Lundin, I., 2013: An eclogite exhumation channel and the P-T-t-d evolution of eclogite-bearing crust in the Sveconorwegian orogen. Abstract 10:th International Eclogite Conference, Courmayeur, 2013, p. 91.

Möller, C., Andersson, J., Dyck, B., Antal Lundin, I., submitted: Exhumation of an eclogite terrane as a hot migmatitic fold nappe, Sveconorwegian orogen, in: Castelli, D., Godard, G., Hirajama, T., Medaris, G. (Eds.), High- and ultrahigh-pressure metamorphism, from microscopic to orogenic scale.), Submitted to Lithos (Special Issue) May, 2014.

Morimoto, N., 1988: Nomenclature of pyroxenes, *American Mineralogist*, 73, 1123-1133.

Mullen E. D., 1983: $MnO/TiO_2/P_2O_5$: a minor element discrimination for basaltic rocks of oceanic environments and its implications for petrogenesis, *Earth Planet. Sci. Lett*., 62, 53-62.

Newton,R.C. & Perkins,D., 1982: Thermodynamic calibration of geobarometers based on the assemblages garnet-plagioclase-orthopyroxene (clinopyroxene)-quartz, *American Mineralogist* 67, 203-22.

Page, L.M., Stephens, M.B. & Wahlgren, C.H., 1996b: 40Ar/39Ar geochronological constraints on the tectonothermal evolution of the Eastern Segment of the Sveconorwegian Orogen, south-central Sweden. InBrewer, T.S. (ed.), Precambrian crustal evolution in the North Atlantic Region. *Geological Society, London, Special Publications* 112, 315-330.

Paria,P., Bhattacharya,A. & Sen,S.K., 1988: The reaction garnet+clinopyroxene+quartz =2 orthopyroxene+anorthite: A potential geobarometer for granulites, *Contributions to Mineralogy and Petrology* 99, 1, 126-133.

Park, R.G., Åhäll, K.-I., & Boland M.P., 1991: The Sveconorwegian shear-zone network of SW Sweden in relation to mid-Proterozoic plate movements, *Precambrian Research* 49, 245-260.

Peccerillo, A. & Taylor, S. R., 1976: Geochemistry of eocene calc-alkaline volcanic rocks from the Kastamonu area, Northern Turkey, *Contributions to Mineralogy and Petrology 58, 1, 63-81.*

Persson, P.-O., Lindh, A., Schöberg, H., Hansen, B.T. & Lagerblad, B., 1995: A comparison of the geochronology of plagioclase-dominated granitoids across a major terrane boundary in the SW Baltic Shield. *Precambrian Research* 74, 57–72.

Pearce, J. A. & Cann, J. R., 1973: Tectonic setting of basic volcanic rocks determined using trace element analyses, *Earth and Planetary Science Letters* 19, 2, 290-300.

Pearce, J. A., 1982: Trace element characteristics of lavas from destructive plate boundaries, Orogenic andesites and related rocks, in *Thorpe, R.S. ed., Chichester, England: John Wiley and Sons*, 528-548.

Perkins III, D. & Chipera, S. J., 1985: Garnet-orthopyroxene-plagioclase-quartz barometry: refinement and application to the English River subprovince and the Minnesota River valley, *Contributions to Mineralogy and Petrology* 89, 1 69-80.

Powell, R. & Holland, T. J. B., 1988: An internally consistent thermodynamic data set for phases of petrological interest, *Journal of Metamorphic Geology, 16, 3, 309-343.*

Pinan-Llamas A., Möller C., Johansson L. & Hansen E., 2013: Structural study of the Eastern Segment of the Sveconorwegian orogen in the Halland Province, SW Sweden. *Abstract Geological Society of America Annual Meating*, Denver, 27-30 October 2013.

Råheim,A. & Green,D.H., 1974: Experimental determination of the temperature and pressure dependence of the Fe-Mg partition coefficient for coexisting garnet and clinopyroxene, *Contributions to Mineralogy and Petrology* 48, 3, 179-203.

Rimša, A., Johansson L., Whitehouse M.J., 2007: Constraints on incipient charnockite formation from zircon geochronology and rare earth element characteristics, *Contributions to Mineralogy and Petrology* 154, 357–369.

Roffeis, C., Corfu, F. & Austrheim H., 2012: Evidence for a Caledonian amphibolite to eclogite facies pressure gradient in the Middle Allochthon Lindås Nappe, SW Norway, *Contributions to Mineralogy and Petrology* 164, 81.

Shervais, J. W., 1982: Ti-V plots and the petrogenesis of modern and ophiolitic lavas, *Earth and Planetary Science Letters* 59,1, 101-118.

Söderlund, U., Jarl, L.-G., Persson, P.-O., Stephens, M. B. & Wahlgren, C.-H., 1999: Protolith ages and timing of deformation in the eastern, marginal part of the Sveconorwegian orogen, southwestern Sweden. *Precambrian Research* 94,29–48.

Söderlund, U., Möller, C., Andersson, J., Johansson, L. & Whitehouse, M., 2002: Zircon geochronology in polymetamorphic gneisses in the Sveconorwegian orogen, SW Sweden: ion microprobe evidence for 1.46–1.42 and 0.98–0.96 Ga reworking. *Precambrian Research* 113, 193–225.

Söderlund, U., Isachsen, C., Bylund, G. et al., 2005: U –Pbbaddeleyite ages and Hf, Nd isotope chemistry constraining repeated mafic magmatism in the Fennoscandian Shield from 1.6 to 0.9 Ga. *Contributions to Mineralogy and Petrology* 150,174–194.

Söderlund, U., Karlsson, C., Johansson, L. & Larsson, K., 2008: The Kullaberg peninsulaça glimpse of the Proterozoic evolution of SW Fennoscandia. *GFF* 130,1-10.

Sørensen, K. & Winter, J.D., 1989: Deformation and Mass Transport in the Nordre Strømfjord Shear Zone, Central West Greenland, *Fluid Movements—Element Transport and the Composition of the Deep Crust NATO ASI Series*, 281, 171.

Stephens M.P., Ripa, M., Lundström, I., Persson, L., Bergman, T., Ahl, M., Wahlgren, C.-H., Persson, P.-O. & Wickström, L., 2009: Synthesis of the bedrock geology in the Bergslagen region, Fennoscandian shield, south -central Sweden. *Geol. Survey Sweden*, Ba 58, 1-259.

Sun, S.-s. & McDonough, W. F., 1989: Chemical and isotopic systematics of oceanic basalts: implications for mantle composition and processes, *Geological Society, London, Special Publications* 42, 313-345.

Ulmius J., Möller C., & Andersson, J., 2013: High T/P metamorphism at 1.45 Ga: P-T evolution and SIMS U-Pb zircon ages of paragneisses from southernmost Sweden. EGU abstract 2013-12115.

Ulmius, J., Andersson, J., Möller, C., submitted. Hallandian high temperature metamorphism at 1.45 Ga in continent Baltica: P-T evolution and SIMS U-Pb zircon ages of aluminous gneisses, SW Sweden, in: Roberts, N., Viola, G., Slagstad, T. (Eds.), The structural, metamorphic and magmatic evolution of

Mesoproterozoic orogens. Submitted to Precambrian Research (Special issue), June, 2014.

Viola, G., Henderson I.H.C., Bingen B., Hendriks, B.W.H., 2011: The Grenvillian–Sveconorwegian orogeny in Fennoscandia: Back-thrusting and extensional shearing along the "Mylonite Zone", *Precambrian Research* 189, 368-388.

Wahlgren, C.A.-H., Cruden, A.R., Stephens, M.B., 1994: Kinematics of a major fanlike structure in the eastern part of the Sveconorwegian orogen, Baltic Shield, south-central Sweden. *Precambrian Research* 70, 67–91.

Wang, X.-D. & Lindh, A., 1996: Temperature-pressure investigation of the southern part of the Southwest Swedish Granulite Region. *European Journal of Mineralogy* 8,51-67.

Wang, X.-D, Söderlund, U., Lindh, A. & Johansson, L., 1998: U–Pb and Sm–Nd dating of high pressure granulite and upper amphibolite facies rocks from the Southwest Swedish Granulite Region. *Precambrian Research* 92, 319-339.

Winter,J.D., 2010: Principles of igenous and metamorphic petrology, Pearson, 2nd edition.

Wood,B.J., 1975: The influence of pressure, temperature and bulk composition on the appearance of garnet in orthogneisses — an example from South Harris, Scotland, *Earth and Planetary Science Letters* 26, 3, 299-311.

Wood, D.A., Joron, J.-L.,Treuil, M., 1979: A re-appraisal of the use of trace elements to classify and discriminate between magma series erupted in different tectonic settings, *Earth and Planetary Science Letters* 62 , 53-62.

13 Appendix

Appendix A: EDX analysis

Amphibole

	Compound %										Number of ions									
	Na_2O	MgO	Al_2O_3	SiO_2	K_2O	CaO	TiO_2	MnO	FeO	**Totals**	Na^+	Mg^{2+}	Al^{3+}	Si^{4+}	K^+	Ca^{2+}	Ti^{4+}	Mn^{2+}	Fe^{2+}	**Cation Sum**
Gas3A51A Prg	1,34	11,55	12,51	41,44	1,80	11,33	1,79		14,72	96,48	0,39	2,61	2,23	6,28	0,35	1,84	0,20		1,87	15,77
Gas3A52A Prg	1,47	11,21	12,37	41,76	1,72	11,72	2,00		14,76	97,01	0,43	2,52	2,20	6,30	0,33	1,89	0,23		1,86	15,76
Gas3A55A Prg	1,28	11,22	12,39	41,45	1,67	11,78	1,8		14,27	95,86	0,38	2,55	2,22	6,31	0,32	1,92	0,21		1,82	15,73
Gas3A105B Prg	1,44	10,56	11,76	40,22	1,76	11,47	2,23		15,72	95,16	0,43	2,44	2,15	6,24	0,35	1,91	0,26		2,04	15,82
Gas3A124C Prg	1,36	10,91	11,95	41,73	1,69	11,57	2,08		15,48	96,77	0,4	2,47	2,14	6,33	0,33	1,88	0,24		1,96	15,75
Gas3A1311D Prg	1,43	10,63	12,16	40,76	1,6	11,41	2,17		15,27	95,43	0,43	2,44	2,21	6,27	0,31	1,88	0,25		1,96	15,75
Gas3B57A Prg	1,42	11,23	12,47	41,68	1,61	11,90	2,25		15,64	98,20	0,41	2,50	2,20	6,23	0,31	1,91	0,25		1,96	15,77
Gas3B81A Prg	1,41	10,65	12,25	41,67	1,72	11,46	2,28		15,91	97,35	0,41	2,40	2,18	6,29	0,33	1,85	0,26		2,01	15,73
Gas3B82A Prg	1,59	11,48	11,77	42,98	1,65	11,97	2,02	0,11	16,23	99,80	0,46	2,52	2,04	6,34	0,31	1,89	0,22	0,01	2,00	15,79
Gas3B131C Prg	1,41	10,69	11,71	40,44	1,83	11,37	2,13	0,17	15,31	95,06	0,42	2,47	2,14	6,27	0,36	1,89	0,25	0,02	1,98	15,80
KB256D Prg	1,54	10,60	11,69	41,46	1,65	11,50	2,66		15,68	96,78	0,45	2,40	2,09	6,30	0,32	1,87	0,30		1,99	15,72
ML252 Prg	1,34	9,60	12,78	39,83	1,96	11,16	1,94		16,69	95,30	0,40	2,22	2,34	6,19	0,39	1,86	0,23		2,17	15,80
Sö233C Prg	1,55	10,83	12,41	41,55	1,73	11,60	2,15		15,57	97,39	0,45	2,43	2,21	6,27	0,33	1,87	0,24		1,96	15,76
GT302A Fe-Prg	1,49	9,17	11,70	41,28	1,72	11,32	2,42		18,66	97,76	0,44	2,08	2,10	6,30	0,33	1,85	0,28		2,38	15,76
StSD162D Prg	1,39	11,34	12,43	42,88	1,71	11,80	1,80		15,02	98,37	0,40	2,51	2,17	6,36	0,32	1,88	0,20		1,86	15,70
StSD192D Prg	1,13	11,69	12,04	42,82	1,74	12,09	1,64		14,42	97,57	0,09	0,68	0,55	1,67	0,09	0,50	0,05		0,47	4,10
	1,24	12,24	12,33	42,93	1,82	12,07	1,92		14,78	99,33	0,17	1,28	1,02	3,02	0,16	0,91	0,10		0,87	7,53

Biotite

	Compound %										Number of ions									
	Na_2O	MgO	Al_2O_3	SiO_2	K_2O	CaO	TiO_2	FeO	MnO	**Totals**	Na^+	Mg^{2+}	Al^{3+}	Si^{4+}	K^+	Ca^{2+}	Ti^{4+}	Fe^{2+}	Mn^{2+}	**Cation Sum**
Gas3A75A	0,06	13,38	14,49	34,96	9,76	0,00	5,98	15,53	0,00	94,16	0,02	3,05	2,61	5,35	1,91	0,00	0,69	1,99	0,00	15,62
Gas3A76A	0,00	13,72	14,42	35,96	9,75	0,00	6,04	15,63	0,00	95,52	0,00	2,82	2,65	5,41	1,86	0,00	0,70	2,05	0,00	15,49
Gas3A138D	0,00	12,90	15,35	36,86	9,94	0,00	6,36	16,68	0,00	98,09	0,00	3,08	2,56	5,41	1,87	0,00	0,68	1,97	0,00	15,57
Gas3A145D	0,00	12,45	14,52	35,56	9,61	0,00	5,80	16,73	0,00	94,67	0,00	2,83	2,61	5,43	1,87	0,00	0,67	2,14	0,00	15,55
Gas3B83A	0,00	13,14	15,00	36,08	9,89	0,09	5,79	15,73	0,00	95,72	0,00	2,94	2,65	5,42	1,89	0,01	0,65	1,97	0,00	15,55
Gas3B101B	0,00	12,63	14,48	36,01	10,08	0,00	6,14	17,58	0,00	96,90	0,00	2,82	2,56	5,40	1,93	0,00	0,69	2,20	0,00	15,60
Gas3B102B	0,00	12,85	14,18	35,50	9,91	0,00	6,29	16,79	0,00	95,51	0,00	2,91	2,53	5,38	1,92	0,00	0,72	2,13	0,00	15,59
Gas3B103B	0,00	12,98	14,08	36,43	9,58	0,00	6,23	17,30	0,00	96,60	0,00	2,89	2,48	5,45	1,83	0,00	0,70	2,16	0,00	15,52
Gas3B127B	0,00	11,60	14,11	34,88	9,60	0,00	6,08	17,19	0,00	93,46	0,00	2,69	2,58	5,42	1,90	0,00	0,71	2,23	0,00	15,53
Gas3B128B	0,00	11,95	14,44	35,38	9,46	0,00	5,48	17,48	0,00	94,18	0,00	2,74	2,62	5,44	1,86	0,00	0,63	2,25	0,00	15,54
Gas3B1310C	0,00	12,20	14,23	34,74	9,75	0,00	6,03	16,47	0,00	93,41	0,00	2,82	2,60	5,39	1,93	0,00	0,70	2,14	0,00	15,57
GT293A	0,00	10,71	14,12	37,12	9,38	0,00	6,06	19,55	0,00	96,94	0,00	1,20	1,25	2,79	0,90	0,00	0,34	1,23	0,00	7,70
Gt301A	0,00	10,77	13,90	36,82	9,42	0,00	5,78	20,19	0,00	96,89	0,00	1,21	1,24	2,78	0,91	0,00	0,33	1,27	0,00	7,73
KB267D	1,25	10,41	11,65	41,47	1,58	11,71	2,50	15,62	0,00	96,20	0,18	1,13	1,00	3,03	0,15	0,92	0,14	0,95	0,00	7,50
Sö204D	0,00	12,64	14,19	35,77	10,06	0,00	5,77	17,66	0,00	96,09	0,00	2,85	2,53	5,42	1,94	0,00	0,66	2,24	0,00	15,63
Sö205D	0,00	12,36	14,34	35,76	9,84	0,00	5,69	16,76	0,00	94,75	0,00	2,81	2,58	5,46	1,92	0,00	0,65	2,14	0,00	15,56
Sö206D	0,00	12,22	14,04	36,13	9,41	0,00	5,66	17,44	0,00	94,90	0,00	2,77	2,52	5,51	1,83	0,00	0,65	2,22	0,00	15,50
Sö2010D	0,00	12,28	14,26	35,37	10,09	0,00	5,76	17,25	0,00	95,01	0,00	2,80	2,57	5,41	1,97	0,00	0,66	2,21	0,00	15,62
Sö212D	0,00	12,24	14,19	35,29	10,06	0,00	5,91	16,90	0,00	94,60	0,00	2,80	2,57	5,42	1,97	0,00	0,68	2,17	0,00	15,60
StSD61A	0,00	15,36	14,52	37,69	8,80	0,00	4,68	15,38	0,00	96,44	0,00	1,68	1,26	2,77	0,83	0,00	0,26	0,95	0,00	7,75
StSD67A	5,45	0,69	27,31	55,42	0,32	10,32	0,00	1,36	0,00	100,89	0,65	0,06	1,99	3,43	0,03	0,68	0,00	0,07	0,00	6,92
StSD86A	0,00	14,93	14,34	37,55	9,55	0,00	5,36	14,73	0,00	96,45	0,00	1,64	1,25	2,77	0,90	0,00	0,30	0,91	0,00	7,76
StSD87A	0,00	14,90	14,35	37,39	9,41	0,00	5,37	14,83	0,00	96,24	0,00	1,64	1,25	2,76	0,89	0,00	0,30	0,92	0,00	7,76
StSD88A	0,00	14,78	14,44	37,50	9,63	0,00	5,36	14,85	0,00	96,56	0,00	1,62	1,25	2,77	0,91	0,00	0,30	0,92	0,00	7,76
StSD121D	0,00	14,71	14,41	37,44	9,59	0,00	5,39	14,92	0,00	96,46	0,00	1,62	1,25	2,76	0,90	0,00	0,30	0,92	0,00	7,76
StSD122D	0,00	14,44	14,01	37,05	9,45	0,00	5,65	14,68	0,00	95,28	0,00	1,61	1,23	2,77	0,90	0,00	0,32	0,92	0,00	7,75
StSD133D	0,00	14,70	14,21	37,58	9,69	0,00	5,51	14,65	0,25	96,60	0,00	1,62	1,23	2,77	0,91	0,00	0,31	0,90	0,02	7,76
StSD134D	0,00	14,48	14,35	36,91	9,45	0,00	5,52	14,63	0,15	95,51	0,00	1,61	1,26	2,75	0,90	0,00	0,31	0,91	0,01	7,76
StSd141D	0,00	14,17	14,22	37,22	9,47	0,00	5,25	15,31	0,00	95,64	0,00	1,58	1,25	2,78	0,90	0,00	0,29	0,96	0,00	7,75
StSd142D	0,00	14,49	14,30	37,40	9,42	0,00	5,37	15,50	0,00	96,49	0,00	1,60	1,25	2,77	0,89	0,00	0,30	0,96	0,00	7,76
StSD211D	0,00	13,99	14,37	37,44	9,57	0,00	5,60	15,69	0,00	96,66	0,00	1,54	1,25	2,77	0,90	0,00	0,31	0,97	0,00	7,75
StSD212D	0,00	13,75	14,23	37,55	9,39	0,00	5,64	15,61	0,00	96,16	0,00	1,52	1,24	2,79	0,89	0,00	0,31	0,97	0,00	7,72

Appendix A: SEM-analysis data for all samples and minerals.

Pyroxenes

	Compound %											Number of ions																		
	SiO_2	TiO_2	Al_2O_3	Cr_2O_3	FeO	MnO	MgO	CaO	Na_2O	K_2O	Totals	Si^{4+}	Ti^{4+}	Al^{3+}	Cr^{3+}	Fe^{2+}	Mn^{2+}	Mg^{2+}	Ca^{2+}	Na^{+}	K^{+}	Cation Sum	Wo	En	Fs	Ac	Wo	En	Fs
Gas58A opx	50,95	0,00	1,46	0,00	24,88	0,51	21,13	0,35	0,00	0,00	99,28	1,94	0,00	0,07	0,00	0,79	0,02	1,20	0,01	0,00	0,00	4,03	0,71	59,50	39,80	0,00			
Gas62A opx	51,15	0,00	1,51	0,00	26,05	0,00	19,83	0,42	0,00	0,00	98,96	1,96	0,00	0,07	0,00	0,83	0,00	1,13	0,02	0,00	0,00	4,01	0,87	57,13	42,00	0,00			
Gas63A opx	50,48	0,00	1,57	0,00	25,61	0,00	19,93	0,42	0,00	0,00	98,01	1,95	0,00	0,07	0,00	0,83	0,00	1,15	0,02	0,00	0,00	4,02	0,87	57,69	41,43	0,00			
Gas64A opx	50,45	0,00	1,62	0,00	26,06	0,00	19,92	0,62	0,00	0,00	98,67	1,94	0,00	0,07	0,00	0,84	0,00	1,14	0,03	0,00	0,00	4,02	1,28	57,07	41,65	0,00			
Gas68A cpx	50,29	0,00	2,76	0,00	9,90	0,00	12,78	21,84	0,65	0,00	98,22	1,92	0,00	0,12	0,00	0,32	0,00	0,73	0,90	0,05	0,00	4,04	45,07	36,70	15,80	2,43	46,19	37,62	16,19
Gas69A cpx	50,15	0,00	3,06	0,00	10,08	0,00	12,80	21,08	0,72	0,00	97,89	1,92	0,00	0,14	0,00	0,32	0,00	0,73	0,87	0,05	0,00	4,03	43,92	37,11	16,25	2,71	45,15	38,15	16,70
Gas610A cpx	50,34	0,00	2,79	0,00	10,10	0,00	12,76	21,65	0,72	0,00	98,36	1,92	0,00	0,13	0,00	0,32	0,00	0,73	0,89	0,05	0,00	4,04	44,63	36,60	16,09	2,69	45,86	37,61	16,53
Gas611A cpx	50,84	0,00	3,08	0,00	11,94	0,00	13,16	19,50	0,62	0,00	99,14	1,93	0,00	0,14	0,00	0,38	0,00	0,74	0,79	0,05	0,00	4,03	40,46	38,00	19,21	2,33	41,43	38,90	19,67
Gas612A cpx	52,24	0,00	1,59	0,00	9,23	0,00	13,78	22,65	0,44	0,00	99,93	1,96	0,00	0,07	0,00	0,29	0,00	0,77	0,91	0,03	0,00	4,02	45,50	38,52	14,38	1,60	46,24	39,15	14,62
Gas79A cpx	51,39	0,00	1,70	0,00	9,26	0,00	13,56	21,98	0,50	0,00	98,39	1,95	0,00	0,08	0,00	0,29	0,00	0,77	0,90	0,04	0,00	4,03	44,92	38,56	14,67	1,85	45,76	39,29	14,95
Gas710A opx	50,07	0,00	1,49	0,00	24,91	0,00	20,18	0,46	0,00	0,00	97,11	1,95	0,00	0,07	0,00	0,81	0,00	1,17	0,02	0,00	0,00	4,02	0,96	58,63	40,41	0,00			
Gas711A cpx	50,70	0,00	3,13	0,00	9,70	0,00	12,59	21,66	0,78	0,00	98,56	1,93	0,00	0,14	0,00	0,31	0,00	0,71	0,88	0,06	0,00	4,03	45,03	36,42	15,62	2,93	46,39	37,52	16,09
Gas91A cpx	50,95	0,00	2,87	0,00	9,91	0,00	12,92	21,35	0,73	0,00	98,73	1,93	0,00	0,13	0,00	0,31	0,00	0,73	0,87	0,05	0,00	4,03	44,18	37,20	15,89	2,73	45,42	38,25	16,34
Gas92A cpx	50,80	0,00	2,70	0,00	9,78	0,00	13,01	21,88	0,78	0,00	98,95	1,93	0,00	0,12	0,00	0,31	0,00	0,74	0,89	0,06	0,00	4,04	44,70	36,98	15,44	2,88	46,02	38,08	15,89
Gas93A cpx	50,83	0,00	2,96	0,00	9,74	0,00	12,98	21,73	0,75	0,00	98,99	1,93	0,00	0,13	0,00	0,31	0,00	0,73	0,88	0,06	0,00	4,04	44,63	37,10	15,48	2,79	45,91	38,17	15,92
Gas106B cpx	50,94	0,00	2,61	0,00	9,47	0,00	13,01	21,93	0,69	0,00	98,65	1,93	0,00	0,12	0,00	0,30	0,00	0,74	0,89	0,05	0,00	4,03	45,11	37,24	15,08	2,57	46,30	38,22	15,48
Gas112C cpx	50,41	0,00	3,20	0,00	10,05	0,00	12,48	21,91	0,71	0,00	98,76	1,92	0,00	0,14	0,00	0,32	0,00	0,71	0,89	0,05	0,00	4,04	45,33	35,93	16,08	2,66	46,57	36,91	16,52
Gas111C cpx	50,20	0,00	3,35	0,00	12,33	0,00	13,27	19,43	0,67	0,00	99,25	1,91	0,00	0,15	0,00	0,39	0,00	0,75	0,79	0,05	0,00	4,04	39,95	37,97	19,58	2,49	40,97	38,94	20,08
Gas113C cpx	46,23	0,99	7,45	0,47	12,92	0,00	12,24	16,05	1,22	0,44	98,01	1,79	0,03	0,34	0,01	0,42	0,00	0,70	0,66	0,09	0,02	4,07	35,50	37,67	21,94	4,88	37,32	39,61	23,07
Gas131D cpx	51,16	0,00	3,14	0,00	9,66	0,00	12,76	22,12	0,75	0,00	99,59	1,93	0,00	0,14	0,00	0,30	0,00	0,72	0,89	0,05	0,00	4,03	45,41	36,45	15,36	2,79	46,71	37,50	15,80
Gas133D cpx	50,64	0,00	2,88	0,00	10,12	0,00	12,92	21,69	0,80	0,00	99,05	1,92	0,00	0,13	0,00	0,32	0,00	0,73	0,88	0,06	0,00	4,04	44,33	36,74	15,97	2,96	45,68	37,86	16,46
Gas1312D opx	50,32	0,00	1,42	0,00	25,96	0,62	19,81	0,48	0,00	0,00	98,61	1,94	0,00	0,06	0,00	0,84	0,02	1,14	0,02	0,00	0,00	4,03	0,99	56,64	42,38	0,00			
Gas141D cpx	51,32	0,00	2,26	0,00	9,19	0,00	13,48	22,35	0,54	0,00	99,14	1,94	0,00	0,10	0,00	0,29	0,00	0,76	0,90	0,04	0,00	4,03	45,42	38,12	14,46	1,99	46,35	38,90	14,76
Gas142D opx	50,98	0,00	1,32	0,00	25,62	0,69	20,25	0,44	0,00	0,00	99,30	1,95	0,00	0,06	0,00	0,82	0,02	1,15	0,02	0,00	0,00	4,02	0,90	57,44	41,66	0,00			
Gas143D cpx	51,08	0,42	3,01	0,00	10,26	0,00	12,78	21,53	0,78	0,00	99,86	1,92	0,01	0,13	0,00	0,32	0,00	0,72	0,87	0,06	0,00	4,03	44,23	36,54	16,33	2,90	45,55	37,63	16,82
Gas3B52A cpx	50,72	0,00	2,64	0,00	9,87	0,00	13,17	22,03	0,70	0,00	99,13	1,92	0,00	0,12	0,00	0,31	0,00	0,74	0,89	0,05	0,00	4,04	44,74	37,22	15,47	2,57	45,92	38,20	15,88
Gas3B53A cpx	51,52	0,00	2,57	0,00	9,87	0,00	13,17	21,89	0,77	0,00	99,79	1,94	0,00	0,11	0,00	0,31	0,00	0,74	0,88	0,06	0,00	4,04	44,45	37,21	15,51	2,83	45,74	38,30	15,96
Gas3B64A opx	50,90	0,00	1,29	0,00	26,07	0,62	20,16	0,61	0,00	0,00	99,65	1,94	0,00	0,06	0,00	0,83	0,02	1,15	0,02	0,00	0,00	4,03	1,24	56,83	41,93	0,00			
Gas3B65A opx	51,01	0,00	1,61	0,00	25,21	0,26	20,17	0,47	0,00	0,00	98,73	1,95	0,00	0,07	0,00	0,81	0,01	1,15	0,02	0,00	0,00	4,01	0,97	58,03	41,00	0,00			
Gas3B62A cpx	51,79	0,00	2,94	0,00	10,28	0,00	13,24	22,14	0,55	0,00	100,94	1,93	0,00	0,13	0,00	0,32	0,00	0,73	0,88	0,04	0,00	4,03	44,71	37,20	16,08	2,01	45,62	37,97	16,41
Gas3B63A cpx	50,80	0,00	2,80	0,00	9,87	0,00	12,78	22,16	0,76	0,00	99,17	1,93	0,00	0,13	0,00	0,31	0,00	0,72	0,90	0,06	0,00	4,04	45,27	36,33	15,58	2,81	46,58	37,38	16,03
Gas3B66A cpx	51,56	0,00	2,97	0,00	9,75	0,00	12,82	21,97	0,87	0,00	99,94	1,93	0,00	0,13	0,00	0,31	0,00	0,72	0,88	0,06	0,00	4,03	44,90	36,46	15,43	3,22	46,39	37,67	15,94
Gas3B74A cpx	51,45	0,00	2,72	0,00	9,44	0,00	13,37	22,79	0,52	0,00	100,29	1,92	0,00	0,12	0,00	0,30	0,00	0,75	0,91	0,04	0,00	4,03	45,91	37,48	14,71	1,90	46,80	38,20	15,00
Gas3B75A cpx	51,44	0,00	2,70	0,00	9,80	0,00	13,02	22,24	0,62	0,00	99,82	1,93	0,00	0,12	0,00	0,31	0,00	0,73	0,90	0,05	0,00	4,03	45,32	36,92	15,47	2,29	46,38	37,79	15,83
Gas3B77A cpx	51,59	0,00	2,90	0,00	10,59	0,00	13,16	21,62	0,59	0,00	100,45	1,93	0,00	0,13	0,00	0,33	0,00	0,73	0,87	0,04	0,00	4,03	43,94	37,22	16,68	2,17	44,91	38,04	17,05
Gas3B91B opx	52,01	0,00	1,35	0,00	26,25	0,00	20,77	0,00	0,00	0,00	100,38	1,96	0,00	0,06	0,00	0,83	0,00	1,17	0,00	0,00	0,00	4,01	0,00	58,59	41,41	0,00			
Gas3B92B opx	51,38	0,00	1,54	0,00	25,27	0,73	20,52	0,43	0,00	0,00	99,87	1,95	0,00	0,07	0,00	0,80	0,02	1,16	0,02	0,00	0,00	4,02	0,87	58,04	41,08	0,00			
Gas3B94B opx	51,79	0,00	1,57	0,00	26,47	0,00	20,48	0,49	0,00	0,00	100,80	1,95	0,00	0,07	0,00	0,83	0,00	1,15	0,02	0,00	0,00	4,02	0,99	57,51	41,51	0,00			
Gas3B113B cpx	51,36	0,00	2,86	0,00	10,12	0,00	13,42	22,54	0,49	0,00	100,79	1,92	0,00	0,13	0,00	0,32	0,00	0,75	0,90	0,04	0,00	4,04	45,15	37,41	15,67	1,78	45,97	38,08	15,95
Gas3B114B cpx	52,23	0,00	3,20	0,00	10,14	0,00	12,99	22,26	0,76	0,00	101,58	1,93	0,00	0,14	0,00	0,31	0,00	0,71	0,88	0,05	0,00	4,03	44,91	36,47	15,85	2,77	46,19	37,51	16,30
Gas3B121B cpx	50,38	0,00	2,78	0,00	9,67	0,00	13,00	21,92	0,59	0,00	98,34	1,92	0,00	0,13	0,00	0,31	0,00	0,74	0,90	0,04	0,00	4,04	45,14	37,26	15,40	2,20	46,16	38,09	15,75
Gas3B126B cpx	49,40	0,00	2,87	0,00	10,26	0,00	12,63	21,57	0,59	0,00	97,32	1,91	0,00	0,13	0,00	0,33	0,00	0,73	0,89	0,04	0,00	4,04	44,81	36,51	16,46	2,22	45,83	37,34	16,83
Gas3B123B cpx	50,24	0,00	2,96	0,00	9,90	0,00	12,76	21,40	0,77	0,00	98,03	1,92	0,00	0,13	0,00	0,32	0,00	0,73	0,88	0,06	0,00	4,04	44,39	36,84	15,88	2,89	45,72	37,93	16,35
Gas3B138C cpx	50,43	0,00	3,33	0,00	10,55	0,00	12,46	20,78	0,89	0,00	98,44	1,92	0,00	0,15	0,00	0,34	0,00	0,71	0,85	0,07	0,00	4,03	43,39	36,20	17,05	3,36	44,90	37,46	17,64
Gas3B151C opx	50,61	0,00	1,60	0,00	26,20	0,57	19,93	0,42	0,00	0,00	98,76	1,95	0,00	0,07	0,00	0,84	0,01	1,14	0,02	0,00	0,00	4,02	0,86	56,68	42,46	0,00			
Gas3B152C opx	50,70	0,00	1,47	0,00	25,13	0,49	20,23	0,36	0,00	0,00	98,38	1,95	0,00	0,07	0,00	0,81	0,02	1,16	0,01	0,00	0,00	4,02	0,74	58,12	41,13	0,00			
Gas3B153C opx	50,87	0,00	1,58	0,00	26,22	0,46	20,06	0,32	0,00	0,00	99,51	1,94	0,00	0,07	0,00	0,84	0,01	1,14	0,01	0,00	0,00	4,02	0,65	57,02	42,32	0,00			
Gas3B154C opx	50,37	0,00	1,26	0,00	25,36	0,75	19,91	0,48	0,00	0,00	98,13	1,95	0,00	0,06	0,00	0,82	0,02	1,15	0,02	0,00	0,00	4,02	0,99	57,16	41,84	0,00			

Gas3B164C cpx	51,08	0,00	2,88	0,00	9,89	0,00	12,63	21,37	0,77	0,10	98,76	1,94	0,00	0,13	0,00	0,31	0,00	0,71	0,87	0,06	0,00	4,03	44,52	36,61	15,97	2,90	45,85	37,71	16,45
Gas3B165C cpx	50,07	0,00	2,94	0,00	9,79	0,00	12,77	21,55	0,82	0,00	98,76	1,92	0,00	0,13	0,00	0,31	0,00	0,73	0,89	0,06	0,00	4,04	44,56	36,74	15,63	3,07	45,97	37,91	16,12
Gas3B191E cpx	51,38	0,00	2,52	0,00	9,79	0,00	13,08	22,34	0,00	0,00	98,76	1,94	0,00	0,11	0,00	0,31	0,00	0,74	0,90	0,00	0,00	4,00	46,37	37,78	15,85	0,00	46,37	37,78	15,85
Gas3B192E cpx	51,00	0,00	2,87	0,00	9,75	0,00	12,89	21,24	0,00	0,00	98,76	1,95	0,00	0,13	0,00	0,31	0,00	0,73	0,87	0,00	0,00	3,99	45,38	38,32	16,30	0,00	45,38	38,32	16,30
KB222B cpx	50,85	0,00	3,03	0,00	10,89	0,00	12,64	21,05	0,55	0,00	99,01	1,93	0,00	0,14	0,00	0,35	0,00	0,72	0,86	0,04	0,00	4,02	43,78	36,58	17,58	2,07	44,70	37,35	17,95
KB223B cpx	51,45	0,00	2,56	0,00	10,05	0,00	12,63	21,24	0,50	0,00	98,43	1,96	0,00	0,11	0,00	0,32	0,00	0,72	0,86	0,04	0,00	4,01	44,67	36,96	16,47	1,90	45,53	37,68	16,79
KB241C cpx	51,23	0,55	3,13	0,62	9,11	0,00	12,34	22,11	0,54	0,00	99,63	1,92	0,02	0,14	0,02	0,29	0,00	0,69	0,89	0,04	0,00	4,00	46,68	36,25	15,00	2,06	47,66	37,02	15,32
KB242C cpx	51,66	0,00	3,08	0,00	11,01	0,00	12,74	20,75	0,60	0,00	99,84	1,94	0,00	0,14	0,00	0,35	0,00	0,71	0,83	0,04	0,00	4,01	43,11	36,84	17,79	2,26	44,11	37,69	18,20
KB253D cpx	42,05	2,95	12,02	0,00	16,18	0,00	10,42	11,45	1,62	1,60	98,29	1,64	0,09	0,55	0,00	0,53	0,00	0,61	0,48	0,12	0,08	4,10	27,78	35,18	29,92	7,11	29,91	37,88	32,21
KB254D cpx	42,14	2,99	11,91	0,00	16,20	0,00	10,85	11,64	1,54	1,58	98,85	1,64	0,09	0,55	0,00	0,53	0,00	0,63	0,48	0,12	0,08	4,10	27,81	36,07	29,46	6,66	29,79	38,64	31,57
KB268D cpx	51,20	0,00	3,61	0,00	12,37	0,00	12,97	19,83	0,58	0,00	100,56	1,92	0,00	0,16	0,00	0,39	0,00	0,72	0,80	0,04	0,00	4,02	40,87	37,20	19,78	2,16	41,77	38,02	20,21
KB273A opx	53,26	0,00	1,18	0,00	25,46	0,00	21,21	0,53	0,00	0,00	101,64	1,97	0,00	0,05	0,00	0,79	0,00	1,17	0,02	0,00	0,00	4,00	1,06	59,14	39,79	0,00			
KB274A opx	53,37	0,00	1,16	0,00	26,31	0,00	20,74	0,00	0,00	0,00	101,58	1,98	0,00	0,05	0,00	0,82	0,00	1,15	0,00	0,00	0,00	3,99	0,00	58,39	41,61	0,00			
KB293A cpx	52,86	0,00	2,88	0,00	10,42	0,00	13,03	21,88	0,63	0,00	101,70	1,95	0,00	0,12	0,00	0,32	0,00	0,72	0,86	0,04	0,00	4,01	44,42	36,81	16,45	2,31	45,47	37,68	16,84
KB294A cpx	51,24	0,00	2,76	0,00	9,84	0,00	12,75	21,94	0,66	0,00	99,19	1,94	0,00	0,12	0,00	0,31	0,00	0,72	0,89	0,05	0,00	4,03	45,23	36,58	15,73	2,46	46,37	37,50	16,13
KB311A cpx	52,91	0,00	2,94	0,00	9,72	0,00	13,12	22,61	0,47	0,00	101,77	1,94	0,00	0,13	0,00	0,30	0,00	0,72	0,89	0,03	0,00	4,01	45,88	37,04	15,35	1,73	46,68	37,69	15,62
KB314A cpx	51,90	0,00	2,94	0,00	10,00	0,00	12,99	22,73	0,51	0,00	101,07	1,93	0,00	0,13	0,00	0,31	0,00	0,72	0,90	0,04	0,00	4,03	45,94	36,53	15,67	1,87	46,81	37,23	15,97
Sö153B cpx	50,48	0,00	2,75	0,00	10,01	0,00	12,65	22,04	0,64	0,00	98,57	1,93	0,00	0,12	0,00	0,32	0,00	0,72	0,90	0,05	0,00	4,04	45,40	36,26	15,95	2,39	46,51	37,15	16,34
Sö161B cpx	49,94	0,38	3,12	0,00	12,85	0,00	13,15	18,89	0,85	0,00	99,18	1,90	0,01	0,14	0,00	0,41	0,00	0,75	0,77	0,06	0,00	4,05	38,84	37,62	20,38	3,16	40,10	38,85	21,05
Sö162B cpx	50,22	0,00	3,35	0,00	9,86	0,00	12,30	21,83	0,80	0,00	98,36	1,92	0,00	0,15	0,00	0,31	0,00	0,70	0,89	0,06	0,00	4,04	45,46	35,64	15,88	3,01	46,87	36,75	16,38
Sö171B opx	50,79	0,00	1,45	0,00	27,31	0,00	19,32	0,62	0,00	0,00	99,49	1,95	0,00	0,07	0,00	0,88	0,00	1,10	0,03	0,00	0,00	4,02	1,27	55,18	43,54	0,00	1,27	55,18	43,54
Sö174B cpx	50,40	0,40	2,78	0,00	10,28	0,00	12,54	21,67	0,00	0,00	98,07	1,93	0,01	0,13	0,00	0,33	0,00	0,72	0,89	0,00	0,00	4,00	45,96	37,01	17,03	0,00	45,96	37,01	17,03
Sö221D cpx	50,64	0,00	2,53	0,00	10,94	0,00	12,89	21,38	0,00	0,00	98,38	1,94	0,00	0,11	0,00	0,35	0,00	0,73	0,88	0,00	0,00	4,01	44,69	37,50	17,81	0,00	44,69	37,50	17,81
Sö222D cpx	50,86	0,00	2,24	0,00	10,01	0,00	13,15	21,89	0,00	0,00	98,15	1,94	0,00	0,10	0,00	0,32	0,00	0,75	0,90	0,00	0,00	4,01	45,62	38,13	16,25	0,00	45,62	38,13	16,25
Sö2210D opx	50,45	0,00	1,25	0,00	27,30	0,00	19,41	0,45	0,00	0,00	98,86	1,95	0,00	0,06	0,00	0,88	0,00	1,12	0,02	0,00	0,00	4,02	0,93	55,52	43,55	0,00			
GT288A opx	51,52	0,00	1,09	0,00	30,27	0,00	17,35	0,46	0,00	0,00	100,69	1,97	0,00	0,05	0,00	0,97	0,00	0,99	0,02	0,00	0,00	4,00	0,95	50,07	48,97	0,00			
GT289A opx	52,03	0,00	1,21	0,00	29,78	0,00	17,01	0,61	0,00	0,00	100,64	1,99	0,00	0,05	0,00	0,95	0,00	0,97	0,02	0,00	0,00	3,99	1,28	49,72	49,00	0,00			
GT294A cpx	52,41	0,00	2,21	0,00	12,62	0,00	11,94	21,76	0,76	0,00	101,70	1,95	0,00	0,10	0,00	0,39	0,00	0,66	0,87	0,05	0,00	4,03	43,93	33,54	19,75	2,78	45,18	34,50	20,31
GT295A cpx	51,64	0,00	1,97	0,00	12,26	0,00	11,85	21,63	0,59	0,00	99,94	1,96	0,00	0,09	0,00	0,39	0,00	0,67	0,88	0,04	0,00	4,02	44,41	33,86	19,54	2,19	45,41	34,62	19,98
GT311A cpx	51,64	0,00	2,27	0,00	12,06	0,00	11,46	21,44	0,67	0,00	99,54	1,96	0,00	0,10	0,00	0,38	0,00	0,65	0,87	0,05	0,00	4,01	44,69	33,24	19,55	2,53	45,84	34,10	20,06
GT312A cpx	50,89	0,00	2,29	0,00	11,83	0,00	11,49	21,20	0,64	0,00	98,34	1,96	0,00	0,10	0,00	0,38	0,00	0,66	0,87	0,05	0,00	4,02	44,59	33,63	19,34	2,44	45,71	34,47	19,82
GT313A cpx	51,36	0,00	1,96	0,00	12,24	0,00	11,93	21,05	0,66	0,00	99,20	1,96	0,00	0,09	0,00	0,39	0,00	0,68	0,86	0,05	0,00	4,02	43,54	34,34	19,65	2,47	44,64	35,21	20,15
GT317A cpx	52,09	0,00	1,17	0,00	11,40	0,00	12,54	22,07	0,41	0,00	99,68	1,97	0,00	0,05	0,00	0,36	0,00	0,71	0,89	0,03	0,00	4,02	44,93	35,52	18,04	1,51	45,62	36,07	18,31
GT318A cpx	51,59	0,00	1,89	0,00	11,70	0,00	11,77	21,79	0,57	0,00	99,31	1,96	0,00	0,08	0,00	0,37	0,00	0,67	0,89	0,04	0,00	4,02	45,12	33,91	18,83	2,14	46,10	34,65	19,24
GT324A opx	50,75	0,00	1,05	0,00	30,35	0,00	16,45	0,57	0,00	0,00	99,17	1,98	0,00	0,05	0,00	0,99	0,00	0,96	0,02	0,00	0,00	4,00	1,21	48,53	50,26	0,00			
GT325A opx	50,50	0,00	1,04	0,00	29,92	0,00	16,21	0,48	0,00	0,00	98,15	1,99	0,00	0,05	0,00	0,98	0,00	0,95	0,02	0,00	0,00	3,99	1,03	48,56	50,41	0,00			
GT334A cpx	51,25	0,00	2,16	0,00	12,13	0,00	11,56	21,05	0,51	0,00	98,66	1,96	0,00	0,10	0,00	0,39	0,00	0,66	0,86	0,04	0,00	4,01	44,31	33,86	19,89	1,94	45,19	34,53	20,28
GT336A opx	49,58	0,00	1,38	0,00	30,72	0,00	15,33	0,80	0,00	0,00	97,81	1,97	0,00	0,06	0,00	1,02	0,00	0,91	0,03	0,00	0,00	4,00	1,73	46,25	52,02	0,00			
StSD93A cpx	52,71	0,00	2,06	0,00	8,27	0,00	13,91	22,91	0,50	0,00	100,36	1,96	0,00	0,09	0,00	0,26	0,00	0,77	0,91	0,04	0,00	4,02	46,19	39,03	12,96	1,82	47,05	39,75	13,20
StSD114A opx	51,98	0,00	1,68	0,00	24,57	0,53	21,00	0,42	0,00	0,00	100,18	1,95	0,00	0,07	0,00	0,77	0,02	1,18	0,02	0,00	0,00	4,01	0,85	59,40	39,74	0,00			
StSD115A opx	52,24	0,00	1,71	0,00	24,58	0,60	20,65	0,76	0,00	0,00	100,54	1,96	0,00	0,08	0,00	0,77	0,02	1,15	0,03	0,00	0,00	4,01	1,55	58,49	39,96	0,00			
StSD81A cpx	52,84	0,00	2,74	0,00	9,23	0,00	13,39	22,27	0,70	0,00	101,17	1,95	0,00	0,12	0,00	0,28	0,00	0,74	0,88	0,05	0,00	4,02	45,13	37,76	14,54	2,57	46,32	38,76	14,92
StSD82A cpx	52,11	0,00	2,55	0,00	9,51	0,00	13,23	22,26	0,63	0,00	100,29	1,94	0,00	0,11	0,00	0,30	0,00	0,74	0,89	0,05	0,00	4,02	45,25	37,43	15,00	2,32	46,33	38,31	15,36
StSD84A cpx	52,23	0,00	2,79	0,00	9,58	0,00	13,11	22,37	0,67	0,00	100,75	1,94	0,00	0,12	0,00	0,30	0,00	0,73	0,89	0,05	0,00	4,02	45,41	37,04	15,09	2,46	46,56	37,97	15,47
StSD85A cpx	52,62	0,00	2,20	0,00	8,77	0,00	13,62	22,63	0,52	0,00	100,36	1,95	0,00	0,10	0,00	0,27	0,00	0,75	0,90	0,04	0,00	4,02	45,86	38,41	13,82	1,91	46,76	39,16	14,09
StSD62A opx	52,40	0,00	1,84	0,00	24,27	0,62	20,75	1,07	0,00	0,00	100,95	1,95	0,00	0,08	0,00	0,76	0,02	1,15	0,04	0,00	0,00	4,01	2,17	58,51	39,32	0,00			
StSD67A opx	52,47	0,00	1,57	0,00	24,51	0,56	21,12	0,52	0,00	0,00	100,75	1,96	0,00	0,07	0,00	0,77	0,02	1,18	0,02	0,00	0,00	4,01	1,05	59,43	39,52	0,00			
StSD124D cpx	52,25	0,00	3,13	0,00	9,53	0,00	13,12	22,16	0,56	0,00	100,75	1,94	0,00	0,14	0,00	0,30	0,00	0,73	0,88	0,04	0,00	4,01	45,37	37,38	15,17	2,07	46,33	38,17	15,50
StSD131D cpx	51,74	0,00	2,85	0,00	8,92	0,00	13,25	22,56	0,59	0,00	99,91	1,93	0,00	0,13	0,00	0,28	0,00	0,74	0,90	0,04	0,00	4,02	46,05	37,64	14,13	2,18	47,08	38,48	14,44
StSD132D cpx	52,10	0,00	3,03	0,00	9,00	0,00	13,09	22,20	0,66	0,00	100,08	1,94	0,00	0,13	0,00	0,28	0,00	0,73	0,89	0,05	0,00	4,02	45,67	37,48	14,39	2,46	46,82	38,42	14,76
StSd143D cpx	52,50	0,00	2,80	0,00	8,89	0,22	13,21	22,25	0,71	0,00	100,58	1,95	0,00	0,12	0,00	0,28	0,01	0,73	0,88	0,05	0,00	4,02	45,41	37,52	14,45	2,62	46,63	38,53	14,84

StSd144D cpx	53,23	0,00	1,95	0,00	8,26	0,00	14,16	22,55	0,61	0,00	100,76	1,96	0,00	0,08	0,00	0,25	0,00	0,78	0,89	0,04	0,00	4,02	45,30	39,58	12,90	2,22	46,33	40,48	13,19
StSD146D opx	52,36	0,00	1,57	0,00	24,38	0,59	20,97	0,44	0,00	0,00	100,31	1,96	0,00	0,07	0,00	0,76	0,02	1,17	0,02	0,00	0,00	4,00	0,90	59,43	39,67	0,00			
StSD151D opx	53,24	0,00	1,72	0,00	23,82	0,58	21,75	0,40	0,00	0,00	101,51	1,96	0,00	0,07	0,00	0,73	0,02	1,20	0,02	0,00	0,00	4,00	0,80	60,88	38,32	0,00			
StSD152D opx	52,87	0,00	1,66	0,00	24,12	0,74	21,14	0,43	0,00	0,00	100,96	1,96	0,00	0,07	0,00	0,75	0,02	1,17	0,02	0,00	0,00	4,00	0,87	59,71	39,41	0,00			
StSD153D cpx	52,17	0,00	3,01	0,00	9,53	0,00	13,01	22,10	0,63	0,00	100,45	1,94	0,00	0,13	0,00	0,30	0,00	0,72	0,88	0,05	0,00	4,02	45,33	37,14	15,20	2,34	46,42	38,02	15,56
StSD154D cpx	52,03	0,00	3,00	0,00	9,06	0,00	12,99	22,21	0,58	0,00	99,87	1,94	0,00	0,13	0,00	0,28	0,00	0,72	0,89	0,04	0,00	4,01	45,90	37,36	14,57	2,17	46,92	38,19	14,89
StSD171D opx	52,44	0,00	1,59	0,00	24,51	0,70	21,03	0,39	0,00	0,00	100,66	1,96	0,00	0,07	0,00	0,77	0,02	1,17	0,02	0,00	0,00	4,01	0,79	59,34	39,87	0,00			
StSD173D opx	52,80	0,00	1,75	0,00	24,11	0,48	21,27	0,54	0,00	0,00	100,95	1,96	0,00	0,08	0,00	0,75	0,02	1,18	0,02	0,00	0,00	4,00	1,09	60,00	38,91	0,00			
StSD224D opx	52,70	0,00	1,44	0,00	24,34	0,55	20,99	0,52	0,00	0,00	100,54	1,97	0,00	0,06	0,00	0,76	0,02	1,17	0,02	0,00	0,00	4,00	1,06	59,41	39,53	0,00			
StSD225D opx	52,52	0,00	1,46	0,00	23,77	0,90	21,02	0,45	0,00	0,00	100,12	1,97	0,00	0,06	0,00	0,74	0,03	1,17	0,02	0,00	0,00	4,00	0,92	59,73	39,35	0,00			

Garnet

	Compound %								Number of ions							
	Na_2O	MgO	Al_2O_3	SiO_2	CaO	MnO	FeO	**Totals**	Na^{+}	Mg^{2+}	Al^{3+}	Si^{4+}	Ca^{2+}	Mn^{2+}	Fe^{2+}	**Cation Sum**
Gas3A3L1A	0,00	5,38	21,59	37,60	6,39	2,08	25,94	98,98	0,00	0,63	2,01	2,97	0,54	0,14	1,72	8,01
Gas3A3L2A	0,00	5,37	21,36	37,28	6,63	2,19	26,06	98,89	0,00	0,64	2,00	2,96	0,56	0,15	1,73	8,04
Gas3A3L3A	0,00	5,41	21,40	37,79	6,57	2,04	26,10	99,31	0,00	0,64	1,99	2,98	0,56	0,14	1,72	8,03
Gas3A3L4A	0,00	5,44	21,62	37,23	6,72	2,29	25,51	98,81	0,00	0,64	2,02	2,95	0,57	0,15	1,69	8,02
Gas3A3L5A	0,00	5,60	21,38	37,76	6,36	2,02	25,69	98,81	0,00	0,66	1,99	2,99	0,54	0,14	1,70	8,02
Gas3A3L6A	0,00	5,34	21,31	37,77	6,79	1,89	25,55	98,65	0,00	0,63	1,99	2,99	0,58	0,13	1,69	8,01
Gas3A3L7A	0,00	5,24	21,61	37,65	6,25	2,04	25,69	98,48	0,00	0,62	2,02	2,99	0,53	0,14	1,71	8,01
Gas3A4L1A	0,00	5,22	21,49	37,81	6,42	2,31	25,78	99,03	0,00	0,61	2,00	2,99	0,54	0,15	1,70	7,99
Gas3A4L2A	0,00	5,19	21,56	37,35	6,73	1,98	26,01	98,82	0,00	0,61	2,02	2,96	0,57	0,13	1,73	8,02
Gas3A4L3A	0,00	5,23	21,30	37,94	6,71	1,96	26,42	99,56	0,00	0,61	1,98	2,99	0,57	0,13	1,74	8,02
Gas3A4L4A	0,00	5,23	21,59	38,11	6,55	2,02	26,23	99,73	0,00	0,61	2,00	2,99	0,55	0,13	1,72	8,00
Gas3A56A	0,00	4,48	21,56	37,50	6,58	2,14	27,57	99,83	0,00	0,53	2,01	2,97	0,56	0,14	1,82	8,03
Gas3A7L1A	0,00	5,64	21,94	38,48	6,61	1,92	25,37	99,96	0,00	0,65	2,01	3,00	0,55	0,13	1,65	7,99
Gas3A7L2A	0,00	5,65	22,05	38,48	7,21	1,79	25,60	100,78	0,00	0,65	2,01	2,98	0,60	0,12	1,66	8,02
Gas3A7L3A	0,00	5,51	21,88	38,73	7,38	1,79	24,65	99,94	0,00	0,64	2,00	3,01	0,61	0,12	1,60	7,98
Gas3A7L4A	0,00	5,64	21,95	37,83	6,60	2,01	25,34	99,37	0,00	0,66	2,03	2,97	0,55	0,13	1,66	8,00
Gas3A94A	0,00	5,34	21,72	37,52	6,60	2,01	26,69	99,88	0,00	0,63	2,01	2,95	0,56	0,13	1,76	8,04
Gas3A10L1B	0,00	6,02	22,52	38,53	6,33	1,77	25,69	100,86	0,00	0,69	2,05	2,97	0,52	0,12	1,66	8,01
Gas3A10L2B	0,00	6,12	22,38	38,28	6,81	1,61	25,47	100,67	0,00	0,71	2,04	2,96	0,56	0,11	1,65	8,03
Gas3A10L3B	0,00	5,78	22,29	38,41	7,01	1,69	25,49	100,67	0,00	0,67	2,03	2,97	0,58	0,11	1,65	8,01
Gas3A121C	0,00	5,68	22,18	38,11	7,03	2,01	26,62	101,63	0,00	0,65	2,02	2,94	0,58	0,13	1,72	8,04
Gas3A122C	0,00	5,59	22,06	38,33	7,72	2,12	25,78	101,60	0,00	0,64	2,01	2,96	0,64	0,14	1,66	8,05
Gas3A139D	0,00	4,94	21,85	37,62	6,46	2,23	26,89	99,99	0,00	0,58	2,03	2,96	0,54	0,15	1,77	8,03
Gas3A1310D	0,00	5,30	21,40	37,69	6,42	1,74	27,17	99,72	0,00	0,62	1,99	2,97	0,54	0,12	1,79	8,03
Gas3B1L1A	0,00	5,79	21,80	38,25	6,32	1,98	25,09	99,23	0,00	0,68	2,01	3,00	0,53	0,13	1,64	7,99
Gas3B1L2A	0,00	5,87	21,98	38,67	6,90	1,83	25,15	100,40	0,00	0,68	2,01	3,00	0,57	0,12	1,63	8,01
Gas3B1L3A	0,00	5,93	21,88	37,79	7,98	1,57	25,05	100,20	0,00	0,69	2,01	2,95	0,67	0,10	1,63	8,05
Gas3B1L4A	0,00	5,63	21,91	38,34	7,27	1,63	24,97	99,75	0,00	0,65	2,01	2,99	0,61	0,11	1,63	8,00
Gas3B1L5A	0,00	5,43	21,41	37,63	6,67	1,78	24,47	97,39	0,00	0,65	2,01	3,00	0,57	0,12	1,63	7,98
Gas3B1L5'A	0,00	5,76	21,33	37,96	7,04	1,36	24,56	98,01	0,00	0,68	1,99	3,01	0,60	0,09	1,63	8,00
Gas3B1L6A	0,00	5,32	21,55	37,95	6,37	1,81	27,01	100,01	0,00	0,62	1,99	2,98	0,54	0,12	1,77	8,02
Gas3B9L1B	0,00	5,69	21,94	38,42	6,39	1,75	26,67	100,87	0,00	0,66	2,01	2,98	0,53	0,11	1,73	8,02
Gas3B9L2B	0,00	5,76	21,67	38,17	7,03	2,26	25,74	100,63	0,00	0,67	1,99	2,97	0,59	0,15	1,68	8,04
Gas3B9L3B	0,00	5,80	22,01	37,99	6,71	2,09	26,60	101,21	0,00	0,67	2,01	2,95	0,56	0,14	1,73	8,05
Gas3B9L4B	0,00	5,81	22,19	39,58	6,35	2,12	26,78	102,83	0,00	0,66	1,99	3,00	0,52	0,14	1,70	8,00
Gas3B9L5B	0,00	5,77	20,00	36,54	6,14	1,48	25,75	95,68	0,00	0,70	1,93	3,00	0,54	0,10	1,77	8,04
Gas3B104B	0,00	5,44	21,92	38,38	6,38	2,35	26,01	100,47	0,00	0,63	2,01	2,99	0,53	0,16	1,69	8,01
Gas3B10L1B	0,00	5,56	22,05	38,66	6,80	2,08	25,86	101,00	0,00	0,64	2,01	2,99	0,56	0,14	1,67	8,01
Gas3B10L2B	0,00	5,36	21,99	38,58	6,86	2,20	26,34	101,34	0,00	0,62	2,00	2,98	0,57	0,14	1,70	8,02
Gas3B10L3B	0,00	5,63	22,28	39,17	6,92	1,78	25,79	101,57	0,00	0,64	2,01	3,00	0,57	0,12	1,65	7,99
Gas3B13L1C	0,00	5,32	21,58	37,71	6,70	1,37	26,24	98,92	0,00	0,63	2,01	2,98	0,57	0,09	1,73	8,01
Gas3B13L2C	0,00	5,67	21,91	37,73	6,42	1,62	25,73	99,08	0,00	0,66	2,03	2,97	0,54	0,11	1,69	8,01
Gas3B13L3C	0,00	5,74	21,63	37,75	6,47	1,73	25,91	99,23	0,00	0,67	2,01	2,97	0,55	0,12	1,71	8,02
Gas3B13L4C	0,00	5,57	21,52	37,43	6,89	2,01	26,19	99,60	0,00	0,65	2,00	2,95	0,58	0,13	1,73	8,05
Gas3B13L5C	0,00	5,40	21,84	37,14	6,47	1,69	25,71	98,24	0,00	0,64	2,05	2,96	0,55	0,11	1,71	8,02
Gas3B14L1C	0,00	4,94	21,18	37,06	6,40	2,10	26,17	97,84	0,00	0,59	2,00	2,98	0,55	0,14	1,76	8,02
Gas3B14L2C	0,00	5,28	21,56	37,07	6,24	1,85	26,30	98,30	0,00	0,63	2,03	2,96	0,53	0,12	1,76	8,03
Gas3B14L3C	0,00	5,32	21,43	36,98	6,57	2,05	26,29	98,64	0,00	0,63	2,01	2,95	0,56	0,14	1,75	8,05
Gas3B16L1C	0,00	5,19	21,77	37,59	6,35	2,25	26,88	100,04	0,00	0,61	2,02	2,96	0,53	0,15	1,77	8,04
Gas3B16L2C	0,00	5,29	21,58	37,52	6,48	2,01	26,74	99,61	0,00	0,62	2,01	2,96	0,55	0,13	1,76	8,04
Gas3B16L3C	0,00	5,44	21,47	37,99	6,12	2,08	26,09	99,19	0,00	0,64	2,00	3,00	0,52	0,14	1,72	8,01
Gas3B196E	0,00	5,58	21,82	37,64	6,30	1,88	26,52	99,74	0,00	0,65	2,02	2,96	0,53	0,12	1,74	8,03
Gas3B197E	0,00	5,69	21,16	37,75	6,78	1,82	26,28	99,48	0,00	0,67	1,97	2,98	0,57	0,12	1,73	8,04
Gas3B198E	1,48	4,37	22,22	40,06	6,95	1,42	21,53	98,04	0,22	0,51	2,04	3,12	0,58	0,09	1,40	7,97
GT281A	0,00	3,98	21,58	37,90	6,97	1,41	28,29	100,12	0,00	0,47	2,01	2,99	0,59	0,09	1,87	8,01
GT282A	0,00	3,81	20,97	38,29	7,03	1,23	28,79	100,11	0,00	0,45	1,95	3,02	0,60	0,08	1,90	3,03
GT283A	0,00	4,23	20,89	37,97	7,14	1,27	28,78	100,28	0,00	0,50	1,94	3,00	0,60	0,08	1,90	8,03
GT284A	0,00	4,10	20,86	38,30	6,81	1,44	28,11	99,63	0,00	0,48	1,95	3,03	0,58	0,10	1,86	8,00
GT285A	0,00	3,87	21,22	38,15	6,82	1,15	27,72	98,92	0,00	0,46	1,99	3,03	0,58	0,08	1,84	7,98
GT291A	0,00	4,45	20,83	38,07	6,60	1,37	28,16	99,48	0,00	0,53	1,95	3,02	0,56	0,09	1,87	8,01
GT292A	0,00	4,46	21,46	37,99	6,34	1,32	28,57	100,14	0,00	0,52	1,99	2,99	0,54	0,09	1,88	8,01
GT305A	0,00	16,14	0,92	50,31	0,67	0,58	29,48	98,10	0,00	1,90	0,09	3,97	0,06	0,04	1,94	7,99
KB211B	0,20	6,19	22,04	38,74	6,64	0,93	25,86	100,59	0,03	0,71	2,01	2,99	0,55	0,06	1,67	8,02
KB212B	0,00	6,41	21,51	39,30	6,37	0,83	25,76	100,18	0,00	0,74	1,96	3,04	0,53	0,05	1,66	7,98
KB213B	0,12	6,54	21,83	38,24	6,40	0,56	25,90	99,59	0,02	0,76	2,01	2,98	0,53	0,04	1,69	8,03
KB214B	0,00	6,14	21,38	38,54	7,17	1,00	25,19	99,43	0,00	0,71	1,97	3,01	0,60	0,07	1,65	8,01
KB215B	0,13	6,31	21,43	38,86	6,30	0,84	25,25	99,12	0,02	0,73	1,97	3,03	0,53	0,06	1,65	7,99
KB216B	-0,05	5,94	21,13	38,49	7,31	1,06	24,52	98,41	-0,01	0,70	1,96	3,03	0,62	0,07	1,61	7,98
KB23L1C	0,00	5,88	21,83	38,89	6,66	0,97	26,41	100,64	0,00	0,68	1,99	3,01	0,55	0,06	1,71	8,00
KB23L2C	0,00	6,03	21,60	38,68	6,70	1,37	26,36	100,76	0,00	0,70	1,97	3,00	0,56	0,09	1,71	8,02
KB23L3C	0,00	6,16	21,27	39,99	6,65	1,02	26,89	101,98	0,00	0,70	1,91	3,05	0,54	0,07	1,72	7,99
KB275A	0,00	5,87	21,86	39,08	6,82	1,39	26,86	101,87	0,00	0,67	1,98	3,00	0,56	0,09	1,72	8,02

KB276A	0,00	6,08	21,69	39,02	6,57	0,93	26,57	100,88	0,00	0,70	1,97	3,01	0,54	0,06	1,71	8,00
KB27L5A	0,00	6,55	22,46	39,82	6,64	0,83	26,55	102,85	0,00	0,74	2,00	3,00	0,54	0,05	1,67	8,00
Sö16L1B	0,00	5,40	21,69	38,19	6,73	0,90	27,33	100,24	0,00	0,63	2,00	2,98	0,56	0,06	1,79	8,02
Sö16L2B	0,00	5,49	21,85	38,47	6,70	0,98	27,09	100,57	0,00	0,64	2,00	2,99	0,56	0,06	1,76	8,01
Sö16L3B	0,00	5,49	21,71	37,60	6,66	1,07	27,04	99,57	0,00	0,64	2,01	2,96	0,56	0,07	1,78	8,03
Sö181B	0,00	5,24	21,75	36,98	6,50	1,08	26,63	98,18	0,00	0,62	2,05	2,95	0,56	0,07	1,78	8,03
Sö182B	0,00	5,31	21,35	37,15	6,60	0,95	26,40	97,76	0,00	0,63	2,01	2,97	0,57	0,06	1,77	8,02
Sö183B	0,00	5,31	21,25	36,53	6,55	1,12	27,32	98,08	0,00	0,64	2,01	2,93	0,56	0,08	1,84	8,06
Sö189B	0,00	5,30	21,14	36,91	6,06	0,96	26,53	96,90	0,00	0,64	2,01	2,98	0,52	0,07	1,79	8,01
Sö195A	0,00	5,48	21,17	37,24	6,40	0,94	25,94	97,17	0,00	0,66	2,00	2,99	0,55	0,06	1,74	8,01
Sö196A	0,00	5,48	21,19	36,64	6,58	0,94	26,23	97,05	0,00	0,66	2,02	2,96	0,57	0,06	1,77	8,04
Sö197A	0,00	5,44	21,04	37,21	6,52	1,01	26,67	97,89	0,00	0,65	1,99	2,98	0,56	0,07	1,79	8,03
Sö201D	0,00	5,03	21,64	37,87	6,78	0,87	27,40	99,59	0,00	0,59	2,01	2,98	0,57	0,06	1,80	8,01
Sö202D	0,00	5,32	21,59	38,04	6,50	1,14	26,88	99,47	0,00	0,62	2,00	2,99	0,55	0,08	1,77	8,01
Sö203D	0,00	4,99	21,52	37,99	6,53	1,06	26,85	98,95	0,00	0,59	2,00	3,00	0,55	0,07	1,78	7,99
Sö2011D	0,00	5,39	21,89	37,77	6,43	1,17	26,84	99,49	0,00	0,63	2,03	2,97	0,54	0,08	1,77	8,02
Sö224D	0,00	5,67	21,93	37,47	6,72	1,15	27,21	100,16	0,00	0,66	2,03	2,94	0,56	0,08	1,78	8,05
Sö225D	0,00	5,50	21,55	37,38	6,13	1,00	27,04	98,59	0,00	0,65	2,02	2,97	0,52	0,07	1,80	8,02
Sö228D	0,00	5,57	21,33	37,20	6,39	0,87	26,93	98,28	0,00	0,66	2,00	2,97	0,55	0,06	1,80	8,03
Sö23L1C	0,00	5,43	21,54	37,65	6,66	1,09	26,45	98,83	0,00	0,64	2,01	2,98	0,56	0,07	1,75	8,02
Sö23L2C	0,00	5,41	21,26	37,57	6,57	1,23	26,65	98,69	0,00	0,64	1,99	2,98	0,56	0,08	1,77	8,02
Sö23L3C	0,00	5,41	21,26	37,57	6,57	1,23	26,65	98,69	0,00	0,64	1,99	2,98	0,56	0,08	1,77	8,02
StML26L1B	0,00	4,53	20,94	37,28	8,28	3,53	23,94	98,51	0,00	0,54	1,97	2,98	0,71	0,24	1,60	8,04
StML26L2B	0,00	4,33	21,75	37,22	8,11	2,91	24,15	98,48	0,00	0,51	2,04	2,96	0,69	0,20	1,61	8,02
StML26L3B	0,00	4,46	21,06	36,77	8,35	3,46	24,32	98,43	0,00	0,53	1,99	2,95	0,72	0,24	1,63	8,06
StML26L4B	0,00	4,38	20,96	36,74	8,23	3,91	24,50	98,72	0,00	0,52	1,98	2,95	0,71	0,27	1,64	8,06
StML26L5B	0,00	4,56	20,78	37,46	8,06	3,15	24,68	98,69	0,00	0,54	1,95	2,99	0,69	0,21	1,65	8,03
StML26L6B	0,00	4,49	20,70	36,69	8,30	3,32	24,36	97,86	0,00	0,54	1,97	2,96	0,72	0,23	1,64	8,06
StML276B	0,00	4,24	20,95	37,29	8,78	3,43	24,29	98,98	0,00	0,50	1,97	2,97	0,75	0,23	1,62	8,04
StML277B	0,00	4,51	21,43	36,49	8,17	3,86	24,91	99,37	0,00	0,54	2,01	2,91	0,70	0,26	1,66	8,08
StML278B	0,00	4,34	21,57	37,15	7,92	3,23	24,47	98,67	0,00	0,52	2,03	2,96	0,68	0,22	1,63	8,03
StSD51A	0,00	6,01	21,72	38,98	6,16	2,36	25,70	100,93	0,00	0,69	1,98	3,01	0,51	0,15	1,66	8,00
StSD52A	0,00	6,26	21,83	39,50	6,42	2,30	25,65	101,96	0,00	0,71	1,96	3,02	0,52	0,15	1,64	8,00
StSD53A	0,00	6,25	21,82	39,14	6,58	2,22	25,35	101,37	0,00	0,72	1,97	3,00	0,54	0,14	1,63	8,01
StSD54A	0,00	6,15	21,70	39,08	6,60	2,09	26,13	101,74	0,00	0,70	1,96	3,00	0,54	0,14	1,68	8,02
StSD55A	0,00	6,14	22,01	39,42	6,38	2,05	25,85	101,85	0,00	0,70	1,98	3,01	0,52	0,13	1,65	8,00
StSD56A	0,00	6,22	21,92	39,26	6,46	2,15	25,33	101,35	0,00	0,71	1,98	3,01	0,53	0,14	1,62	8,00
StSD56*A	0,00	6,28	21,97	38,79	6,44	2,41	25,13	101,02	0,00	0,72	2,00	2,99	0,53	0,16	1,62	8,01
StSD201D	0,00	6,14	21,73	39,32	6,44	2,39	25,15	101,17	0,00	0,70	1,97	3,02	0,53	0,16	1,62	7,99
StSD202D	0,00	5,89	21,99	39,40	7,13	2,41	25,96	102,78	0,00	0,67	1,97	3,00	0,58	0,16	1,65	8,02
StSD203D	0,00	6,02	21,59	39,53	6,72	2,26	25,42	101,55	0,00	0,69	1,95	3,03	0,55	0,15	1,63	8,00

Opaque Phases

	Compound %											Number of ions										
	CaO	MgO	Al_2O_3	TiO_2	FeO	SiO_2	CaO	MnO	V2O5	Cr2O3	**Totals**	Ca^{2+}	Mg^{2+}	Al^{3+}	Ti^{4+}	Fe^{2+}	Si^{4+}	Ca^{2+}	Mn^{2+}	V	Cr	**Cation Sum**
Gas3A46A Ilm	0,00	0,94	0,00	48,38	47,96	0,00	0,00	0,00	0,00	0,00	97,28	0,00	0,04	0,00	0,96	1,05	0,00	0,00	0,00	0,00	0,00	2,05
Gas3A47A Ilm	0,00	0,75	0,41	47,58	48,45	0,00	0,00	0,00	0,00	0,00	97,19	0,00	0,03	0,01	0,94	1,07	0,00	0,00	0,00	0,00	0,00	2,05
Gas3A54A Hem	0,00	0,00	0,68	0,00	98,81	0,00	0,00	0,00	0,00	0,00	99,49	0,00	0,00	0,02	0,00	1,98	0,00	0,00	0,00	0,00	0,00	2,00
Gas3A61A Ilm	0,00	1,22	0,00	49,76	46,65	0,00	0,00	0,00	0,00	0,00	97,63	0,00	0,05	0,00	0,97	1,01	0,00	0,00	0,00	0,00	0,00	2,03
Gas3A95A Ilm	0,00	0,00	0,37	16,09	70,49	0,00	0,00	0,00	0,00	0,00	86,95	0,00	0,00	0,02	0,43	2,11	0,00	0,00	0,00	0,00	0,00	2,56
Gas3A123C Hem	0,00	0,00	0,55	0,00	99,27	0,00	0,00	0,00	0,00	0,00	99,82	0,00	0,00	0,02	0,00	1,98	0,00	0,00	0,00	0,00	0,00	2,00
Gas3A136D	0,00	0,63	0,35	33,65	60,20	0,00	0,00	0,00	0,00	0,00	94,83	0,00	0,03	0,01	0,74	1,47	0,00	0,00	0,00	0,00	0,00	2,25
Gas3A137D	0,00	0,78	0,00	46,52	49,01	0,00	0,00	0,00	0,00	0,00	96,31	0,00	0,03	0,00	0,94	1,10	0,00	0,00	0,00	0,00	0,00	2,07
Gas3B55A Ilm	0,00	1,30	0,00	50,55	49,50	0,00	0,00	0,00	0,00	0,00	101,36	0,00	0,05	0,00	0,96	1,04	0,00	0,00	0,00	0,00	0,00	2,04
Gas3B56A	0,00	1,00	0,00	48,94	48,46	0,00	0,00	0,00	0,00	0,00	98,40	0,00	0,04	0,00	0,95	1,05	0,00	0,00	0,00	0,00	0,00	2,05
Gas3B93B Ilm	0,00	0,98	0,00	44,85	52,74	0,00	0,00	0,00	0,00	0,00	98,57	0,00	0,04	0,00	0,90	1,17	0,00	0,00	0,00	0,00	0,00	2,10
GT286A Ilm	0,00	0,79	0,00	48,04	47,75	0,00	0,00	0,00	0,00	0,00	96,57	0,00	0,03	0,00	0,96	1,06	0,00	0,00	0,00	0,00	0,00	2,04
GT287A Ilm	0,00	0,52	0,00	47,61	49,86	0,00	0,00	0,00	0,00	0,00	97,99	0,00	0,02	0,00	0,94	1,10	0,00	0,00	0,00	0,00	0,00	2,06
GT315A Ilm	0,66	0,00	0,00	48,39	48,05	0,00	0,00	0,00	0,00	0,00	97,09	0,02	0,00	0,00	0,96	1,06	0,00	0,00	0,00	0,00	0,00	2,04
GT331A Ilm	0,00	0,46	0,00	43,91	49,80	0,00	0,00	0,00	0,00	0,00	94,16	0,00	0,02	0,00	0,91	1,15	0,00	0,00	0,00	0,00	0,00	2,09
KB225B Ilm	14,12	0,66	1,82	62,39	3,13	16,68	0,00	0,00	0,00	0,00	98,80	0,30	0,02	0,04	0,94	0,05	0,34	0,00	0,00	0,00	0,00	1,70
KB251D Ilm	0,00	0,73	0,00	44,14	52,64	0,00	0,00	0,00	0,00	0,00	97,51	0,00	0,03	0,00	0,89	1,18	0,00	0,00	0,00	0,00	0,00	2,11
KB281A Ilm	0,00	0,00	0,48	44,86	52,70	0,44	0,00	0,00	0,00	0,00	98,48	0,00	0,00	0,01	0,89	1,17	0,01	0,00	0,00	0,00	0,00	2,09
KB283A Ilm	0,00	0,73	0,00	46,31	51,21	0,05	0,00	0,00	0,00	0,00	98,30	0,00	0,03	0,00	0,92	1,13	0,00	0,00	0,00	0,00	0,00	2,08
Sö152B Hem	0,00	0,00	0,77	0,00	90,14	1,00	0,00	0,00	0,00	0,00	91,91	0,00	0,00	0,03	0,00	1,94	0,03	0,00	0,00	0,00	0,00	1,99
Sö155B Hem	0,00	0,46	0,67	0,00	90,33	1,66	0,00	0,00	0,00	0,00	93,12	0,00	0,02	0,02	0,00	1,90	0,05	0,00	0,00	0,00	0,00	1,99
Sö191A Ilm	0,00	0,00	0,00	44,20	51,36	0,00	0,00	0,00	0,00	0,00	95,56	0,00	0,00	0,00	0,91	1,18	0,00	0,00	0,00	0,00	0,00	2,09
Sö198A Ilm	0,00	0,00	0,00	45,53	48,35	0,00	0,00	1,04	0,00	0,00	94,92	0,00	0,00	0,00	0,94	1,10	0,00	0,00	0,02	0,00	0,00	2,06
Sö199A Ilm	0,00	0,00	0,00	45,37	48,94	0,00	0,00	1,27	0,00	0,00	95,58	0,00	0,00	0,00	0,93	1,11	0,00	0,00	0,03	0,00	0,00	2,07
Sö 231C Ilm	0,00	0,00	0,00	45,72	50,08	0,00	0,00	0,95	0,00	0,00	96,75	0,00	0,00	0,00	0,93	1,13	0,00	0,00	0,02	0,00	0,00	2,07
ML243A Hem	0,00	0,48	0,79	0,00	70,09	1,38	0,00	0,00	0,00	0,00	72,73	0,00	0,03	0,03	0,00	1,88	0,05	0,00	0,00	0,00	0,00	1,99
ML253A Ilm	0,00	0,00	0,00	21,80	66,55	0,00	0,00	0,00	0,00	0,00	88,35	0,00	0,00	0,00	0,56	1,89	0,00	0,00	0,00	0,00	0,00	2,44
ML263B Ilm	0,00	0,67	0,00	14,24	72,68	0,00	0,00	0,00	0,00	0,00	87,58	0,00	0,03	0,00	0,39	2,19	0,00	0,00	0,00	0,00	0,00	2,60
ML264B Ilm	0,00	0,46	0,00	48,46	42,03	0,00	0,00	0,00	0,00	0,00	90,95	0,00	0,02	0,00	1,01	0,97	0,00	0,00	0,00	0,00	0,00	1,99
StSD71A Hem	0,00	0,00	0,42	13,45	86,23	0,00	0,00	0,00	0,71	0,00	100,82	0,00	0,00	0,01	0,25	1,63	0,00	0,00	0,00	0,01	0,00	1,91
StSD72A Ilm	0,00	0,00	0,43	13,23	76,35	0,00	0,00	0,00	0,70	0,00	90,71	0,00	0,00	0,02	0,35	2,24	0,00	0,00	0,00	0,02	0,00	2,62
StSD73A Ilm	0,00	0,79	0,00	46,08	49,79	0,00	0,00	0,00	0,00	0,00	96,66	0,00	0,03	0,00	0,93	1,11	0,00	0,00	0,00	0,00	0,00	2,07
StSD74A Hem	0,00	0,78	0,00	46,50	55,79	0,00	0,00	0,00	0,00	0,00	103,07	0,00	0,03	0,00	0,78	0,94	0,00	0,00	0,00	0,00	0,00	1,75
StSD64A Fe2TiO5	0,00	0,00	0,00	16,5	83,24	0,00	0,00	0,00	0,00	0,00	99,74	0,00	0,00	0,00	1,04	5,27	0,00	0,00	0,00	0,00	0,00	6,32
StSD63A Fe2TiO5	0,00	0,60	0,47	16,13	81,26	1,20	0,00	0,00	0,96	0,00	100,62	0,00	0,07	0,05	1,00	5,02	0,10	0,00	0,00	0,05	0,00	6,29
StSD171D Fe2TiO5	0,00	0,40	0,39	0,59	72,41	0,00	24,49	0,00	0,74	0,78	99,81	0,00	0,05	0,04	0,05	4,44	0,00	1,50	0,00	0,04	0,05	6,17
StSD221D Ilm	0,00	0,42	0,00	40,17	55,98	0,00	0,00	0,00	0,00	0,00	96,58	0,00	0,02	0,00	0,84	1,30	0,00	0,00	0,00	0,00	0,00	2,16
StSD222D Fe2TiO5	0,00	0,00	0,34	16,58	84,89	0,00	0,00	0,00	0,00	0,00	101,81	0,00	0,00	0,03	1,03	5,26	0,00	0,00	0,00	0,00	0,00	6,32

Feldspar

	Compound %										Number of ions									
	Na2O	MgO	Al2O3	SiO2	K2O	CaO	TiO_2	FeO	BaO	**Totals**	Na^{+}	Mg^{2+}	Al^{3+}	Si^{4+}	K^{+}	Ca^{2+}	Ti^{4+}	Fe^{2+}	Ba^{2+}	**Cation Sum**
Gas3A311Aplag	7,11	0,00	26,64	57,09	0,24	8,26	0,00	0,00	0,00	99,34	0,62	0,00	1,42	2,58	0,01	0,40	0,00	0,00	0,00	5,03
Gas3A312Aplag	6,97	0,00	26,42	56,50	0,38	8,36	0,00	0,00	0,00	98,63	0,62	0,00	1,42	2,57	0,02	0,41	0,00	0,00	0,00	5,04
Gas3A313Aplag	7,01	0,00	26,56	57,09	0,30	8,05	0,00	0,00	0,00	99,01	0,61	0,00	1,42	2,58	0,02	0,39	0,00	0,00	0,00	5,02
Gas3A314APlg	7,02	0,00	26,58	56,97	0,33	8,10	0,00	0,00	0,00	99,00	0,62	0,00	1,42	2,58	0,02	0,39	0,00	0,00	0,00	5,03
Gas3A45Aplag	7,06	0,00	27,03	57,09	0,27	8,15	0,00	0,00	0,00	99,60	0,62	0,00	1,43	2,57	0,02	0,39	0,00	0,00	0,00	5,03
Gas3A48Aplag	7,39	0,00	26,95	57,60	0,26	7,96	0,00	0,00	0,00	100,16	0,64	0,00	1,42	2,58	0,01	0,38	0,00	0,00	0,00	5,03
Gas3A57Aplag	6,89	0,00	26,38	57,06	0,27	7,97	0,00	0,00	0,00	98,57	0,61	0,00	1,41	2,59	0,02	0,39	0,00	0,00	0,00	5,02
Gas3A66Aplag	7,26	0,00	26,35	57,89	0,27	7,88	0,00	0,00	0,00	99,65	0,63	0,00	1,40	2,60	0,02	0,38	0,00	0,00	0,00	5,03
Gas3A67Aplag	7,32	0,00	26,35	57,57	0,35	7,86	0,00	0,00	0,00	99,45	0,64	0,00	1,40	2,60	0,02	0,38	0,00	0,00	0,00	5,04
Gas3A77Aplag	7,34	0,00	26,52	58,02	0,38	7,81	0,00	0,00	0,00	100,07	0,64	0,00	1,40	2,60	0,02	0,37	0,00	0,00	0,00	5,03
Gas3A78Aplag	7,37	0,00	26,31	58,15	0,40	7,63	0,00	0,00	0,00	99,86	0,64	0,00	1,39	2,61	0,02	0,37	0,00	0,00	0,00	5,03
Gas3A712Aplag	7,33	0,00	26,52	57,61	0,36	8,07	0,00	0,00	0,00	99,89	0,64	0,00	1,40	2,59	0,02	0,39	0,00	0,00	0,00	5,04
Gas3A713Aplag	7,48	0,00	26,02	58,69	0,35	7,18	0,00	0,00	0,00	99,72	0,65	0,00	1,37	2,63	0,02	0,34	0,00	0,00	0,00	5,01
Gas3A714Aplag	7,52	0,00	25,94	58,41	0,43	7,38	0,00	0,00	0,00	99,68	0,66	0,00	1,37	2,62	0,02	0,36	0,00	0,00	0,00	5,03
Gas3A715Aalk	0,43	0,00	18,72	60,90	15,51	0,00	0,00	0,00	0,00	95,56	0,04	0,00	1,07	2,95	0,96	0,00	0,00	0,00	0,00	5,02
Gas3A716Aplag	7,17	0,00	26,10	57,77	0,25	8,15	0,00	0,00	0,00	99,44	0,63	0,00	1,39	2,60	0,01	0,39	0,00	0,00	0,00	5,02
Gas3A1010Bplag	7,18	0,00	27,17	58,30	0,33	8,36	0,00	0,00	0,00	101,34	0,62	0,00	1,42	2,58	0,02	0,40	0,00	0,00	0,00	5,04
Gas3A125Cplag	7,93	0,00	25,76	59,54	0,49	7,08	0,00	0,00	0,00	100,80	0,68	0,00	1,35	2,64	0,03	0,34	0,00	0,00	0,00	5,04
Gas3A134Dplag	7,93	0,00	25,95	59,24	0,49	7,07	0,00	0,00	0,00	100,68	0,68	0,00	1,36	2,63	0,03	0,34	0,00	0,00	0,00	5,04
Gas3A135Dplag	7,61	0,00	25,40	58,26	0,39	7,34	0,00	0,00	0,00	99,00	0,67	0,00	1,35	2,63	0,02	0,36	0,00	0,00	0,00	5,03
Gas3A144Dplag	7,56	0,00	26,09	58,90	0,38	7,47	0,00	0,00	0,00	100,40	0,65	0,00	1,37	2,63	0,02	0,36	0,00	0,00	0,00	5,03
Gas3B32Aplag	7,55	0,00	26,10	59,06	0,39	7,44	0,00	0,00	0,00	100,54	0,65	0,00	1,37	2,63	0,02	0,35	0,00	0,00	0,00	5,02
Gas3B33Aplag	7,40	0,00	26,04	58,34	0,34	8,00	0,00	0,00	0,00	100,12	0,64	0,00	1,37	2,61	0,02	0,38	0,00	0,00	0,00	5,02
Gas3B34Aplag	7,25	0,00	27,12	58,03	0,42	8,50	0,00	0,00	0,00	101,32	0,62	0,00	1,42	2,57	0,02	0,40	0,00	0,00	0,00	5,03
Gas3B36Aplag	7,55	0,00	26,62	58,37	0,41	7,63	0,00	0,00	0,00	100,58	0,65	0,00	1,40	2,60	0,02	0,36	0,00	0,00	0,00	5,03
Gas3B37Aplag	7,30	0,00	26,41	58,40	0,47	7,82	0,00	0,00	0,00	100,40	0,63	0,00	1,39	2,61	0,03	0,37	0,00	0,00	0,00	5,03
Gas3B39Aalkali	0,47	0,00	19,29	61,07	15,52	0,00	0,00	0,00	2,90	96,35	0,04	0,00	1,08	2,91	0,94	0,00	0,00	0,00	0,05	4,97
Gas3B110Aalkali	0,55	0,00	19,51	62,67	15,47	0,00	0,00	0,00	3,21	98,20	0,05	0,00	1,07	2,92	0,92	0,00	0,00	0,00	0,06	4,96
Gas3B111Aalkali	0,55	0,00	19,32	62,48	15,58	0,00	0,00	0,00	3,29	97,93	0,05	0,00	1,07	2,93	0,93	0,00	0,00	0,00	0,06	4,98
Gas3B41Aplag	7,13	0,00	25,97	58,63	0,39	7,73	0,00	0,00	0,00	99,85	0,62	0,00	1,37	2,63	0,02	0,37	0,00	0,00	0,00	5,01
Gas3B42Aplag	7,63	0,00	26,07	59,02	0,53	7,48	0,00	0,00	0,00	100,73	0,66	0,00	1,37	2,63	0,03	0,36	0,00	0,00	0,00	5,05
Gas3B95Bplag	7,13	0,00	27,12	58,07	0,38	8,92	0,00	0,00	0,00	101,63	0,61	0,00	1,41	2,57	0,02	0,42	0,00	0,00	0,00	5,04
Gas3B96Bplag	6,94	0,00	27,27	58,1	0,00	8,53	0,00	0,00	0,00	100,84	0,6	0,00	1,43	2,58	0,00	0,41	0,00	0,00	0,00	5,01
Gas3B134Cplag	6,86	-0,13	26,26	57,14	0,44	7,91	0,00	0,00	0,00	98,47	0,6	0	1,41	2,6	0,03	0,39	0,00	0,00	0,00	5,01
Gas3B135Cplag	7,33	0,11	25,91	56,52	0,48	7,6	0,00	0,67	0,00	98,63	0,65	0,01	1,39	2,58	0,03	0,37	0,00	0,03	0,00	5,06
Gas3B136Cplag	6,67	0,04	26,21	55,86	0,39	8,5	0,00	0,00	0,00	97,67	0,6	0	1,42	2,57	0,02	0,42	0,00	0,00	0,00	5,03
Gas3B144Cplag	6,83	0,00	26,64	55,73	0,36	8,69	0,00	0,00	0,00	98,25	0,61	0,00	1,44	2,55	0,02	0,43	0,00	0,00	0,00	5,04
Gas3B145Cplag	7,22	0,00	25,71	57,91	0,42	7,38	0,00	0,00	0,00	98,64	0,63	0,00	1,37	2,63	0,02	0,36	0,00	0,00	0,00	5,02
Gas3B146Cplag	7,54	0,00	25,81	57,5	0,46	7,27	0,00	0,00	0,00	98,6	0,66	0,00	1,38	2,61	0,03	0,35	0,00	0,00	0,00	5,04
Gas3B148Cplag	7,81	0,00	26,85	59,83	0,00	7,71	0,00	0,00	0,00	102,2	0,66	0,00	1,38	2,62	0,00	0,36	0,00	0,00	0,00	5,02
Gas3B147Calkali	0,00	0,00	18,64	60,09	15,42	0,00	0,96	0,00	0,00	95,11	0,00	0,00	1,07	2,92	0,96	0,00	0,03	0,00	0,00	4,99
Gas3B157Cplag	6,55	0,00	26,83	57,1	0,00	8,41	0,00	0,00	0,00	98,88	0,57	0,00	1,43	2,58	0,00	0,41	0,00	0,00	0,00	4,99
Gas3B161Cplag	6,87	0,00	27,62	57,69	0,49	8,31	0,00	0,00	0,00	100,99	0,59	0,00	1,45	2,56	0,03	0,4	0,00	0,00	0,00	5,02
Gas3B162Cplag	7,53	0,00	26,12	58,56	0,43	7,65	0,00	0,00	0,00	100,29	0,65	0,00	1,38	2,62	0,02	0,37	0,00	0,00	0,00	5,03
Gas3B163Cplag	7	0,00	26,18	57,83	0,34	7,66	0,00	0,00	0,00	99,02	0,61	0,00	1,39	2,61	0,02	0,37	0,00	0,00	0,00	5,01
Gas3B182Dplag	7,25	0,00	26,36	58,15	0,00	7,79	0,00	0,00	0,00	99,55	0,63	0,00	1,39	2,61	0,00	0,37	0,00	0,00	0,00	5,01
Gas3B183Dplag	7,55	0,00	26,44	58,64	0,00	7,82	0,00	0,00	0,00	100,45	0,65	0,00	1,39	2,61	0,00	0,37	0,00	0,00	0,00	5,02
Gas3B189Dplag	7,18	0,00	26,46	57,76	0,00	8,02	0,00	0,00	0,00	99,43	0,63	0,00	1,4	2,6	0,00	0,39	0,00	0,00	0,00	5,01
Gas3B193Eplag	7,38	0,00	26,43	59,05	0,00	7,74	0,00	0,00	0,00	100,6	0,63	0,00	1,38	2,62	0,00	0,37	0,00	0,00	0,00	5,01
Gas3B194Eplag	7,2	0,00	26,83	58,22	0,00	8,36	0,00	0,00	0,00	100,62	0,62	0,00	1,41	2,59	0,00	0,4	0,00	0,00	0,00	5,02
Gas3B195Eplag	7,41	0,00	26,15	57,88	0,00	7,87	0,00	0,00	0,00	99,32	0,65	0,00	1,39	2,61	0,00	0,38	0,00	0,00	0,00	5,02
GT2811Aplag	7,37	0,00	25,05	59,82	0,64	7,14	0,00	0,00	0,00	100,01	0,64	0,00	1,32	2,67	0,04	0,34	0,00	0,00	0,00	5,01
GT2812Aplag	7,22	0,00	25,72	59,54	0,57	7,28	0,00	0,00	0,00	100,34	0,62	0,00	1,35	2,65	0,03	0,35	0,00	0,00	0,00	5
GT2813Aplag	6,46	0,57	23,6	55,84	0,45	7,01	0,00	4,8	0,00	98,73	0,58	0,04	1,29	2,59	0,03	0,35	0,00	0,19	0,00	5,07
GT2814Aplag	7,02	0,00	26,27	59,86	0,33	8,09	0,00	0,00	0,00	101,58	0,6	0,00	1,36	2,63	0,02	0,38	0,00	0,00	0,00	4,99
GT2815Aplag	6,94	0,00	26,31	58,88	0,48	8,07	0,00	0,00	0,00	100,68	0,6	0,00	1,38	2,62	0,03	0,38	0,00	0,00	0,00	5,01
GT296Aplag	7,51	0,00	25,62	60,33	0,23	7,64	0,00	0,00	0,00	101,33	0,64	0,00	1,33	2,66	0,01	0,36	0,00	0,00	0,00	5
GT297Aplag	7,61	0,00	25,99	59,85	0,53	7,55	0,00	0,00	0,00	101,53	0,65	0,00	1,35	2,64	0,03	0,36	0,00	0,00	0,00	5,03
GT298Aplag	7,8	0,00	25,39	60,73	0,39	7,07	0,00	0,00	0,00	101,38	0,67	0,00	1,32	2,67	0,02	0,33	0,00	0,00	0,00	5,01
GT321Aplag	0,46	0,00	18,24	64,53	15,29	0,00	0,00	0,00	0,00	98,52	0,04	0,00	1	3,01	0,91	0,00	0,00	0,00	0,00	4,96
GT322Aplag	7,33	0,00	25,86	59,55	0,42	7,65	0,00	0,00	0,00	100,81	0,63	0,00	1,35	2,64	0,02	0,36	0,00	0,00	0,00	5,01
KB217Bplag	7,06	0,00	26,71	59,01	0,38	8,17	0,00	0,00	0,00	101,33	0,6	0,00	1,39	2,61	0,02	0,39	0,00	0,00	0,00	5,01
KB218Bplag	7,25	0,00	25,22	58,46	0,52	7,33	0,00	0,00	0,00	98,78	0,64	0,00	1,35	2,65	0,03	0,36	0,00	0,00	0,00	5,01
KB219Bplag	6,96	0,00	26,92	59,2	0,38	8,5	0,00	0,00	0,00	101,97	0,59	0,00	1,39	2,6	0,02	0,4	0,00	0,00	0,00	5,01
KB2110Bplag	6,2	0,00	27,07	57,03	0,00	8,99	0,00	0,00	0,00	99,3	0,54	0,00	1,44	2,57	0,00	0,43	0,00	0,00	0,00	4,98
KB2111Bplag	6,67	0,00	26,5	57,64	0,48	8,43	0,00	0,00	0,00	99,73	0,58	0,00	1,4	2,59	0,03	0,41	0,00	0,00	0,00	5,01
KB233Cplag	7,38	0,00	25,97	59,33	0,5	7,74	0,00	0,00	0,00	100,91	0,63	0,00	1,36	2,63	0,03	0,37	0,00	0,00	0,00	5,02
KB234Cplag	7,7	0,00	25,63	59,57	0,53	6,96	0,00	0,00	0,00	100,4	0,66	0,00	1,34	2,65	0,03	0,33	0,00	0,00	0,00	5,02
KB235Cplag	7,25	0,00	26,12	60,08	0,46	7,72	0,00	0,00	0,00	101,63	0,62	0,00	1,35	2,64	0,03	0,36	0,00	0,00	0,00	5
KB264Dplag	6,89	0,00	26,46	57,83	0,26	8,46	0,00	0,00	0,00	99,9	0,6	0,00	1,4	2,59	0,01	0,41	0,00	0,00	0,00	5,01
KB265Dplag	7,05	0,00	25,83	59,56	0,4	7,73	0,00	0,00	0,00	100,57	0,61	0,00	1,35	2,64	0,02	0,37	0,00	0,00	0,00	4,99

KB269Dplag	7,08	0,00	27,06	58,97	0,00	8,37	0,00	0,00	0,00	101,49	0,6	0,00	1,4	2,6	0,00	0,4	0,00	0,00	0,00	5
KB2610Dplag	6,88	0,00	26,65	58,43	0,34	8,76	0,00	0,00	0,00	101,07	0,59	0,00	1,39	2,59	0,02	0,42	0,00	0,00	0,00	5,02
KB302Aplag	6,49	0,00	27,98	58,59	9,42	0,00	0,00	0,00	0,00	102,49	0,55	0,00	1,44	2,56	0,44	0,00	0,00	0,00	0,00	4,99
KB303Aplag	7,35	0,00	27,04	60,63	8,12	0,00	0,00	0,00	0,00	103,14	0,62	0,00	1,38	2,62	0,38	0,00	0,00	0,00	0,00	5
KB304Aplag	7,16	0,00	27,45	60,8	8,39	0,00	0,00	0,00	0,00	103,8	0,6	0,00	1,39	2,61	0,39	0,00	0,00	0,00	0,00	4,99
KB305Aplag	6,31	0,00	27,92	58,53	0,37	10,19	0,00	0,00	0,00	103,31	0,53	0,00	1,43	2,55	0,02	0,48	0,00	0,00	0,00	5,01
KB306Aplag	6,12	0,00	28,68	57,68	0,31	10,36	0,00	0,00	0,00	103,17	0,52	0,00	1,48	2,52	0,02	0,48	0,00	0,00	0,00	5,01
KB312Aplag i (cpx)	6,13	0,00	27,77	58,04	0,34	10,24	0,00	0,00	0,00	102,51	0,52	0,00	1,44	2,55	0,02	0,48	0,00	0,00	0,00	5,01
Sö185Bplag	7,59	0,00	25,48	58,53	0,00	6,97	0,00	0,00	0,00	98,57	0,67	0,00	1,36	2,65	0,00	0,34	0,00	0,00	0,00	5,01
Sö186Bplag	7,32	0,00	25,53	57,85	0,00	7,3	0,00	0,00	0,00	98	0,65	0,00	1,37	2,63	0,00	0,36	0,00	0,00	0,00	5
Sö192Aplag	6,79	0,00	26,23	56,25	0,42	8,39	0,00	0,00	0,00	98,08	0,6	0,00	1,42	2,58	0,02	0,41	0,00	0,00	0,00	5,03
Sö193Aplag	6,42	0,00	26,73	55,7	0,47	8,99	0,00	0,00	0,00	98,32	0,57	0,00	1,44	2,55	0,03	0,44	0,00	0,00	0,00	5,03
Sö194Aplag	7,04	0,00	25,86	55,95	0,49	8,13	0,00	0,00	0,00	97,48	0,63	0,00	1,41	2,58	0,03	0,4	0,00	0,00	0,00	5,05
Sö207Dplag	7,17	0,00	26,1	57,38	0,37	7,87	0,00	0,00	0,00	98,88	0,63	0,00	1,39	2,6	0,02	0,38	0,00	0,00	0,00	5,03
Sö208Dplag	7,19	0,00	25,82	57,81	0,3	7,97	0,00	0,00	0,00	99,09	0,63	0,00	1,38	2,61	0,02	0,39	0,00	0,00	0,00	5,02
Sö2014Dplag	7,11	0,00	26,5	59,21	0,00	8,45	0,00	0,00	0,00	101,27	0,61	0,00	1,38	2,61	0,00	0,4	0,00	0,00	0,00	5
Sö215Dplag	7,04	0,00	25,76	57,42	0,00	7,66	0,00	0,00	0,00	97,88	0,62	0,00	1,38	2,62	0,00	0,37	0,00	0,00	0,00	5
Sö227Dplag	7,07	0,00	26,79	57,03	0,00	8,41	0,00	0,00	0,00	99,3	0,62	0,00	1,42	2,57	0,00	0,41	0,00	0,00	0,00	5,02
Sö229Dplag	7,1	0,00	26	56,95	0,31	8,03	0,00	0,00	0,00	98,4	0,63	0,00	1,4	2,6	0,02	0,39	0,00	0,00	0,00	5,03
Sö232Cplag	7	0,00	26,54	57,83	0,4	8,31	0,00	0,00	0,00	100,08	0,61	0,00	1,4	2,59	0,02	0,4	0,00	0,00	0,00	5,02
Sö236Cplag	7,41	0,00	25,72	58,43	0,58	7,44	0,00	0,00	0,00	99,6	0,65	0,00	1,36	2,63	0,03	0,36	0,00	0,00	0,00	5,03
Sö240Cplag	7,01	0,00	26,06	57	0,49	8,04	0,00	0,00	0,00	98,6	0,62	0,00	1,4	2,59	0,03	0,39	0,00	0,00	0,00	5,03
Sö23L1Cplag	7,21	0,00	26,35	57,2	0,35	8,09	0,00	0,00	0,00	99,2	0,63	0,00	1,4	2,59	0,02	0,39	0,00	0,00	0,00	5,04
Sö23L2Cplag	7,42	0,00	25,77	57,54	0,44	7,55	0,00	0,00	0,00	98,73	0,65	0,00	1,38	2,61	0,03	0,37	0,00	0,00	0,00	5,04
Sö23L3Cplag	7,28	0,00	25,42	58,6	0,41	7,28	0,00	0,00	0,00	98,99	0,64	0,00	1,35	2,64	0,02	0,35	0,00	0,00	0,00	5,01
Sö23L4Cplag	6,49	0,00	26,62	55,92	0,31	8,69	0,00	0,00	0,00	98,03	0,58	0,00	1,44	2,56	0,02	0,43	0,00	0,00	0,00	5,02
StML244Aplag	6,59	0,00	27,01	55,81	0,42	8,29	0,00	0,00	0,00	98,13	0,58	0,00	1,46	2,55	0,02	0,41	0,00	0,00	0,00	5,02
StML245Aplag	6,2	0,00	27,25	55,14	0,54	8,69	0,00	0,00	0,00	97,83	0,55	0,00	1,48	2,53	0,03	0,43	0,00	0,00	0,00	5,02
StML265Bplag	6,39	0,00	26,42	55,29	1,12	7,09	0,00	0,00	0,00	96,3	0,58	0,00	1,45	2,57	0,07	0,35	0,00	0,00	0,00	5,02
StML266Bplag	6,7	0,00	24,17	58,4	2,06	5,95	0,00	0,00	0,00	97,28	0,6	0,00	1,31	2,69	0,12	0,29	0,00	0,00	0,00	5,01
ML273Bplag	6,21	0,00	27,31	55,15	0,52	9,09	0,00	0,00	0,00	98,29	0,55	0,00	1,47	2,53	0,03	0,45	0,00	0,00	0,00	5,03
StML274BPlag	6,3	0,00	26,69	55,71	0,49	8,48	0,00	0,00	0,00	97,67	0,56	0,00	1,45	2,56	0,03	0,42	0,00	0,00	0,00	5,01
StML275Bplag	6,35	0,00	27,11	54,6	0,52	9	0,00	0,00	0,00	97,58	0,57	0,00	1,48	2,52	0,03	0,45	0,00	0,00	0,00	5,04
StSD58Aplag i (grt)	6,77	0,00	27,04	58,42	0,00	9,02	0,00	0,00	0,00	101,26	0,58	0,00	1,41	2,58	0,00	0,43	0,00	0,00	0,00	5
StSD63Aplag i (opx)	6,5	0,00	27,64	58,18	0,22	9,51	0,00	0,00	0,00	102,05	0,55	0,00	1,43	2,56	0,01	0,45	0,00	0,00	0,00	5,01
StSD101Aplag	6,86	0,00	27,18	59,18	0,26	8,82	0,00	0,00	0,00	102,29	0,58	0,00	1,4	2,59	0,01	0,41	0,00	0,00	0,00	5,01
StSD102Aplag	7,03	0,00	26,9	59,38	0,5	8,4	0,00	0,00	0,00	102,21	0,6	0,00	1,39	2,6	0,03	0,39	0,00	0,00	0,00	5,01
StSD111Aplag	6,7	0,00	27,23	58,59	0,34	8,7	0,00	0,00	0,00	101,56	0,57	0,00	1,42	2,58	0,02	0,41	0,00	0,00	0,00	5
StSD112Aplag	6,72	0,00	26,73	58,75	0,27	8,85	0,00	0,00	0,00	101,33	0,58	0,00	1,39	2,6	0,02	0,42	0,00	0,00	0,00	5
StSD113Aplag	7	0,00	26,49	59,12	0,35	8,47	0,00	0,00	0,00	101,42	0,6	0,00	1,38	2,61	0,02	0,4	0,00	0,00	0,00	5,01
StSD135Dplag	6,72	0,00	26,64	58,95	0,39	8,69	0,00	0,00	0,00	101,4	0,58	0,00	1,39	2,6	0,02	0,41	0,00	0,00	0,00	5
StSD136Dplag	6,64	0,00	27,28	57,78	0,35	8,92	0,00	0,00	0,00	100,97	0,57	0,00	1,43	2,57	0,02	0,42	0,00	0,00	0,00	5,01
StSD155Dplag	6,55	0,00	26,91	57,6	0,41	8,83	0,00	0,00	0,00	100,29	0,57	0,00	1,42	2,58	0,02	0,42	0,00	0,00	0,00	5,01
StSD165Dplag i (cpx)	6,54	0,00	27,06	58,29	0,4	9,03	0,00	0,00	0,00	101,32	0,56	0,00	1,41	2,58	0,02	0,43	0,00	0,00	0,00	5,01
StSD213Dplag	5,93	0,00	27,92	57,63	0,23	10,09	0,00	0,00	0,00	101,8	0,51	0,00	1,45	2,54	0,01	0,48	0,00	0,00	0,00	4,99
StSD226Dplag	7,24	0,00	26,59	60,01	0,32	8,05	0,00	0,00	0,00	102,21	0,61	0,00	1,37	2,63	0,02	0,38	0,00	0,00	0,00	5
StSD227Dplag	6,94	0,00	26,46	59,64	0,4	8,2	0,00	0,00	0,00	101,65	0,59	0,00	1,37	2,62	0,02	0,39	0,00	0,00	0,00	5
StSD251Dplag i (cpx)	6,13	0,00	27,6	58,71	0,00	9,43	0,00	0,00	0,00	101,86	0,52	0,00	1,43	2,58	0,00	0,44	0,00	0,00	0,00	4,97

i = inclusion
(mineral) = host mineral of inclusion

Other Minerals

	Compound %								Number of ions							
	P2O5	CaO	FeO	SO3	Al_2O_3	SiO_2	CuO	**Totals**	P^{5+}	Ca^{2+}	Fe^{2+}	S^{2-}	Al^{3+}	Si^{4+}	Cu	**Cation Sum**
Gas3B64A Ap	43,94	54,26	0,00	0,00	0,00	0,00	0,00	98,20	2,95	4,62	0,00	0,00	0,00	0,00	0,00	7,57
Gas3B187D Ap	44,26	55,12	0,27	0,00	0,00	0,00	0,00	99,38	2,94	4,63	0,02	0,00	0,00	0,00	0,00	7,57
Sö209D Fe-sulphide	0,00	0,00	84,50	9,35	0,58	0,96	0,00	95,39	0,00	0,00	5,97	0,59	0,06	0,08	0,00	6,70
Sö 211D Cu-sulphide	0,00	0,00	41,81	90,07	0,00	0,00	46,1	177,94	0,00	0,00	1,03	1,98	0,00	0,00	1,02	4,03

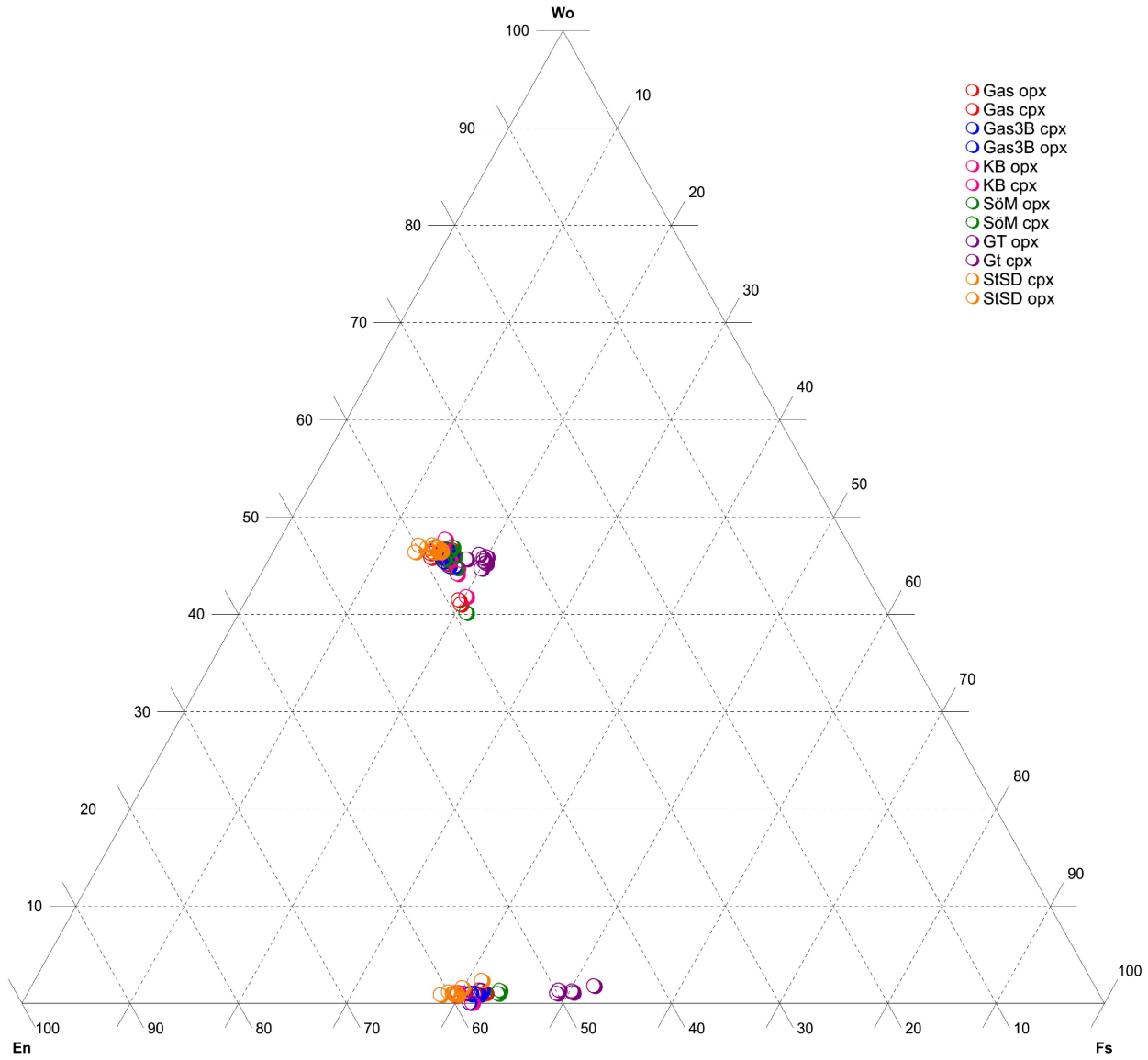

Appendix B: Wo-En-Fs discrimiantion diagram for pyroxenes. The used classification method is by Morimoto (1988).

P-T results Thermocalc

Gas3B	AvT [°C]	sd(T) [°C]	AvP [kbar]	sd(P) [kbar]	corr
1	782	95	10,2	1,2	0,718
2	713	90	9,3	1,2	0,731
3	779	91	10,0	1,2	0,695
4	789	93	10,0	1,2	0,688
5	813	98	10,4	1,2	0,681
6	783	92	9,9	1,2	0,695
7	719	88	9,2	1,2	0,707
8	782	95	10,2	1,2	0,718
Average	**770**	**92,75**	**9,9**	**1,2**	**0,704**

Gas3A	AvT [°C]	sd(T) [°C]	AvP [kbar]	sd(P) [kbar]	corr
1	860	93	10,3	1,2	0,631
2	874	100	11,0	1,3	0,656
3	854	94	10,2	1,2	0,636
4	840	95	10,2	1,2	0,672
5	860	90	10,3	1,1	0,629
6	854	90	10,2	1,1	0,633
7	840	93	10,1	1,2	0,668
8	839	99	10,1	1,2	0,659
Average	**852,6**	**94,3**	**10,3**	**1,2**	**0,648**

StSD	AvT [°C]	sd(T) [°C]	AvP [kbar]	sd(P) [kbar]	corr
1	809	91	9,7	1,2	0,628
2	803	96	9,6	1,2	0,625
3	810	100	10,0	1,3	0,640
4	802	96	9,6	1,2	0,622
5	803	94	9,6	1,2	0,611
6	808	89	9,7	1,1	0,612
7	800	87	9,8	1,1	0,626
8	810	89	9,7	1,1	0,616
9	810	87	9,6	1,1	0,615
Average	**806,1**	**92,1**	**9,7**	**1,2**	**0,622**

KB	AvT [°C]	sd(T) [°C]	AvP [kbar]	sd(P) [kbar]	corr
1	816	98	9,6	1,3	0,637
2	798	90	9,4	1,2	0,633
3	817	96	9,7	1,2	0,639
4	817	99	9,6	1,2	0,636
5	817	95	9,7	1,2	0,639
Average	**813,0**	**95,6**	**9,6**	**1,2**	**0,637**

Gt	AvT [°C]	sd(T) [°C]	AvP [kbar]	sd(P) [kbar]	corr
1	756	80	8,8	1,1	0,731
2	766	80	8,8	1,1	0,739
3	771	81	9,1	1,2	0,737
4	760	80	9,0	1,2	0,745
5	775	83	9,5	1,2	0,718
6	776	83	9,5	1,2	0,719
Average	**767,3**	**81,2**	**9,1**	**1,2**	**0,732**

SöM	AvT [°C]	sd(T) [°C]	AvP [kbar]	sd(P) [kbar]	corr
1	797	94	10,0	1,3	0,701
2	802	101	9,9	1,4	0,694
3	797	92	10,0	1,3	0,703
4	801	91	10,0	1,3	0,701
5	817	100	10,8	1,4	0,727
6	801	91	10,0	1,3	0,701
7	801	91	10,0	1,3	0,701
8	799	92	10,1	1,3	0,702
Average	**801,9**	**94,0**	**10,1**	**1,3**	**0,704**

Appendix C: All results of temperature-pressure estimates, calculated by AvePT (Thermocalc). AvT = average temperature. AvP = average pressure, sd(T) = standard deviation of temperature, sd(P) = standard deviation of pressure, corr = correlated ellipse.

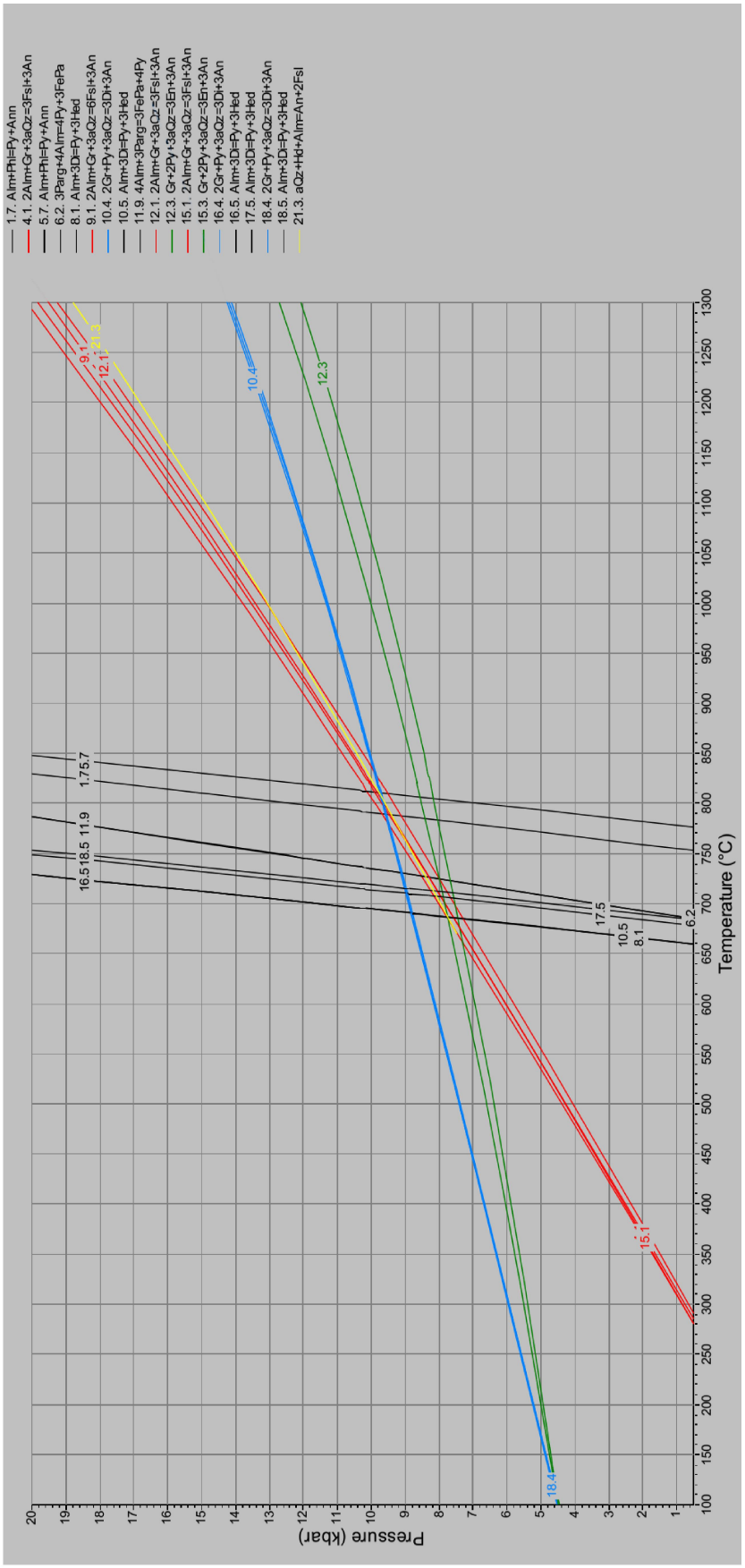

Appendix D: Calculated PT-diagram for different geothermobarometers (WinTWQ). Sample: GT1.

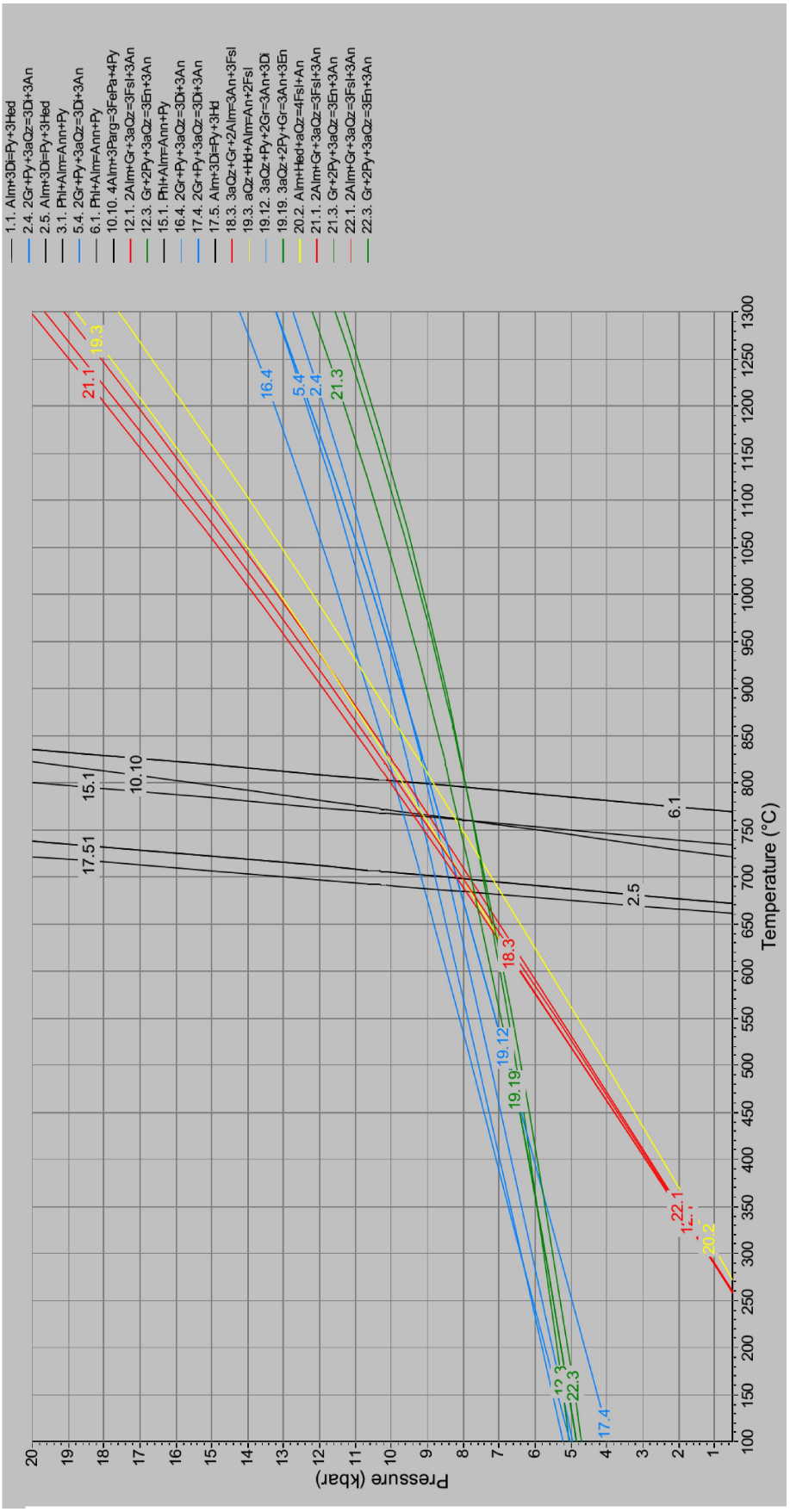

Appendix D: Calculated PT-diagrams for different geothermobarometers (WinTWQ). Sample: StSD.

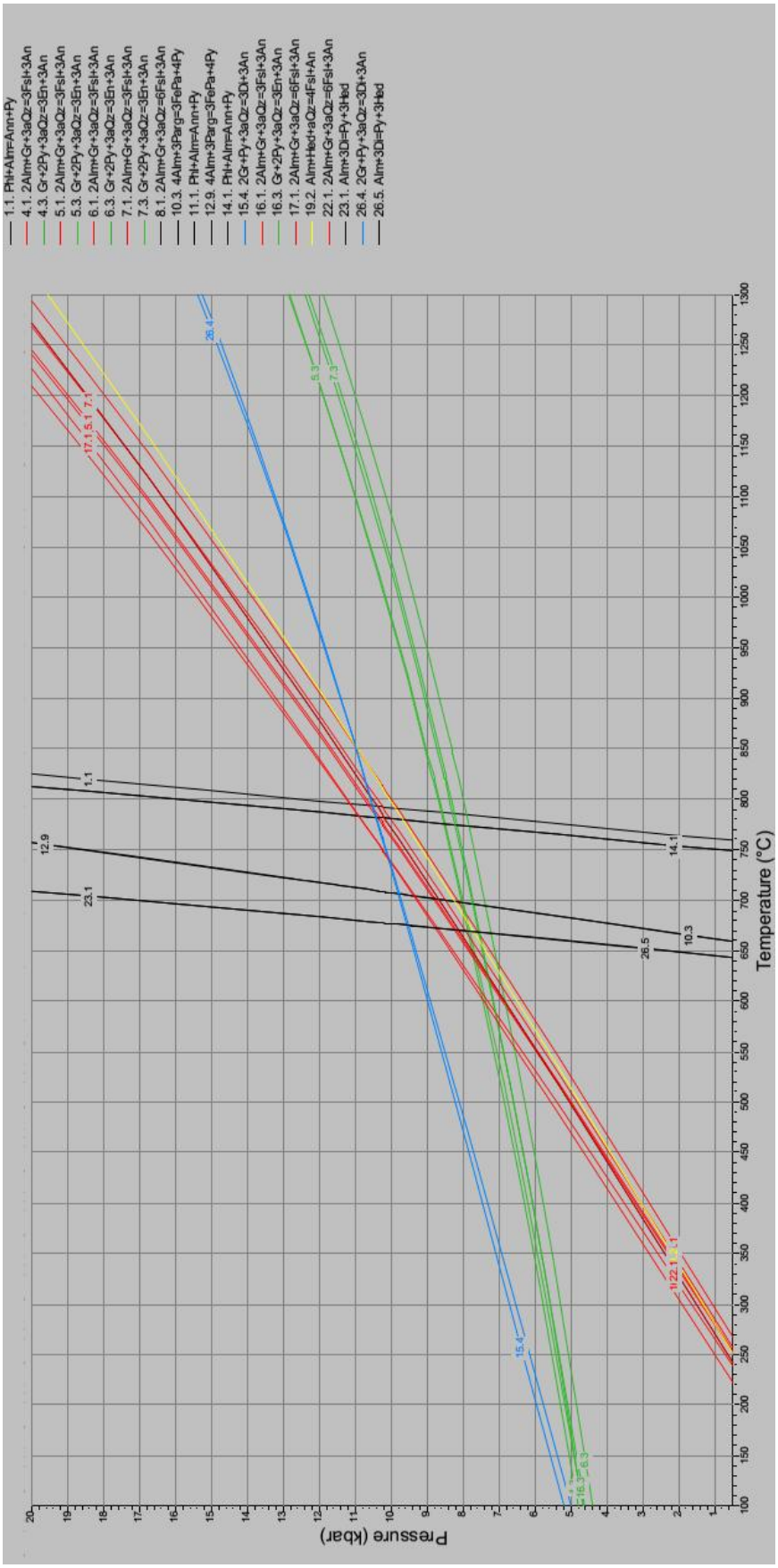

Appendix D: Calculated PT-diagrams for different geothermobarometers (WinTWQ). Sample: Gas3A.

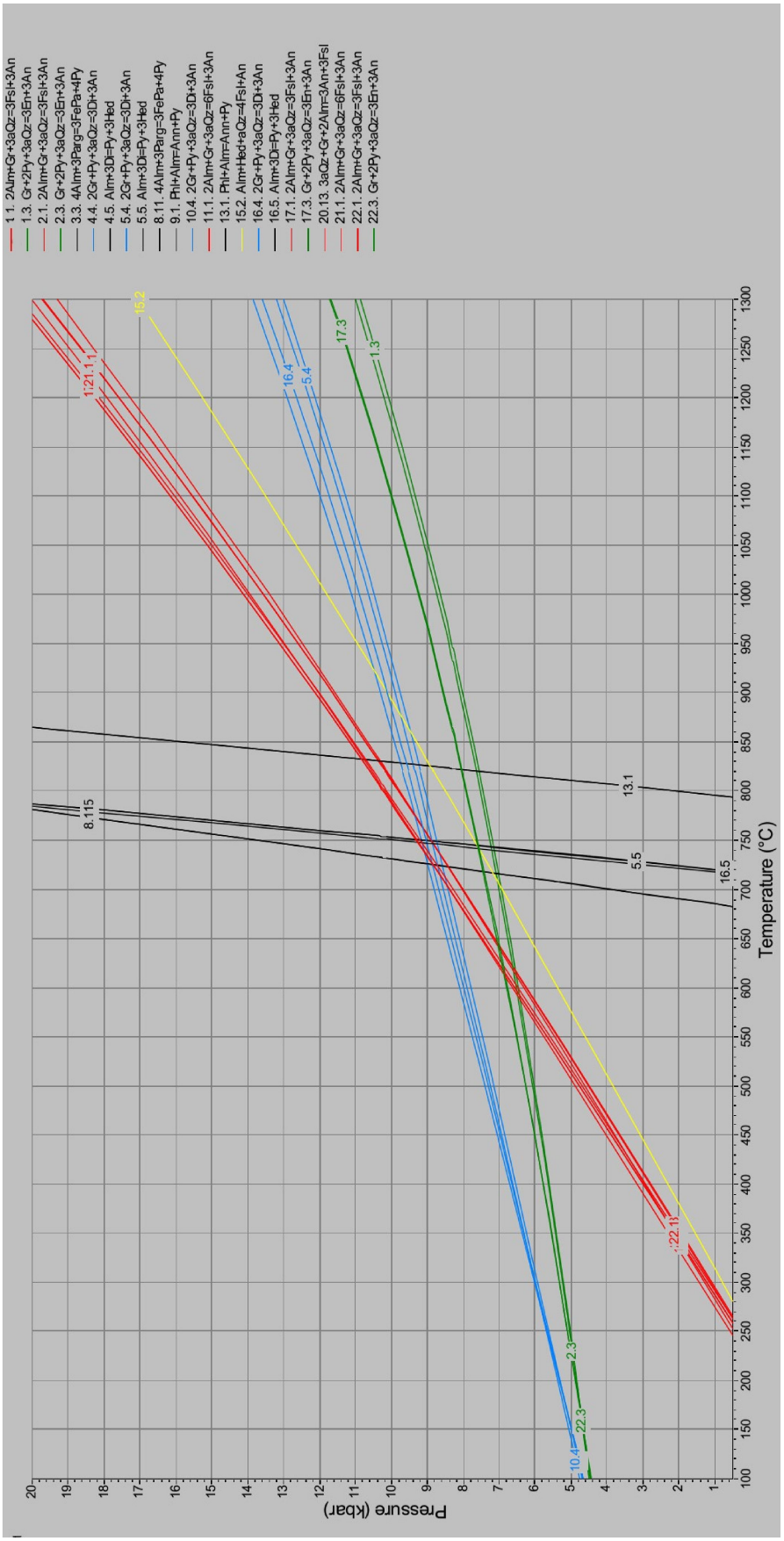

Appendix D: Calculated PT-diagrams for different geothermobarometers (WinTWQ). Sample: Gas3B.

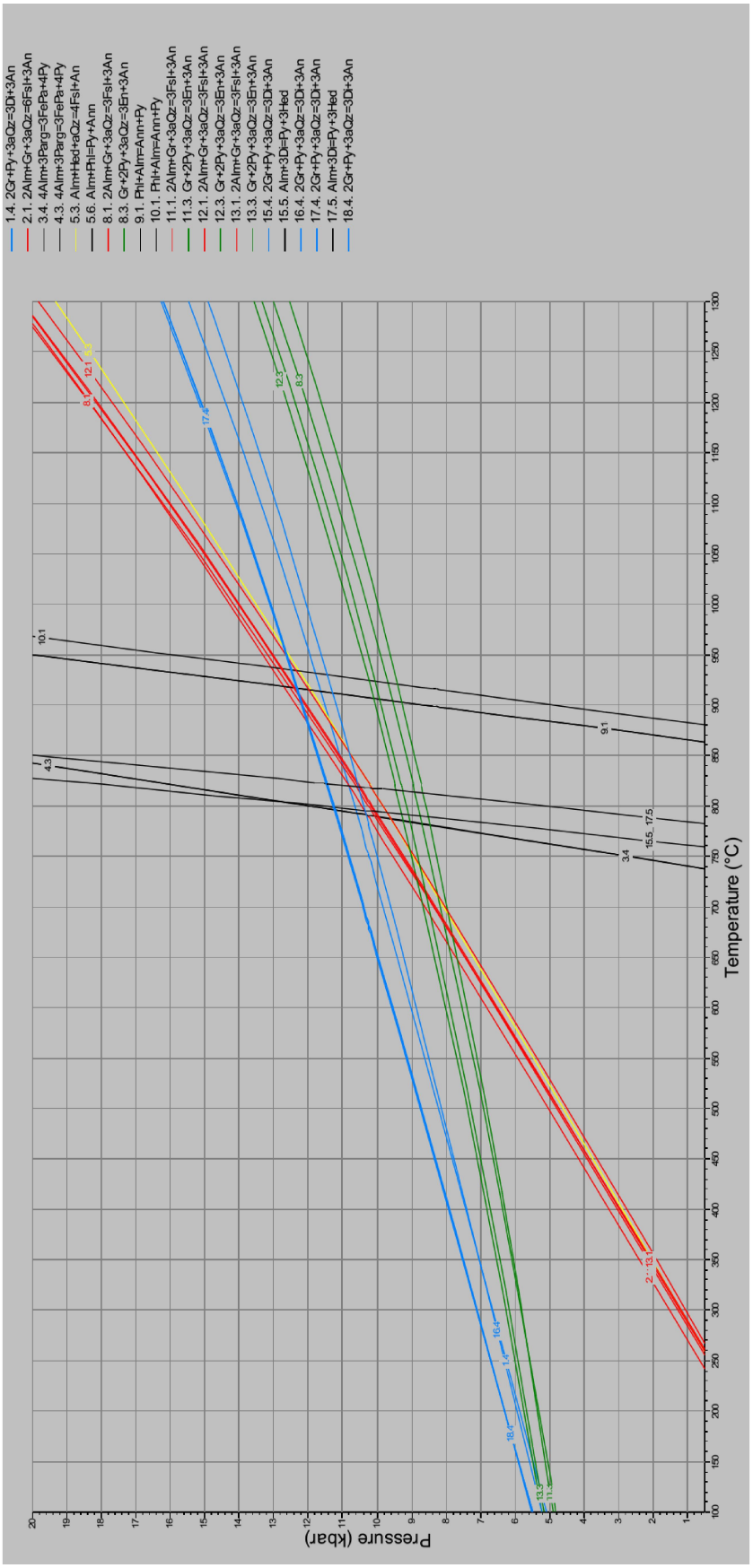

Appendix D: Calculated PT-diagrams for different geothermobarometers (WinTWQ). Sample: KB2.

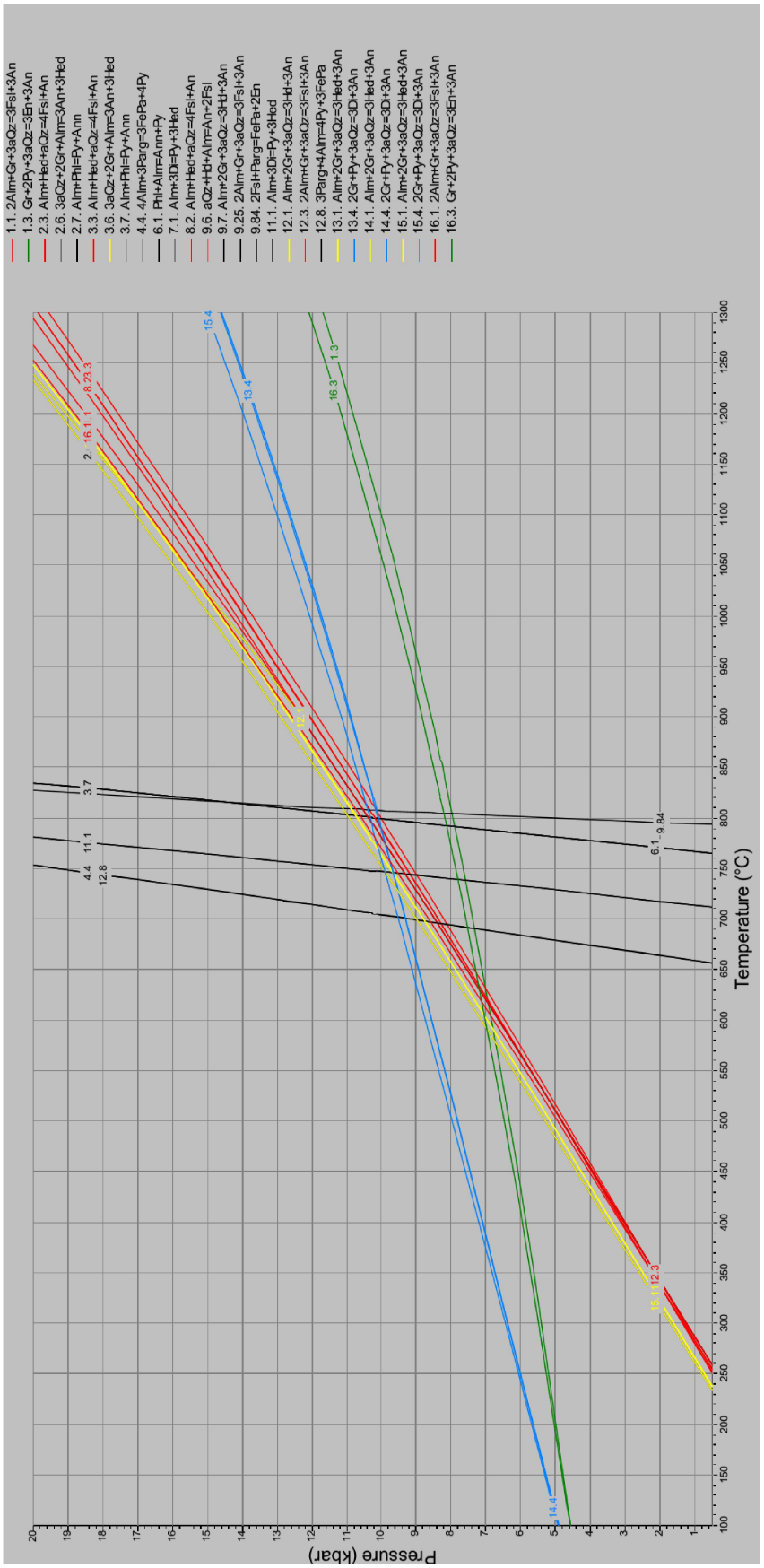

Appendix D: Calculated PT-diagrams for different geothermobarometers (WinTWQ). Sample: SöM1.

CIPW norm calculation

Normative	KB2		AV1		TL1		GT1		SöM1		SöPD		SöHf1		StSD1		StHD1		StHD2		Gas3B		Gas3		StML1		StML2		StML3	
Minerals	Wt.%	Vol%	Wt.%	Vol%	Wt.%	Vol%	Wt.%	Vol%	Wt.%	Vol%	Wt.%	Vol%	Wt.%	Vol%	Wt.%	Vol%	Wt.%	Vol%	Wt.%	Vol%	Wt.%	Vol%	Wt.%	Vol%	Wt.%	Vol%	Wt.%	Vol%	Wt.%	Vol%
Quartz	0,00	0,00	0,00	0,00	0,00	0,00	0,00	0,00	0,00	0,00	0,00	0,00	1,32	1,57	0,95	1,10	0,00	0,00	0,56	0,65	0,00	0,00	0,00	0,00	11,46	12,48	6,06	6,65	3,31	3,73
Plagioclase	47,82	54,39	43,18	49,04	51,85	58,78	39,24	45,87	45,88	52,22	59,44	64,66	39,60	46,31	47,09	53,60	48,39	55,07	47,48	54,02	48,94	55,75	47,73	54,43	57,54	61,60	58,79	63,41	50,70	56,27
Orthoclase	2,90	3,47	3,96	4,71	4,49	5,37	5,91	7,26	5,97	7,16	13,53	15,45	7,56	9,29	6,26	7,51	5,61	6,73	5,56	6,67	5,67	6,79	6,09	7,30	5,50	6,19	8,75	9,93	6,09	7,10
Nepheline	0,00	0,00	0,23	0,27	0,00	0,00	0,00	0,00	0,00	0,00	0,00	0,00	0,00	0,00	0,00	0,00	0,00	0,00	0,00	0,00	0,00	0,00	0,00	0,00	0,00	0,00	0,00	0,00	0,00	0,00
Diopside	22,73	20,93	26,86	24,86	12,88	11,83	19,84	18,56	17,80	16,32	6,25	5,36	17,55	16,22	15,39	14,29	15,77	14,55	13,97	12,92	16,58	15,28	16,62	15,33	9,26	8,04	2,43	2,11	13,15	11,85
Hypersthene	15,98	14,17	0,00	0,00	10,11	8,95	20,45	18,26	18,28	16,07	3,26	2,63	20,16	17,56	15,84	14,33	15,23	13,59	19,56	17,53	9,19	8,19	14,68	13,09	7,28	6,11	14,11	11,78	17,41	15,20
Olivine	2,07	1,76	18,90	16,66	9,43	8,01	2,29	1,94	2,74	2,30	7,86	5,96	0,00	0,00	0,00	0,00	2,24	1,92	0,00	0,00	6,79	5,81	1,75	1,49	0,00	0,00	0,00	0,00	0,00	0,00
Ilmenite	3,40	2,20	1,88	1,20	3,61	2,32	5,49	3,64	3,51	2,27	4,16	2,56	6,04	4,00	4,29	2,77	4,25	2,75	4,18	2,70	4,41	2,84	4,60	2,97	1,84	1,12	2,07	1,27	2,03	1,28
Magnetite	5,00	2,95	4,65	2,72	7,10	4,18	5,94	3,60	5,32	3,14	4,87	2,74	6,89	4,16	9,29	5,48	7,63	4,50	7,86	4,64	7,61	4,49	7,64	4,51	6,23	3,46	6,76	3,78	6,58	3,78
Apatite	0,07	0,07	0,25	0,24	0,53	0,51	0,83	0,82	0,49	0,47	0,67	0,61	0,88	0,87	0,93	0,89	0,90	0,87	0,88	0,85	0,86	0,82	0,93	0,89	1,09	0,98	1,16	1,05	0,83	0,78
Zircon	0,03	0,02	0,01	0,01	0,03	0,02	0,03	0,02	0,03	0,02	0,03	0,02	0,03	0,02	0,03	0,02	0,03	0,02	0,03	0,02	0,03	0,02	0,03	0,02	0,01	0,01	0,01	0,01	0,01	0,01
Chromite	0,07	0,04	0,46	0,27	0,04	0,03	0,06	0,04	0,04	0,03	0,00	0,00	0,00	0,00	0,01	0,01	0,01	0,01	0,01	0,01	0,01	0,01	0,01	0,01	0,00	0,00	0,00	0,00	0,03	0,02

Appendix E: Results of the CIPW norm calculation. The Fe2+/Fe3+ ratio is based on the chemical analysis.

Tidigare skrifter i serien "Examensarbeten i Geologi vid Lunds universitet":

364. Cederberg, Julia, 2013: U-Pb baddeleyite dating of the Pará de Minas dyke swarm in the São Francisco craton (Brazil) - three generations in a single swarm. (45 hp)
365. Björk, Andreas, 2013: Mineralogisk och malmpetrografisk studie av disseminerade sulfider i rika och fattiga prover från Kleva. (15 hp)
366. Karlsson, Michelle, 2013: En MIFO fas 1 -inventering av förorenade områden: Kvarnar med kvicksilverbetning Jönköpings län. (15 hp)
367. Michalchuk, Stephen P., 2013: The Säm fold structure: characterization of folding and metamorphism in a part of the eclogite-granulite region, Sveconorwegian orogen. (45 hp)
368. Praszkier, Aron, 2013: First evidence of Late Cretaceous decapod crustaceans from Åsen, southern Sweden. (15 hp)
369. Alexson, Johanna, 2013: Artificial groundwater recharge – is it possible in Mozambique? (15 hp)
370. Ehlorsson, Ludvig, 2013: Hydrogeologisk kartering av grundvattenmagasinet Åsumsfältet, Sjöbo. (15 hp)
371. Santsalo, Liina, 2013: The Jurassic extinction events and its relation to CO_2 levels in the atmosphere: a case study on Early Jurassic fossil leaves. (15 hp)
372. Svantesson, Fredrik, 2013: Alunskiffern i Östergötland – utbredning, mäktigheter, stratigrafi och egenskaper. (15 hp)
373. Iqbal, Faisal Javed, 2013: Paleoecology and sedimentology of the Upper Cretaceous (Campanian), marine strata at Åsen, Kristianstad Basin, Southern Sweden, Scania. (45 hp)
374. Kristinsdóttir, Bára Dröfn, 2013: U-Pb, O and Lu-Hf isotope ratios of detrital zircon from Ghana, West-African Craton – Formation of juvenile, Palaeoproterozoic crust. (45 hp)
375. Grenholm, Mikael, 2014: The Birimian event in the Baoulé Mossi domain (West African Craton) — regional and global context. (45 hp)
376. Hafnadóttir, Marín Ósk, 2014: Understanding igneous processes through zircon trace element systematics: prospects and pitfalls. (45 hp)
377. Jönsson, Cecilia A. M., 2014: Geophysical ground surveys of the Matchless Amphibolite Belt in Namibia. (45 hp)
378. Åkesson, Sofia, 2014: Skjutbanors påverkan på mark och miljö. (15 hp)
379. Härling, Jesper, 2014: Food partitioning and dietary habits of mosasaurs (Reptilia, Mosasauridae) from the Campanian (Upper Cretaceous) of the Kristianstad Basin, southern Sweden. (45 hp)
380. Kristensson, Johan, 2014: Ordovicium i Fågelsångskärnan-2, Skåne – stratigrafi och faciesvariationer. (15 hp)
381. Höglund, Ida, 2014: Hiatus - Sveriges första sällskapsspel i sedimentologi. (15 hp)
382. Malmer, Edit, 2014: Vulkanism - en fara för vår hälsa? (15 hp)
383. Stamsnijder, Joaen, 2014: Bestämning av kvartshalt i sandprov - metodutveckling med OSL-, SEM– och EDS-analys. (15 hp)
384. Helmfrid, Annelie, 2014: Konceptuell modell över spridningsvägar för glasbruksföroreningar i Rejmyre samhälle. (15 hp)
385. Adolfsson, Max, 2014: Visualizing the volcanic history of the Kaapvaal Craton using ArcGIS. (15 hp)
386. Hajny, Casandra, 2014: Ett mystiskt ryggradsdjursfossil från Åsen och dess koppling till den skånska, krittida ryggradsdjursfaunan. (15 hp)
387. Ekström, Elin, 2014: – Geologins betydelse för geotekniker i Skåne. (15 hp)
388. Thuresson, Emma, 2014: Systematisk sammanställning av större geoenergianläggningar i Sverige. (15 hp)
389. Redmo, Malin, 2014: Paleontologiska och impaktrelaterade studier av ett anomalt lerlager i Schweiz. (15 hp)
390. Artursson, Christopher, 2014: Comparison of radionuclide-based solar reconstructions and sunspot observations the last 2000 years. (15 hp)
391. Svahn, Fredrika, 2014: Traces of impact in crystalline rock – A summary of processes and products of shock metamorphism in crystalline rock with focus on planar deformation features in feldspars. (15 hp)
392. Järvin, Sara, 2014: Studie av faktorer som påverkar skredutbredningen vid Norsälven, Värmland. (15 hp)
393. Åberg, Gisela, 2014: Stratigrafin i Hanöbukten under senaste glaciationen: en studie av borrkärnor från IODP's expedition nr 347. (15 hp)
394. Westlund, Kristian, 2014: Geomorphological evidence for an ongoing transgression on northwestern Svalbard. (15 hp)
395. Rooth, Richard, 2014: Uppföljning av

utlastningsgrad vid Dannemora gruva; april 2012 - april 2014. (15 hp)

396. Persson, Daniel, 2014: Miljögeologisk undersökning av deponin vid Getabjär, Sölvesborg. (15 hp)
397. Jennerheim, Jessica, 2014: Undersökning av långsiktiga effekter på mark och grundvatten vid infiltration av lakvatten – fältundersökning och utvärdering av förhållanden vid Kejsarkullens avfallsanläggning, Hultsfred. (15 hp)
398. Särman, Kim, 2014: Utvärdering av befintliga vattenskyddsområden i Sverige. (15 hp)
399. Tuvesson, Henrik, 2014: Från hav till land – en beskrivning av geologin i Skrylle. (15 hp)
400. Nilsson Brunlid, Anette, 2014: Paleoekologisk och kemisk-fysikalisk undersökning av ett avvikande sedimentlager i Barsebäcks mosse, sydvästra Skåne, bildat för ca 13 000 år sedan. (15 hp)
401. Falkenhaug, Jorunn, 2014: Vattnets kretslopp i området vid Lilla Klåveröd: ett kunskapsprojekt med vatten i fokus. (15 hp)
402. Heingård, Miriam, 2014: Long bone and vertebral microanatomy and osteohistology of 'Platecarpus' ptychodon (Reptilia, Mosasauridae) – implications for marine adaptations. (15 hp)
403. Kall, Christoffer, 2014: Microscopic echinoderm remains from the Darriwilian (Middle Ordovician) of Västergötland, Sweden – faunal composition and applicability as environmental proxies. (15 hp)
404. Preis Bergdahl, Daniel, 2014: Geoenergi för växthusjordbruk – Möjlig anläggning av värme och kyla i Västskåne. (15 hp)
405. Jakobsson, Mikael, 2014: Geophysical characterization and petrographic analysis of cap and reservoir rocks within the Lund Sandstone in Kyrkheddinge. (15 hp)
406. Björnfors, Oliver, 2014: A comparison of size fractions in faunal assemblages of deep-water benthic foraminifera—A case study from the coast of SW-Africa.. (15 hp)
407. Rådman, Johan, 2014: U-Pb baddeleyite geochronology and geochemistry of the White Mfolozi Dyke Swarm: unravelling the complexities of 2.70-2.66 Ga dyke swarms on the eastern Kaapvaal Craton, South Africa. (45 hp)
408. Andersson, Monica, 2014: Drumliner vid moderna glaciärer — hur vanliga är de? (15 hp)
409. Olsenius, Björn, 2014: Vinderosion, sanddrift och markanvändning på Kristianstadsslätten. (15 hp)
410. Bokhari Friberg, Yasmin, 2014: Oxygen isotopes in corals and their use as proxies for El Niño. (15 hp)
411. Fullerton, Wayne, 2014: REE mineralisation and metasomatic alteration in the Olserum metasediments. (45 hp)
412. Mekhaldi, Florian, 2014: The cosmic-ray events around AD 775 and AD 993 - Assessing their causes and possible effects on climate. (45 hp)
413. Timms Eliasson, Isabelle, 2014: Is it possible to reconstruct local presence of pine on bogs during the Holocene based on pollen data? A study based on surface and stratigraphical samples from three bogs in southern Sweden. (45 hp)
414. Hjulström, Joakim., 2014: Bortforsling av kaxblandat vatten från borrningar via dagvattenledningar: Riskanalys, karaktärisering av kaxvatten och reningsmetoder. (45 hp)
415. Fredrich, Birgit, 2014: Metadolerites as quantitative P-T markers for Sveconorwegian metamorphism, SW Sweden. (45 hp)

LUNDS UNIVERSITET

Geologiska institutionen
Lunds universitet
Sölvegatan 12, 223 62 Lund